RAM ROBOTICS AND MECHATRONICS

IMPROVING THE ELECTRONICS OF A ROBOTIC STAND FOR WOUND CARE MONITORING

M.A. (Max) Liebe

BSC ASSIGNMENT

Committee:
dr. ir. J. Canyelles Pericàs
dr. ir. E. Dertien

July, 2025

051RaM2025
Robotics and Mechatronics
EEMCS
University of Twente
P.O. Box 217
7500 AE Enschede
The Netherlands

UNIVERSITY OF TWENTE. | TECHMED CENTRE
UNIVERSITY OF TWENTE. | DIGITAL SOCIETY INSTITUTE

Abstract

This graduation project addresses the electronic limitations of a robotic stand designed for automated wound care monitoring in patients with diabetic foot ulcers (DFUs). The primary purpose was to enhance the integration, manufacturing, safety, and functionality of the device's hardware. Through a structured design process involving background research, ideation and detailed specifications, the project proposes an extensive overhaul of the electronics of the existing prototype. Key improvements include transitioning from primitive point-to-point wiring and development modules to integrated Printed Circuit Board (PCB) designs with embedded sensors, significantly improving component integration and manufacturability. The design also includes new functionality, such as an onboard power storage solution with USB Type-C power delivery, an emergency stop mechanism, an LED drive circuit and preparations for a user interface. While theoretical designs and schematics were developed, the physical prototype was not realised due to a lack of time, which led to mostly qualitative evaluation. The proposed designs successfully meet most established user and design requirements. Although these designs will still require practical verification, they lay a strong theoretical foundation for a more capable and integrated wound monitoring device that could help DFU patients worldwide.

Acknowledgement

I want to express my gratitude to everyone who assisted me throughout this graduation project. First, I would like to thank my supervisor, Pep Canyelles Pericàs, for their continuous support, insights, understanding and motivational words throughout this project. Next, I would like to thank my critical observer, Edwin Dertien, who gave very insightful feedback on my presentation that steered the project in the right direction. As this report builds on previous research by Imme Ebben, René van Koolwijk and Filip van der Kroft, I would also like to express my gratitude for their invaluable contributions to this project; without their elaborate research, this project would not have been possible. A special thanks to Filip, with whom I spent numerous brainstorming sessions working on improvements and new designs for the device. I would also like to thank Arnoud Hartemink, who worked on the device's interface simultaneously, for being a helpful project partner and a good motivator. Also, a special thanks to my housemate, David de Groot, for motivating me for multiple days and nights while working on our graduation projects. I would also like to thank my family and friends for their continuous support throughout this project. And finally, thanks to the RAM group for making this project possible and providing me with a fun and welcoming working environment.

Contents

List of Figures

List of Tables

1 Introduction

1.1 Project Background

Each year, more than eighteen million people worldwide develop a diabetic foot ulcer **(DFU)**. These wounds can have a significant impact on physical fitness and quality of life and are associated with a higher mortality rate among diabetes patients [1]. DFUs are susceptible to infection, which can compromise the healing process and may eventually lead to the need for foot amputation [1, 2]. Treatment of these wounds is a complex and lengthy process, with only between 30% and 40% of ulcers healing after twelve weeks and a recurrence rate of 65% in five years [1]. This infection risk poses the need for fast and reliable wound assessment strategies.

In the Netherlands, such assessment information is usually recorded in the PatDoc format [3]. Per protocol, the wound is described in text and is accompanied by a picture taken with a mobile device. Estimating wound area, reading temperature data, and testing for bacterial presence are performed through separate manual tests, which, although cost-effective, are also very time-consuming, sometimes rendering the test data outdated and unusable [4]. Various wound analysis techniques using image analysis exist that can (partially) automate this process, with recent developments in neural networks and deep learning having further accelerated the performance of these techniques.

Figure 1.1: Demonstration of using Visitrak, a manual wound analysis method [5]

Figure 1.2: Cutimed, a chronic wound analysis method using a mobile phone

Two significant aspects of wound analysis using imaging are segmenting the wound from the healthy skin and background, and classification of the most important wound tissues, such as granulation, fibrin, and necrosis. While studies have shown these algorithms to be effective [6, 7], the major challenge seems to be gathering accurate and reliable image data. This is mainly due to the lacklustre accuracy and lighting conditions of the pictures, resulting from smartphone photography [6].

Last year, Filip van der Kroft designed a prototype for a wound monitoring device that can improve the quality of visual data gathered from DFU patients. This prototype was constructed based on previous research done by Imme Ebben and René van Koolwijk and is a Raspberry Pi-based device that uses a motorised robotic arm with a camera and sensing module attached at the end to capture data accurately. This is achieved by moving the arm around the foot to direct the camera at the patient's wound. The foot is held stationary by a footrest. The device also has a time-of-flight distance sensor for focusing the camera. This allows the device to capture images without movement and perform accurate thermal sensing. In the end, its functions will be easily accessible from an interface wirelessly connected to the device over Bluetooth or WiFi [4].

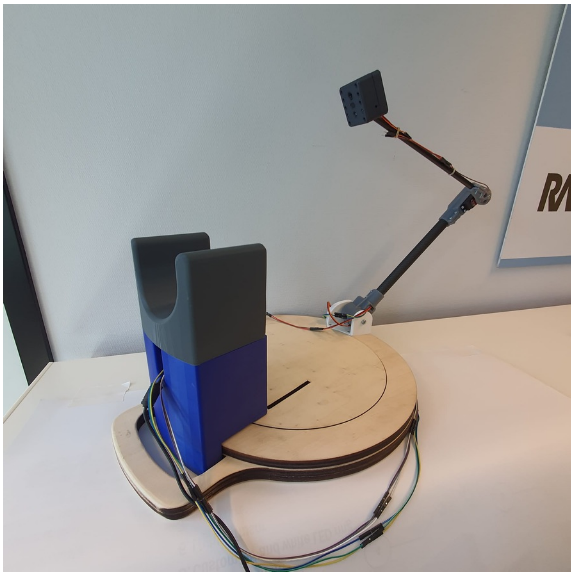

Figure 1.3: The prototype wound monitoring device constructed by van der Kroft

1.2 Prototype Limitations & Solutions

The prototype in its current stage is still quite unfinished. It utilises a combination of development boards (Raspberry Pi 4B and Arduino Uno) and sensors embedded in modules, all of which are interconnected via rudimentary wiring. Some features are also still left unfinished, like the ability to drive its LEDs. To further develop this prototype in preparation for manufacturing and to enhance its integration, safety, and functionality, this project will investigate potential issues and areas of improvement with the current prototype and propose possible solutions that could be applied in an updated iteration of the design. While most of the previously established user requirements have been satisfied by the prototype, some requirements remain unmet. Changes to the prototype design may enable these to be met. For example, van der Kroft specifies that the device has no onboard power storage [4]. There may also be certain features mandated by international standards that are currently not incorporated into the prototype, which could be added. This project aims to investigate all of these points and provide improved designs and implementations for the electronics that could be used in the next iteration of the prototype.

1.3 Research Questions

The main research question of this thesis is defined as follows: *"How can the electronics of the wound care monitoring device be modified to improve the integration, manufacturability, safety and functionality of the hardware?"*

Six sub-questions are defined to answer the main research question:

Literature Review SRQ1: *"What techniques are used to analyse chronic wounds, and which of these techniques are suitable for a wound monitoring device designed for home use?"*

Prototype Design SRQ2: *"What does the operation of the prototype look like, and what electronic components are used in the current version of the prototype?"*

User & Design Requirements SRQ3: *"Which design requirements should be added to the list of current requirements, based on issues with the current design or international standards?"*

Ideation SRQ4: *"What potential issues do the current components present, and what changes to implementation or new technologies can be used to solve these issues?"*

Ideation SRQ5: *"What new features should be added to the device based on the user and design requirements, and how are these implemented?"*

Evaluation SRQ6: *"What impact do the changes implemented in the new prototype designs have on the integration, manufacturability, safety and functionality of the device?"*

1.4 Thesis Outline

This thesis begins with background research to answer SRQ1 to SRQ3, starting with a literature review on data acquisition strategies for wound analysis to gain insight into the project's context. Then, a study is done on the workings and components of the prototype to gain a thorough understanding of its operation, along with its strengths and weaknesses regarding the electronics. As part of the background research, the project introduces a "Foundation" stage where the user & design requirements are defined, and potentially updated based on the prototype design or international standards. The next chapter describes the design method used for this project and explains the various phases of each stage of the design cycle. Following this, the Ideation process is documented, along with different sketches and ideas for improving aspects of the device's electronics. A final idea is then selected for further development. In Chapter 5, the specifications for this idea are established, to then develop it into a series of (physical) designs in Chapter 6. Chapter 7 evaluates the proposed designs based on the user & design requirements, and documents the differences compared to the old design. Chapter 8 interprets and comments on these results, aiming to answer the main research question. It also evaluates the research method itself and specifies the implications of this research. The final chapter concludes whether the project's goals have been achieved and highlights potential improvements that could be investigated for further renditions of the prototype wound monitoring device.

The structure looks like this:

- Introduction
- Background Research
- Methods
- Ideation
- Specification
- Realisation
- Evaluation
- Discussion
- Conclusion

2 Background Research

This chapter provides an overview of the project's background. First, a review of various literature on chronic wound analysis will be conducted to gain more insight into the limitations of current chronic wound analysis methods and identify potential technologies that could be utilised in a wound monitoring device for home settings. The results of this literature review are compared against the technologies in the current device to verify that the choices of these technologies are sufficient.

2.1 Literature Review

2.1.1 Introduction

Recent years have seen a steady increase in skin disease cases worldwide [8]. Chronic wounds, which can be referred to as "wounds that do not heal within three months and are difficult to treat" [9, p. 1], constitute a significant portion of these cases [8]. In a 2014 study commissioned by the Nederlandse Zorgautoriteit ("Dutch healthcare authority"), the prevalence in the Netherlands was estimated to be 1 to 3% [10], indicating approximately 500,000 cases in the Netherlands alone. Due to its common prevalence, numerous methods have been developed to assess the state of a chronic wound. A standard method for at-home wound assessment involves photographing the wound with a digital or smartphone camera. These images can then be processed by algorithms for tissue classification and wound analysis [6]. Although advances in algorithms and artificial intelligence have significantly improved these methods in recent years, Marijanovic and Filko note that no single current approach provides the comprehensive data required for practical implementation in medical centres [6]. According to the researchers, the primary limitation is not the analysis techniques, but rather the need for greatly improved wound measurement to generate accurate and consistent data for the algorithms [6]. Previous research by Imme Ebben, René van Koolwijk and Filip van der Kroft investigated the potential for constructing a device to improve the measurement of imaging data for at-home chronic wound monitoring [3, 4, 11]. A prototype of such a device was constructed that uses optical imaging and thermal imaging technologies to acquire wound data. Aside from these two imaging techniques, numerous other imaging modalities could be used to gain insights into the state of a chronic wound. Investigating the potential for incorporating other imaging techniques into this device could be insightful.

Therefore, this literature review aims to provide an overview of various imaging data acquisition techniques, focusing on their potential for reliable and robust wound monitoring in a home or care centre setting.

The first part of this review presents various methods for gathering imaging data on the wound. Next, the relevant variables for at-home wound assessment are discussed. The final part of this review will compare the data acquisition techniques based on the previously mentioned variables and propose some possible combinations of these techniques that can be utilised in a home wound-monitoring device.

2.1.2 Wound Imaging Data Acquisition Methods

Medical professionals utilise various imaging techniques to evaluate the condition of a chronic wound. The most basic, but also widely used technique is optical imaging. As previously stated, this method involves taking photographs of the wound with a digital camera. An example of this is the inSight CR app, which utilises a smartphone camera to capture imaging data and then processes the RGB data using an AI algorithm [12]. Despite being such a simple method, optical imaging offers a high spatial resolution and allows for accurate shape measurement [7, 13]. Its main weakness is that it does not help measure the depth or volume of a wound [7, 13, 14] unless it is combined with some depth-measuring technique like stereo-vision [13, 15]. This technique involves using a second digital camera or a dual-lens camera to take a picture at a slightly different angle, thereby triangulating the depth. While this approach enables the 3D reconstruction of the wound, its accuracy is relatively low, and the results are also heavily influenced by lighting conditions [15].

The main limitation of optical imaging is that every algorithm only has RGB data to work with. That is why some researchers have opted to employ a technique based on hyperspectral imaging (HSI). This method involves taking a series of images and measuring the intensity of various light wavelengths. Whereas routine optical imaging is limited to just red, green, and blue channels, HSI data can have up to several hundred narrow bands [13]. HSI makes it possible to measure oxygen saturation, detect the presence of bacteria, and allow for even more advanced wound shape classification [7, 13, 14]. Research by Chin et al. has shown that such oxygen saturation data could be used to measure burn depth in a mouse's wound [16].

Optical Coherence Tomography (OCT) produces real-time cross-sectional images of a wound's internal microstructure using interferometry [7]. Research has shown it could be helpful to monitor structural changes during the wound-healing process of certain cutaneous wounds [17]. Depending on the specific OCT technique used, it may also be helpful for high-speed burn depth evaluation [14, 18]. OCT can also be used for wound shape measurement [19]. However, it has poor tissue penetration and is therefore limited to use in cutaneous wound monitoring [7]. OCT scan devices are also expensive, particularly when compared to other low-cost techniques, such as optical imaging.

A more affordable technique that has also been used to gain insights into the healing process of chronic wounds is thermal imaging. Thermal imaging involves using an infrared camera to measure infrared radiation emitted from wound tissue [7]. As inflammatory reactions generally increase tissue temperature, thermal imaging can give insights into the stage of wound healing and detect the existence of infections [20]. Yi et al. developed a smartphone add-on to enhance conventional wound healing monitoring by combining thermal sensing and optical sensing [21]. The main drawbacks of thermal imaging are its accuracy, specificity and sensitivity [7, 22].

Time-of-Flight (ToF) 3D imaging involves measuring the time it takes for light to travel from a point to the camera sensor and back. By translating this travel time into depth, a 3D reconstruction of the wound can be made, which in turn can be used to perform shape and volume analysis on the wound [13]. ToF technology is already being embedded into numerous high-end smartphones and smartphone add-ons. This technology is still in its infancy, as researchers in 2024 tried to use ToF 3D imaging for reconstructing a wound, but were not yet able to gather sufficient data to create an accurate reconstruction of said wound [23].

Near-infrared (NIR) spectroscopy measures the balance between oxygen delivery and consumption in tissues of the sample under study [14, p.9], this is done by detecting the maximum light absorption wavelengths of different components [7, 24]. This technique can determine oxygen saturation and haemoglobin content around wound sites [7, 24], which can be used to estimate wound burn depth and monitor the wound healing progress. [25–27]. NIRS is a simple imaging method, with few restrictions on lighting conditions. However, like thermal imaging, it lacks specificity [14].

Laser Doppler Imaging (LDI) is an imaging modality that visualises blood movement in the skin. It does so by focusing a raster pattern with a red laser on the surface of the wound [14, 28]. This makes it possible to observe changes in blood flow over time, which can be used to assess burn wound depth [28, 29]. According to Li et al., LDI has a limited application for imaging chronic wounds due to a lack of accuracy and lower measurable blood flow in the lower limbs of diabetic patients [7].

Another technique that relies on reflecting specific wavelengths of light is fluorescence imaging. This involves visualising bacteria that become fluorescent when a particular light is shone upon the tissue of the wound. An example of such an implementation is the i:X Wound Intelligence Device developed by MolecuLight. This device emits a monochromatic violet light onto the wound tissue, resulting in green fluorescence of the wound. For harmful bacteria, this fluorescence turns red [13]. This information can give insights into tissue health and the potential for a wound to heal [13].

Terahertz (THz) spectroscopy analyses changes in water content between healthy and unhealthy wound tissue [7]. It has been used for the evaluation of burn wounds [30] and is safe as the photon emissions from THz are non-ionising [7, 31]. It has a similar resolution to Magnetic Resonance Imaging (MRI) for detecting tissue hydration [32] and also does not require contact with a patient. It is also able to penetrate deeper than imaging techniques like NIRS [7].

Although the penetration depth may be worse than THz spectroscopy, ultrasound imaging offers a cheap and high spectral resolution solution for imaging cutaneous wounds [7]. It involves sending an acoustic pulse to the wound and using a transducer to pick up the reflected signal. By scanning over the wound, a 2D image can be reconstructed based on the intensity of the signals. Research has shown that this can assess wound depth, area and volume [33]. Like THz spectroscopy, it is safe as no ionising radiation is involved. However, physical contact is often required due to the limited range of ultrasound imaging [7].

More established techniques, such as MRI and computed tomography (CT) and their derivatives, have also proven to be effective for analysing soft tissue, bone, and joint pathology around the wounded region, as well as vascularisation of chronic wounds, respectively [34–36]. However, the ionising radiation associated with these techniques immediately eliminates any potential for using these technologies in a home setting, not to mention the great economic costs associated with them. For this reason, these technologies will not be considered when comparing imaging techniques in the next section.

2.1.3 Relevant Variables

To narrow down the previously mentioned imaging methods to a list of potential candidates for at-home use, it is important to establish the variables based on which the techniques will be compared. One of the variables, whether the device emits ionising radiation, was already deemed to eliminate that modality as a potential candidate in the previous section and thus will not be considered for this comparison.

As the project's intention is for the device to be used at home, cost and portability are important factors to consider. As previously stated, the healthcare costs associated with chronic wounds are already significant; therefore, if this device is intended to mitigate these costs, any excessive cost would render the use of the related technology invalid. The need for portability was emphasised by the QualityZorg staff in van Koolwijk's interviews [3], and therefore, any technology that is not or barely portable should also be eliminated from consideration for the device.

Many wound analysis methods focus on wound shape and segmentation, this is because wound shape and size are easily quantifiable metrics that can be tracked over time to show the status and progress (or lack thereof) of the wound [37, 38]. This is already the metric used by common methods such as Visitrak™ (Smith & Nephew, Watford, United Kingdom), and some studies have shown that measurement of this metric by image data can even be more accurate than manual measurements [39]. While wound shape and depth are often used in the same context, the wound shape can be analysed from the surface of the wound, while depth and, by extension, volume require some penetrative technology. For this reason, depth will be treated as a separate variable in this analysis.

Infections pose a significant risk for patients with chronic wounds. For example, in 15-20% of cases of patients with infected diabetic foot ulcers, the lower limb has to be amputated [40]. Infections cannot be detected solely based on wound shape or depth, but may require measuring other metrics, such as bacterial presence, temperature fluctuations, or variations in oxygen saturation [7, 14]. For the sake of simplicity, the analysis will consider the capability to measure any of these metrics as an indicator of the ability to detect infections.

As it may be difficult to control the ambient lighting in a home setting, it is also useful to consider the restrictions certain technologies may require concerning ambient lighting conditions. Although the prototype of the wound monitoring device created by van der Kroft aims to mitigate these restrictions with a light-shielding lid [4], this has not yet been implemented; thus, it is also essential to consider this factor.

Finally, although the interviews by van Koolwijk indicate that an at-home wound-monitoring device would likely still for 80% be operated by medical staff or home care workers [3], physical contact could still pose a risk of infections or sanitary problems. Therefore, although not a critical restriction, the requirement for physical contact by the device is undesirable and should be carefully considered when deciding on the techniques to use for that device.

2.1.4 Technique Comparison

The discussed variables are now assessed and compared across the previously discussed data acquisition modalities, as shown in Table 2.1.

Imaging Method	Cost	Portability	Wound shape classification	Wound depth classification	Can detect infections	Requires contact with skin	Impact of ambient lighting conditions
Optical Imaging	Low	High	Yes	No	No	No	Medium
Optical Imaging + Stereovision	Low	High	Yes	Yes, low accuracy and limited depth	No	No	High
Hyperspectral Imaging	High	Medium	Yes	Yes, limited depth	Yes	No	High
Optical Coherence Tomography	High	Medium	Yes	Yes, limited depth	Limited, structural changes can be detected which in turn could signify infections	No	None
Thermal Imaging	Medium	High	Limited, low resolution	Yes, low resolution	Yes	No	None
Time of Flight 3D Imaging	Medium	High	Yes	Yes, limited depth	No	No	Medium, other NIR light sources may influence results
Near-Infrared Spectroscopy	Medium	Medium	No	No	Yes	No	Low
Laser Doppler Imaging	Medium	Medium	Limited, blood flow is visualised but not the wound shape directly	Yes	Limited, increased perfusion can be a sign of inflammation	No	Medium, light of similar wavelengths could interfere
Fluorescence Imaging	Low	High	No	No	Yes	No	High, only suitable for use in darkened environments
Terahertz Imaging	Medium-High	Medium	Limited, by mapping differences in water content wound boundaries could be identified	Yes	Yes	No	None
Ultrasound imaging	Low	High	Yes, requires scanning	Yes, limited depth	Yes	Yes	None

Table 2.1: Data acquisition techniques compared by relevant variables. A red highlight indicates a critical factor for not considering this technique, and a yellow highlight indicates something that should be carefully considered.

As can be seen from the data in Table 2.1, no single technique currently provides all the data needed to perform a full analysis of the wound without containing a restriction for at-home use. This means that to create a device capable of analysing most aspects of a chronic wound, the device would need to incorporate multiple techniques.

It is clear to see why many wound-monitoring approaches opt to use optical imaging. Its low cost and high portability make it accessible to a wide range of users while offering excellent wound shape classification. The fact that most smartphones are equipped with cameras that have sufficient resolution to perform this analysis also greatly benefits this technology. However, it is also obvious that this technology is limited in its capabilities concerning depth and volume classification, as well as detecting infections. Stereo-vision can offer a solution to the lack of depth measurement; however, ambient lighting conditions significantly impact it, resulting in less accuracy compared to other techniques.

If the goal is to create a cost-effective device capable of full wound analysis, it could be argued that combining optical imaging with ultrasound imaging is the most economical way to achieve this. A combination of these techniques will still lack depth measurement, but the cost-benefit of having such inexpensive technologies could outweigh this. The requirement for physical contact means the device would need to be sanitised before and after use, which might be something a device manufacturer would want to avoid.

If physical contact is restricted, a combination of optical imaging and thermal imaging will likely still be a very viable alternative that can fully analyse the wound. For more accurate depth measurement, thermal imaging could also be combined with ToF imaging, although this would drive up the cost. All of these techniques are highly portable and thus could likely be integrated into the same module. Fluorescence imaging could enhance the reliability of infection measurement data without adding significant complexity to the device, as, in theory, all that is needed are a few 405 nm ultraviolet LEDs.

Although LDI offers in-depth classification and NIR spectroscopy, providing insightful information regarding infections, both technologies fall short in terms of cost and portability, and thus should only be considered if the goal is to create a device that can perform analysis with a high degree of accuracy. The other technologies are considered eliminated as potential candidates due to their high cost and should therefore not be considered for the device.

2.1.5 Reflecting on Current Prototype

The prototype created by van der Kroft is designed to combine digital imaging, thermal imaging and fluorescence imaging [4]. The literature review suggests that these choices are excellent for the goals of the wound monitoring device. It does not make sense to add an ultrasound sensor to the device, as physical contact would require sanitisation of the device and mandate extra care taken with the robotic arms. Additionally, the three technologies already meet all the measurement requirements. Therefore, this project will not consider alternative imaging modalities for the prototype and will continue using the same techniques that were already chosen for the prototype. This does not necessarily mean that any sensors used in the device will remain the same.

2.2 Analysis of Current Electronics

This chapter aims to summarise the functionality of the current prototype designed by van der Kroft and explain the rationale behind their design choices. An overview of its components is provided to serve as the basis for ideating improvements to the electronics, which will be discussed in Chapter 3.

2.2.1 Introduction of the Device

The wound monitoring device, which will be referred to from now on by either "the device" or "the prototype", was designed by van der Kroft in 2024 to provide an automated solution for at-home wound monitoring [4]. The core concept of the device was inspired by research conducted by Ebben, who primarily investigated the needs for such a device [11], and van Koolwijk, who determined the user and design requirements for the device [3]. The device is pictured in Figure 2.1.

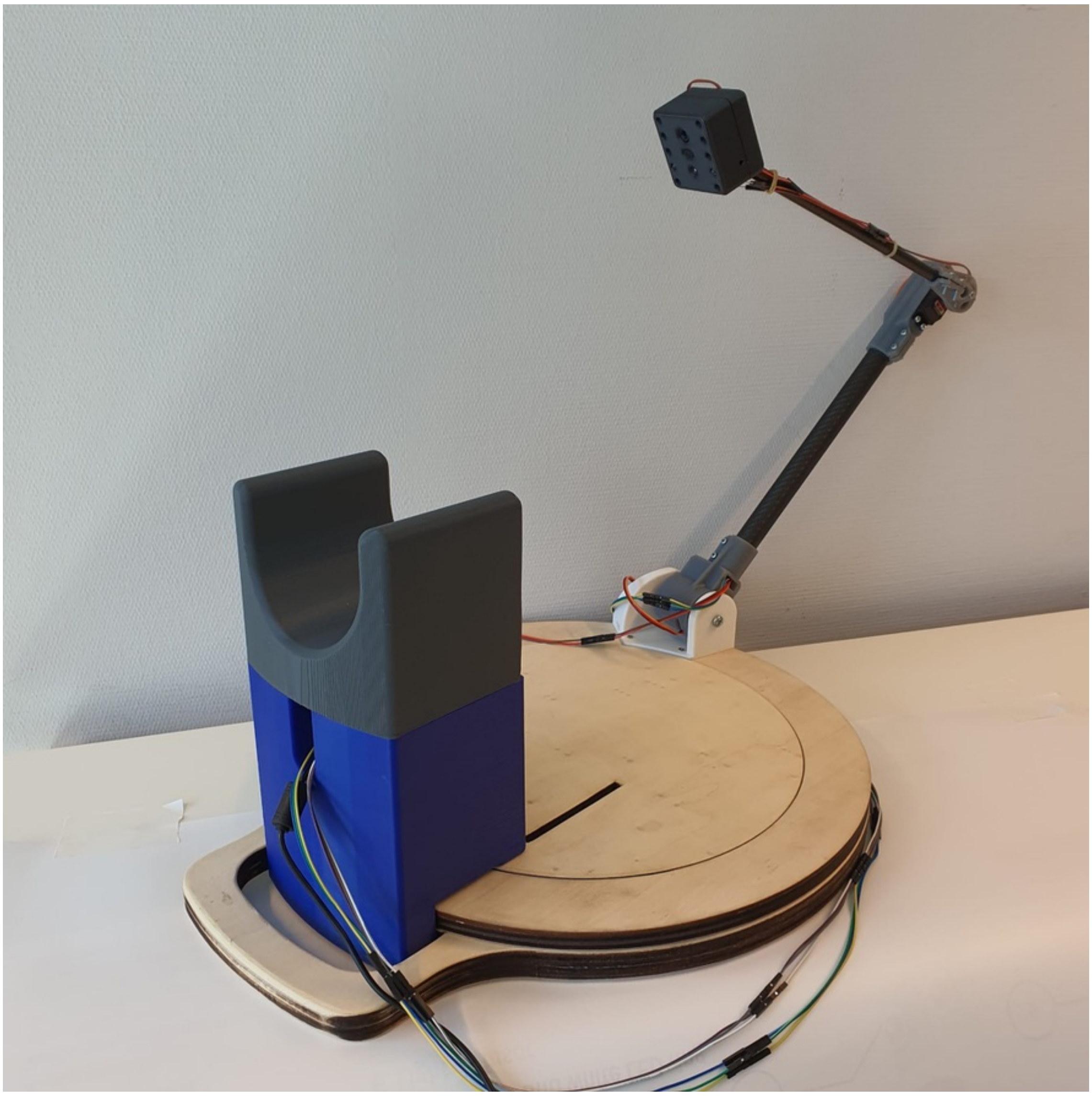

Figure 2.1: The wound monitoring device prototype as created by van der Kroft [4]

The idea of the prototype is to be a rotating robotic arm with four degrees of freedom, equipped with a module at the end that features multiple cameras and sensors. A DFU patient first lays their foot down on a designated leg rest or steps on the centre of the device. The device can then control the robotic arm and process sensor data autonomously to analyse the wound. The autonomous and controlled nature of the device ensures consistent and accurate wound measurement data, which can then be used for various purposes. In addition to regular wound monitoring, the data can also be utilised as training data for wound analysis algorithms. These functions are all still theoretical, though, as the device is still a very early prototype with numerous functions still missing [4]. These limitations are further explained later in this chapter.

2.2.2 Stakeholder Requirements

An analysis of the device's relevant stakeholders and their needs was previously performed by Ebben [11]. Van Koolwijk used this data to determine design requirements for the device [3]. This project will assume that this data is still accurate. If, during research or the design process, uncertainties arise regarding stakeholder needs or intentions that cannot be resolved based on research alone, the relevant stakeholder groups may be consulted for clarification.

Stakeholders

It is essential to identify the stakeholders for this project, as any changes to the device may necessitate feedback from a specific stakeholder group. Ebben's stakeholder analysis identifies the following groups [11]:

- "Patients", patients with a DFU or any other chronic wound
- "Healthcare professionals", nurses, doctors and wound care specialists responsible for performing diagnoses and treatment on the wound
- "Caregivers", family members or home care workers who assist the patients with wound care
- "Product development team", designers, engineers and developers of the device

User & Design Requirements

The user and design requirements are based on the criteria indicated in the papers by Ebben, van Koolwijk and van der Kroft [3, 4, 11]. They are divided into functional requirements and corresponding technical requirements. As this project primarily focuses on hardware and electronics, the design requirements related to comfort and aesthetics, such as the foot stand, have been omitted for conciseness. The table may be extended at the end of this chapter if the background research reveals additional requirements.

Assessment of Requirement Implementation

As van der Kroft indicates in their research, most of the previously established requirements have already been met by the current implementation of the prototype. However, changes to the hardware have the potential to alter the implementation status of stakeholder requirements. Therefore, all hardware modifications must be assessed for their impact on requirement fulfilment.

Aside from the already implemented requirements, some have not yet been met. The current device notably lacks an onboard power storage solution, which means that the requirements for wireless operation are not fully met [4]. The simplest way to fulfil this requirement would

[1] There are no specifications for the exact amount of processing power required for this task. It is assumed that most modern single-board computers are capable of doing this task.

[2] The interface is currently still under development by Arnoud Hartemink and is therefore subject to change.

[3] No exact amount of storage was mentioned in any of the papers by Ebben, van Koolwijk or van der Kroft [3, 4, 11], it is assumed that the recommended amount of storage needed to run the Raspberry Pi is sufficient.

Functional requirements	**Technical requirements**
High-resolution images of the wound	Minimum camera resolution of 12.3 MP
	Camera with built-in autofocus
No impact of variations of lighting	External light shield
	Built-in illumination
Blurring and distortion prevention	Ability for cameras and sensors to be completely stationary
Capability to accurately determine the surface area of the wound	Adequate processing power[1] or external processing device
Capability to determine the percentage of colour corresponding to the three different tissue types	Adequate processing power[1] or external processing device
Display with the possibility to input data	Mobile user interface or built-in touch display[2]
On-board storage space to store multiple images and analysis results	Sufficient amount of internal or external flash storage[3]
Wireless functionality (should last throughout a full day of use)	On-board power storage (battery)
	WiFi or Bluetooth connectivity
Sending updates on wound status remotely	WiFi connectivity
Capability to measure temperature	Infrared thermal camera with an accuracy of +-0.2 degrees Celsius ideally, a minimum of +-1.0 degrees
Capability to measure bacteria presence in wound	High-efficiency UV LEDs with a wavelength of 405 nm
Consistent exposure for the camera	Dimmable white LEDs with a diffuser plate
Accurate positioning	Accurate stepper and servo motors
Easy (automatic) alignment of camera with the wound	Range finder sensor with a minimum sensing distance of 8 cm and an accuracy of +-5 mm
	Automatic positioning
Monitoring all areas of the foot	4 degrees of freedom servo arm with wide range of motion
	Ability for the camera to be positioned perpendicular to every surface of the foot
Sufficient safety measures	No contact with the wound necessary
Lightweight	Weight in between 1 kg and 15 kg, according to ARBO regulations

Table 2.2: Functional and technical requirements of the device determined after stakeholder analysis.

be to embed a battery in the device. Further details regarding this implementation are outlined in section 4.2.1.

Van der Kroft also indicates that the current prototype does not have a light shield to minimise external light, and also does not have a diffuser plate for the dimmable LEDs. While these are both design-specific requirements, it is relevant to consider them during the analysis, as their implementation may impact the available space for the other components.

2.2.3 Device Components

Understanding both the mechanical and electronic components of the device is crucial for determining any possible improvements that can be made to it. Therefore, this section dissects

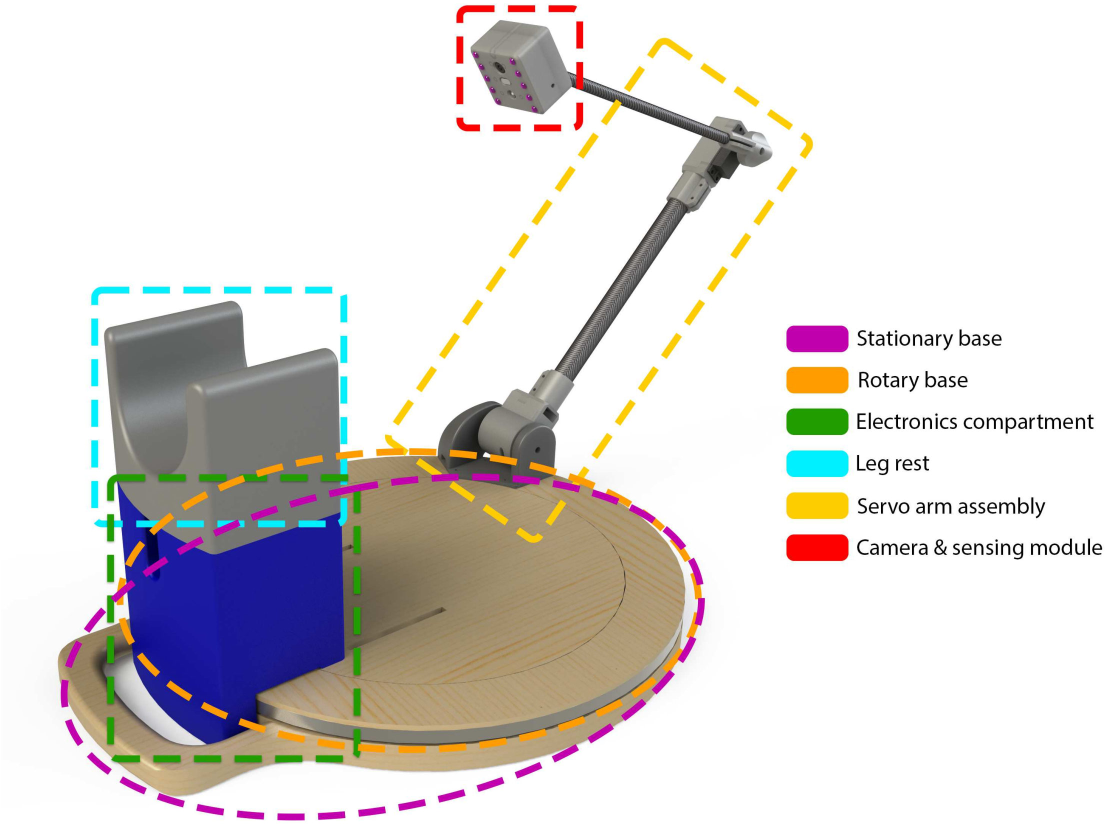

Figure 2.2: Layout of mechanical and structural parts of the prototype.

and explains all the components of the prototype, providing in-depth explanations of their functions within the device and the rationale behind the choice of each specific component.

Mechanical & Structural Components

To explain the inner workings of the device and establish some space restrictions for the hardware, the mechanical and structural components of the device are briefly described here. Some parts have been renamed for conciseness from those in van der Kroft's design. Figure 2.2 highlights the placement of each part in the design.

The stationary base is made of thick plywood and contains a carry handle for easy transportation. This carry handle is positioned near the electronics compartment, which accounts for most of the weight, making it easier to carry. The slits allow the footrest to clip into the base, providing a slimmer profile during transportation. There are also slits with bearings embedded in the bottom, allowing the rotating base to rotate with less friction. There are two mounting holes for the electronics compartment [4].

The rotary base is rotated on the vertical axis by the stepper motor embedded in the electronics compartment. The gear ring seen in Figure 2.3 is attached to the rotating base, which is then rotated by the small gear attached to the stepper motor [4]. This axis is one of the device's four degrees of freedom.

The electronics compartment is 3D printed and houses the stepper motor, Raspberry Pi 4B and the Arduino Uno. There is a slit in the front for any cables to pass through. Like the stationary base, it has two bearings embedded to allow the rotary base to rotate with less friction. It features mounting holes for the stepper motor, as well as holes for bolts to pass through, allowing it to be securely attached to the base. To cover the electronics, a cover plate is screwed into the top [4].

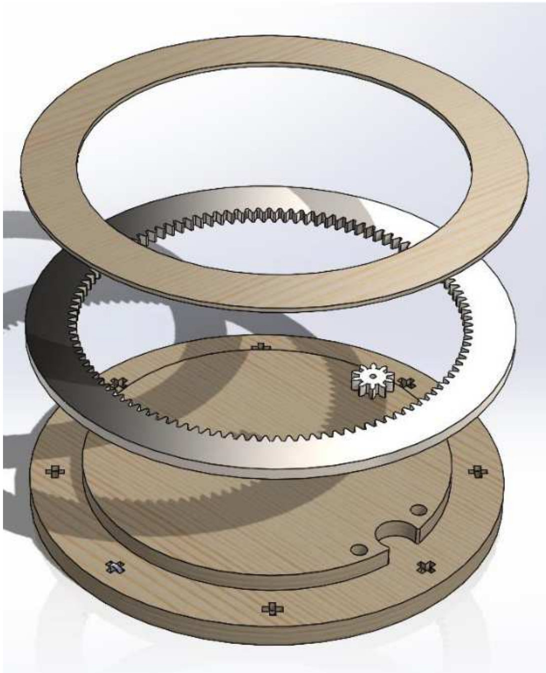

Figure 2.3: Exploded view of the base [4]

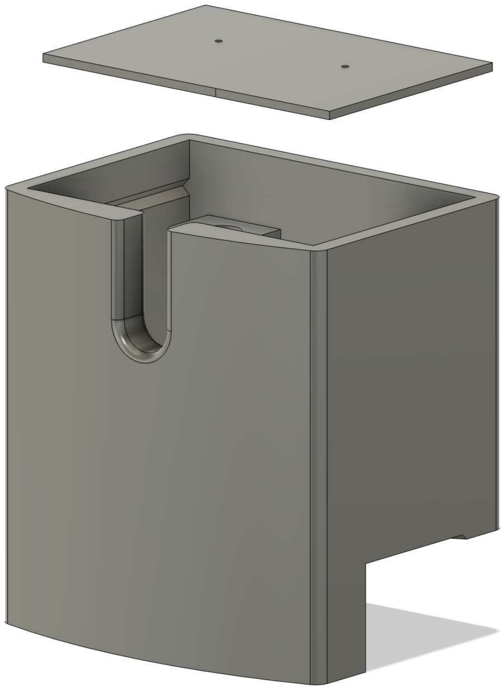

Figure 2.4: Exploded view of electronics compartment

The design of the leg rest has already undergone numerous iterations by van der Kroft, and the current design is likely to require no adjustments in this project. Nevertheless, it is a simple 3D-printed leg rest that slots into the electronics compartment. Its slits also allow it to be slotted into the stationary base for transport [4].

The servo arm assembly consists of two carbon fibre rods, which are moved by servos within the assembly. It attaches to the rotary base through a 3D-printed bracket. One servo is located in the bottom bracket, one in the joint between the rods, and one at the end, attached to the camera and sensing module. Together, they add three additional degrees of freedom. In the current prototype, the wires for the servos and camera module are guided around the arms [4].

The camera and sensing module is an enclosure that houses the digital camera, infrared camera, and laser distance sensor. The modules of these components are stacked together as tightly as possible to give the closest possible perspective. It has holes for the white and UV LEDs, as well as a small hole where the cables exit. Like the brackets of the servo arm, this enclosure is 3D printed [4]. Notably absent in the current prototype is an external light shield. This would likely be attached to this module.

Hardware & Electronics

The device is based on a Raspberry Pi 4B, a small, open-source single-board computer (SBC) featuring a quad-core 64-bit ARM Cortex-A72 processor and 1 to 4 gigabytes of LPDDR4 memory. The Raspberry Pi functions like a full desktop computer, featuring an embedded GPU, HDMI output, USB support, WiFi, Ethernet, Bluetooth, and running a custom Linux distribution from an SD card. It also houses several GPIO pins that can be used for various applications. There is a specific MIPI CSI port for cameras and a MIPI DSI port for displays [41]. Ebben spe-

Figure 2.5: Camera and sensing module [4]

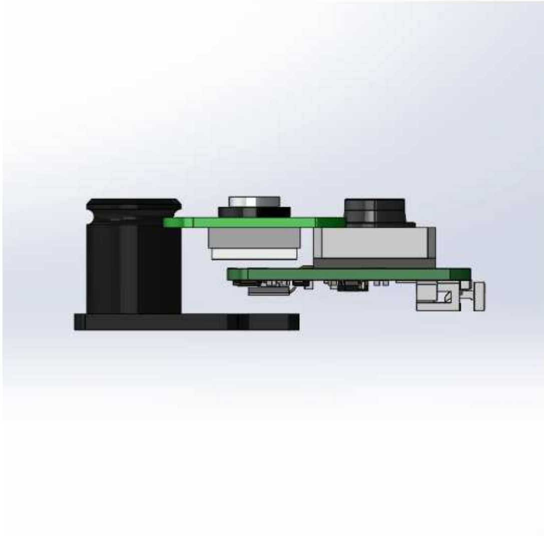

Figure 2.6: Layout of sensors within the camera module [4]

cifies that the main motivations for choosing this SBC are its low cost, ongoing developer support, and its wireless networking and Bluetooth capabilities [11]. It is located in the electronics compartment [4].

To drive the stepper and servo motors, the device uses an Arduino Uno [3, 4]. This is a small development board created by Arduino S.r.l. for Atmel's ATmega328P microcontroller [42]. While no explicit motivation is given for the choice of this development board, its open-source nature and wide adaptation worldwide make the board a beginner-friendly and logical choice for a prototype. The Arduino Uno is also housed in the electronics compartment and presumably connected to the Raspberry Pi over USB to supply power and to control it. However, this is never confirmed in the paper by van der Kroft.

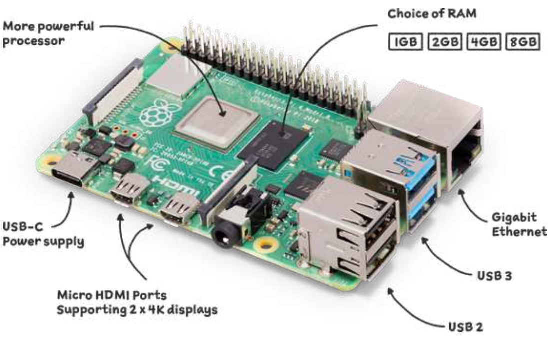

Figure 2.7: Raspberry Pi 4B [43]

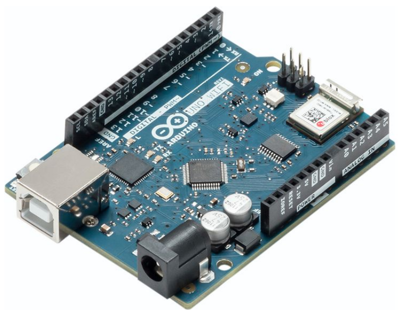

Figure 2.8: Arduino Uno R3 [42]

Attached to the Arduino Uno is the VNGARD967058 CNC shield by VNG Systems [3]. This board is directly inserted into the Arduino's Dupont headers and supports up to four stepper drivers & motors to be connected to it [42]. The purpose of this board is to make it easy to mount a DRV8825 stepper driver module [3]. This module can drive a stepper motor with a voltage ranging from 8.2 to 45 V, supply 1.5 A of current continuously (2.5 A peak), has a micro-step resolution of 1/32, and has built-in overcurrent and thermal protection [44].

The stepper motor is responsible for rotating the base. The prototype uses the SF2423-10B41 stepper motor [4]. It uses 24 V and has a current rating of 2 A [47]. Note that this is above the current rating of the stepper motor driver [44], which will be further expanded upon in section

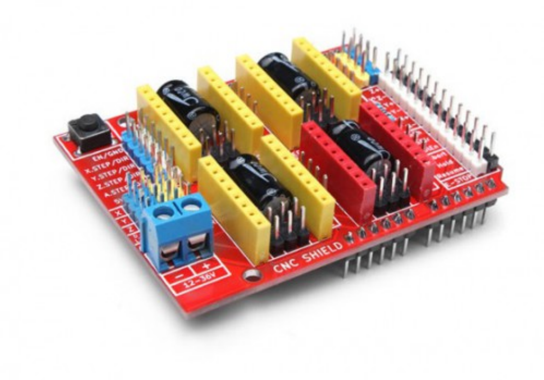

Figure 2.9: VNGARD967058 Arduino CNC Shield [45]

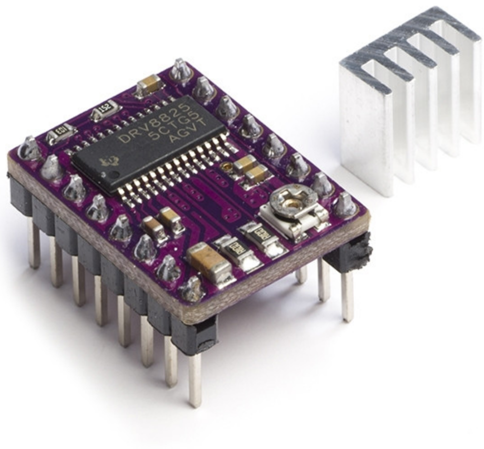

Figure 2.10: DRV8825 Stepper Driver Module [46]

4.1. It is rated for a holding torque of 0.48 Nm. The motor is also a two-phase design and utilises a four-wire interface. The resolution is 200 steps per revolution [48]. It is mounted within the electronics compartment [4].

The device uses three different servo motors. The bottom servo of the servo arm assembly is an Absima S150MH. This servo is rated for 4.8-6 V and supports a weight of 1.5 Nm [49]. It makes sense that this is also the strongest of the servo motors, as it has to carry the most weight. The middle servo is the Reely S-0060 MG [3]. It is rated for 6-7.4 V with a torque of 0.54 Nm [50]. Finally, the servo attached to the end of the camera module is the Reely S-0008, rated for 4.8-6 V and 0.11 Nm [51]. The Arduino Uno drives all of the motors [4].

Figure 2.11: SF2423-10B41 Stepper Motor [47]

Figure 2.12: S150MH Servo Motor [49]

The camera and sensing module contains various sensors. For digital photography, it houses the Arducam Hawkeye B0399 module [4]. This small 25x24 mm camera module features a 64 MP sensor (9152x6944 resolution) and supports autofocus. It has a view angle of 84° and a focus range of 8 cm to infinity. It connects to the Raspberry Pi over the CSI interface [52]. In the prototype, custom loose cables are soldered to the CSI ribbon cable to extend its length [4].

Figure 2.13: S-0060 MG Servo Motor [50]

Figure 2.14: S-0008 Servo Motor [51]

Next to the camera, a laser distance sensor is located. The sensor is mainly used to focus the camera. The prototype features a TOF050F ToF distance sensor. It has an accuracy of 5%. Van der Kroft specifies ToF was preferred during the selection over ultrasonic distance sensors as sound can reflect inside the wound before returning to the sensor [4, 53].

Figure 2.15: Hawkeye B0399 Camera Module [52]

Figure 2.16: TOF050F ToF Distance Sensor [54]

The camera and sensing module also houses an infrared thermal camera. The prototype uses an MLX90640-D55 thermal camera breakout module with a 32x24 resolution and 55° view angle. The thermal camera features a variable refresh rate ranging from 0.5 Hz to 64 Hz and a Noise Equivalent Temperature Difference (NETD) of 0.1 K RMS at a 1 Hz refresh rate [55]. It is connected over I^2C to the Raspberry Pi].

The underside of the camera and sensing module contains five white LEDs and five 405nm UV LEDs, arranged in alternating pairs. The prototype utilises standard 5 mm LEDs for this purpose. The white LEDs are used for illuminating the subject, assuming an external light shield is in place. The UV LEDs serve to make bacteria fluorescent when their light is shone upon the wound [4] [56]. Although the paper mentions the existence of these LEDs, it does not propose a method for driving them.

Finally, a small slot is provided in the bottom servo bracket for a limit switch, which is used to calibrate the position of the stepper motor. The cables from the camera, sensing module, and servo motors are all guided around the device to connect to the Arduino Uno and Raspberry Pi. There are also cables connected to the Raspberry Pi to power it [4], although the power supply used is not mentioned.

Figure 2.17: MLX90640-D55 Thermal Camera Module [57]

Figure 2.18: Limit switch used to calibrate stepper motor position [58]

2.3 International Standards

One aspect that was not addressed in any paper is the requirements that may be mandated (or at least highly recommended) by international standards. Van der Kroft only verified the required accuracy of the thermal camera, which was determined to be +/-0.3°C according to the ISO 80601-2-56:2017 standard [59]. The goal of this section is to investigate whether some parts of the device have particular design requirements associated with them that are mandated by international standards. As the source of most international standards is not free of charge, articles that are based on these standards will be used as a substitute.

For medical electronic devices, the IEC 60601 standard is one of the most relevant. It covers a wide range of topics regarding medical equipment, specifically. IEC 60601-1, which establishes basic safety principles, emphasises the need for protection against electric shock [60]. In the case of the wound monitoring device, this would mean that no electronic contacts that have the potential to short a voltage rail to ground should be exposed. This consequently means that any exposed wires pose a risk; therefore, the device should cover all electronics and wires going to these electronics carefully. The standard also enforces restrictions for moving mechanical parts, mandating the use of safety distances, protective devices, and/or stops [60]. The device's use of servo and stepper motors makes this point relevant. The stepper motors are currently already physically stopped from reaching the user's leg, as the leg rest is in the way. However, the servo motors have no physical or software-based limits in place to prevent them from exceeding their intended range. It is therefore highly recommended that a mechanism to stop the motors be added to the design requirements. IEC 60601-1 also mandates that all components are cooled sufficiently to prevent the device from overheating [60]. The thermal output of the device's components should be analysed, and, where necessary, sufficient cooling should be implemented.

2.4 Additional Design Requirements

After reviewing the device's current electronics and finding new requirements according to the IEC 60601-1 standard, new design requirements can be added to the list of user & design requirements outlined in Section 2.2.2. These are listed in Table 2.3.

Functional requirements	**Technical requirements**
Robust power delivery solution	Power supply able to handle the amount of current used by the device's components
Ability to drive the LEDs	A driver circuit to toggle the LEDs on demand
Sufficient safety measures	(Hardware) emergency stop features
Sufficient safety measures	Hardware stops for the servo motors
Sufficient electrical protection	No exposed wires or electrical contacts with risk of shorting
Proper thermal regulation and protection measures	Sufficient cooling to handle the heat output of every component

Table 2.3: Additional functional and technical requirements of the device determined after analysing the device and international standards.

3 Methods and Techniques

To identify potential improvements for the device, it is essential to employ a well-structured approach in the design process. The chosen approach is explained in this chapter. It is partly based on the Creative Technology design process as explained by Mader & Eggink [61]. This method consists of four phases: Ideation, Specification, Realisation and Evaluation.

However, for this project, it is fundamental to get a foundational understanding of the current state of the design. As the main aspects of the device have already been designed, this project does not involve ideation, user testing, and evaluation of an entirely new concept, as most Creative Technology projects would. Instead, a deep foundational understanding of the current design and design requirements is more essential. Therefore, a fifth stage of the design process is inserted before the others, defined as "Foundation".

3.1 Foundation

The goal of the Foundation stage is to lay the groundwork for the rest of the design process. It starts by establishing the current design requirements of the project and the state of implementation of these design requirements. Next, the mechanical and physical aspects of the current design are highlighted. Finally, criteria are established that should be focused on when ideating improvements for the hardware of the design. It should be noted that this phase is not part of the iterative process described by Mader & Eggink, but rather a step that lays the groundwork and motivation for the other phases. This work is all documented in the Background Research part of this paper.

3.2 Ideation

Mader & Eggink consider the Ideation stage an iterative stage in the design process that focuses on the user requirements, available technologies and creative ideas. In their approach, Mader & Eggink suggest tinkering with various technologies and sketching and building low-fidelity prototypes [61]. As highlighted above, this project defines the user requirements and, to some extent, the technologies used in the Foundation stage rather than the Ideation stage.

The Ideation phase in this project primarily serves to generate ideas for improvements to the current design. Its purpose is to identify better, newer, or more robust technologies compared to the current design, ideating concepts to integrate these technologies into the design and propose alterations to the mechanical design that could facilitate these changes. Ultimately, a concept is developed and further refined in the Specification phase.

3.3 Specification

The Specification phase described by Mader & Eggink is, for the most part, applicable to the context of this project. The main difference is that Mader & Eggink's approach considers the creation and subsequent evaluation of multiple prototypes [61]. Instead of developing ideas into low-fidelity prototypes, this phase will be focused on establishing concrete specifications for the abstract ideas and concepts generated in the Ideation phase. This entails a well-detailed component & circuit selection process, performing calculations where necessary. Where applicable, use scenarios are used to evaluate a theoretical implementation of these designs. These specifications can then be used in the Realisation stage to manifest the designs.

3.4 Realisation

The Realisation phase further develops the designs defined during the Specification phase into actual prototypes. The designs are implemented in order of perceived importance. The definition of "implement" differs depending on the type of improvement. For example, improvements to the electronics may require the creation of circuit schematics and printed circuit boards. In contrast, new features may require modelling mechanical CAD parts. At this stage, the footprints and dimensional restrictions of the physical design are strictly adhered to. If time allows, any necessary components will be purchased to build the first real prototype.

3.5 Evaluation

The created prototype designs are tested with an appropriate testing methodology. A new analysis is made on the status of the functional and non-functional requirements. The designs are compared to those of the current prototype based on relevant quantitative or qualitative metrics. Suppose it is not possible to compare the new prototype with the old one, which would be the case for new features. In that case, the implementation of this feature is evaluated through other means, such as focusing on how these features may impact the aspects specified in the (sub) research question(s). Where applicable, potential improvements for future renditions of the designs are suggested.

4 Ideation

The goal of this chapter is to identify areas for improvement for the prototype and generate ideas for possible solutions to these problems. First, issues with the current design and electronics are addressed, after which suggestions for new features are presented based on the user & design requirements defined in the Foundation stage/background research part of this paper. All proposed ideas are used to generate a few design concepts that incorporate all improvements. Finally, a single design is chosen that will be further developed in the Specification stage.

4.1 Suggestions for Improvements & Alternatives

This section utilises the knowledge gained about the device in Section 2.2 to identify issues or areas for improvement in the prototype. Solutions or alternatives to these issues are ideated so that they can be incorporated into the final concept.

4.1.1 Printed Circuit Board Designs

The components in the device are connected by individual, loose wires. This method of connecting electronics, known as point-to-point wiring, is generally inefficient, time-consuming and takes up a lot of space. Connections that need to be shared between three or more components, such as the ground connection, also require a means to split the connection or connect multiple wires at a single terminal. This is generally undesirable, even in the prototyping stage.

For circuits with relatively simple layouts or schematics, breadboards provide a convenient, centralised way to connect components at a single point. When prototyping the device, these boards could offer a simple solution to improve integration and quickly test and verify components, thanks to the modular nature of the breadboard. Unfortunately, they still leave a lot to be desired. If the designs become too complex, a breadboard-based prototype would become challenging to manage and work with due to the large number of wires. As breadboard connections are designed to be easily removed and adjusted, they are generally quite loose; therefore, the design carries a high risk of breaking during use. This is detrimental to testing a motorised device, even during the prototyping stage. Manufacturing the device would not become much easier than point-to-point wiring, as each connection still has to be made manually.

Printed Circuit Boards (PCBs) are constructed by adhering a conductive material, such as copper, to an insulating material. By shaping the conductive material to have specific geometric shapes, like rectangles, circles and squares, and interconnecting these shapes with thin lines, called "traces", a circuit can be "printed" onto the insulating material, with the large shapes functioning as connection terminals for components [62]. This eliminates the need for individual wires to connect components, significantly simplifying and speeding up the manufacturing process. These layers of conductive and insulating material can be stacked on top of each other to allow even more complex circuits within the same area. This also allows one layer to be dedicated to a single contact, like ground, which significantly simplifies the design process of more complex circuits [62].

PCBs offer numerous features and benefits not found in other connection methods, including the ability to shape the PCB to any footprint accurately. Components can be soldered directly to the board. Although traditional Through-Hole Technology (THT) components, which are also used in breadboard designs, are supported, PCBs also support mounting components directly on the surface pads of the PCB itself through Surface-Mount Technology (SMT) and Surface-Mount Devices (SMDs). SMDs typically have smaller footprints than their THT counterparts and are generally more efficient, both in terms of power consumption and manufacturing efficiency [63]. Copper pours, which are large sections of the PCB filled with conductive material, can provide a low-resistance or low-inductance path for connecting electronics. They can also be used to dissipate heat through the PCB itself [62]. Vias, which are small holes that run through the entire PCB, are used to carry signals from one layer to another. The act of drilling holes through the PCB can also be used to insert mounting holes into the PCB to screw it down. Finally, a layer of silkscreen can be printed on top of the PCB, which can be used to visually indicate the placement of components on the PCB or other miscellaneous details, such as the pinout of a chip.

As PCBs are inexpensive and ubiquitous, and numerous CAD modelling software options are available, making PCB design simple, even with all the aforementioned features, it makes sense to convert the wiring of the prototype to a PCB-based design. This can significantly improve the integration of components, simplify manufacturing and even allow for much safer electrical connections thanks to PCB headers. Although creating a digital design and waiting for the physical prototype to be manufactured may take more time than simply debugging breadboard connections, the reliability, flexibility, and efficiency of PCBs make them a much-preferred option over breadboard-based designs for complex prototypes. It should be noted that, as PCBs are flat, 2D surfaces, it may still be necessary to use wire connections between components and other PCBs to allow, for example, elements in the camera and sensing module to be connected to components in the electronics enclosure. However, as mentioned, the usage of breadboard headers can drastically simplify this process and provide rigid connections from the wires to the board.

4.1.2 Raspberry Pi Model

The current device version uses a Raspberry Pi 4B for computing power. This is a logical choice given the design requirements, as the Raspberry Pi 4B has plenty of computing power, has onboard Wi-Fi and Bluetooth and has a well-established open-source ecosystem [41]. Although it may be helpful to search for an alternative SBC or opt for a different processor, the ease of integrating sensors with the Raspberry Pi makes it a suitable choice for this project.

At the time of writing, the newest, most powerful edition of the Raspberry Pi is the Raspberry Pi 5. Although this is mostly a performance uplift compared to the Raspberry Pi 4B, the amount of image processing required for the device means it would likely benefit significantly from the 2-3x performance improvement [64] compared to the old model. As the upgrade to a Raspberry Pi 5 seems almost inevitable, the rest of the improvements for the design will assume the model of Pi used to be a Pi 5 instead of the current Pi 4B.

The Raspberry Pi also offers the Compute Module 5, a version of the Pi 5 designed for use in embedded systems. It contains the same internal hardware as a standard Raspberry Pi 5 but uses two 100-pin high-density connector sockets on the PCB to slot into an embedded design [65]. This can potentially save space in the final design and is arguably more robust than using the full development board, which also contains unused I/O ports. The Compute Module 5 also offers options for embedded eMMC storage, which is generally faster than SD storage and can provide a performance boost when performing image analysis.

4.1.3 Obsolete Hardware

Currently, all motors are controlled by the Arduino Uno. While this solution works, it adds a second development board to the device, which induces several engineering challenges. For example, the Uno needs to be flashed separately from the Pi 5. It also means there needs to be multiple codebases for the device's operation, which complicates development. Furthermore, this implementation requires continuous communication between the Pi and the Uno, which may introduce unwanted delays and unresponsiveness. Finally, the addition of a second

Figure 4.1: VL53L4CD ToF distance sensor module by Adafruit [70].

development board may cause problems when dealing with space constraints. Aside from engineering challenges, it also imposes extra costs for the manufacturer.

The inclusion of an Arduino Uno is unnecessary, as the Raspberry Pi is theoretically capable of driving the servo and stepper motors using its General Purpose Input and Output (GPIO) pins. The Pi 5 has 40 GPIO pins, with varying functions for some specific pins [65]. One potential issue with using a Pi 5 to drive the servo motors is that the Pi 5 only has two pins that support hardware Pulse Width Modulation (PWM). PWM signals are necessary to drive the servo motors. This issue can likely be mitigated easily by using either software PWM solutions, such as pigpio [66], or external PWM controllers like the I2C-based PCA9685 [67]. This ultimately means that the VNGARD967058 CNC shield, which is currently only used to mount the stepper motor driver, would also become obsolete.

While all of the other components are still in production, the TOF050F distance sensor is a module that uses the discontinued VL6180X sensor by STMicroelectronics [68]. As it is not desirable to use components that are no longer in production, a replacement should be used. The VL53L4CD, produced by the same manufacturer, supersedes the VL6180X. It has a great range (1 to 1200 mm) and similar accuracy (+-7 mm) to the TOF050F [54, 69]. There are various modules made for the VL53L4CD that are similar in size to the TOF050F. One such module with the same name is developed by Adafruit [70].

4.1.4 Embedding Separate Modules Onto PCBs

Many of the sensors used in the camera and sensing module are composed of individual modules. This is because these modules are development modules. Although the sensors do fit together in the constrained space of the camera and sensing module, wiring all these modules separately in a robust way is challenging. Ideally, all sensors and their corresponding components would fit onto a single PCB, providing maximum flexibility for the physical design and allowing for easier wiring and manufacturing.

For the distance sensor, the TOF050F module can be replaced with a standalone VL53L4CD ToF sensor. There are only a few pull-up resistors and capacitors required to make this sensor function [69]. The MLX90640 thermal array used in the prototype is still in production and available as a standalone IR array in various form factors. The current prototype uses a module by PIM365 containing the MLX90640ESF-BAB-000-TU sensor, which is a variant of the sensor with an FOV of 110°. Its datasheet suggests that this sensor also works with only a few pull-up resistors and capacitors on the supply voltage [55].

Given the simplicity of these sensors' applications, it should not be challenging to embed both of these sensors directly onto the PCB. Both sensors communicate through I^2C, which uses addressing to address each device individually using a shared data bus. This means that only two GPIO pins are required from the Raspberry Pi to address both sensors. If a daughterboard-based approach is used, this means fewer wires need to be contained in the cable that connects to the motherboard. It is also noteworthy that the passive components required for both sensors are also only needed for I^2C to function correctly [55, 69], so it is likely that these components can be shared as well.

Aside from these sensors, the white and UV LEDs can also be embedded directly into the daughterboard for ease of manufacturing. Changing their footprint from through-hole to surface mount also reduces their size.

Unfortunately, this approach is not feasible for the camera module. The high throughput required to read the 64 MP camera sensor necessitates the use of the Raspberry Pi's CSI connector. While it is theoretically possible to find a loose camera sensor and add all the necessary components and processing required for it to function over CSI, the Arducam Hawkeye is already a highly optimised and well-researched solution that is a sufficient option given the project's time frame.

However, the wiring for the camera module can still be drastically improved by embedding a CSI connector on a carrier board. This way, the camera module can be connected directly with a short, likely folded CSI cable, to the carrier board. This carrier board can be the daughterboard suggested in the previous section. This is a significant enhancement over the current solution, which uses two short CSI cables with wires soldered to them to connect them over a distance. Aside from significantly improving robustness, this would also improve safety and make manufacturing the device less labour-intensive. Figure 4.2 depicts a concept of embedding the sensors on a daughterboard.

If a PCB is designed to contain the electronics in the electronics enclosure, there is also an opportunity to embed the stepper motor driver onto a PCB. The DRV8825 stepper motor driver is available as a standalone IC, specifically the DRV8825PWPR, which only requires a few extra resistors and capacitors to function [44].

4.1.5 Cable Routing Enhancements

The previous section briefly discussed the rough state of the CSI connector wiring in the current prototype. However, many other aspects of the device's cables can be improved. As shown in Figure 1.3, the device has various servo and sensor wires exposed. For obvious reasons, these wires should be shielded from the outside of the device to improve safety and durability.

Currently, the wires are fed through the wire hole in the back of the electronics compartment, surrounding the device, to the servo holder bracket, where they are then routed to the rest of the components. One potential way to prevent routing around the device and shield the wires is to route them underneath either the rotary or the stationary base and then route them back up through a hole in the servo bracket, thereby eliminating the need for the wires to be exposed on the outside. This approach is illustrated in Figure 4.3.

One issue with this approach is that the rotary base, as its name suggests, rotates. This means that the necessary length of wire needed to reach the servo bracket is variable. However, there is an even bigger problem that prevents this simple solution from even being physically possible at all. The cable "cuts" through the entirety of the top of the base. This means that it is not possible to support it anywhere, and thus, the top of the base would be floating. The ring that is cut through with this approach is highlighted in Figure 4.4.

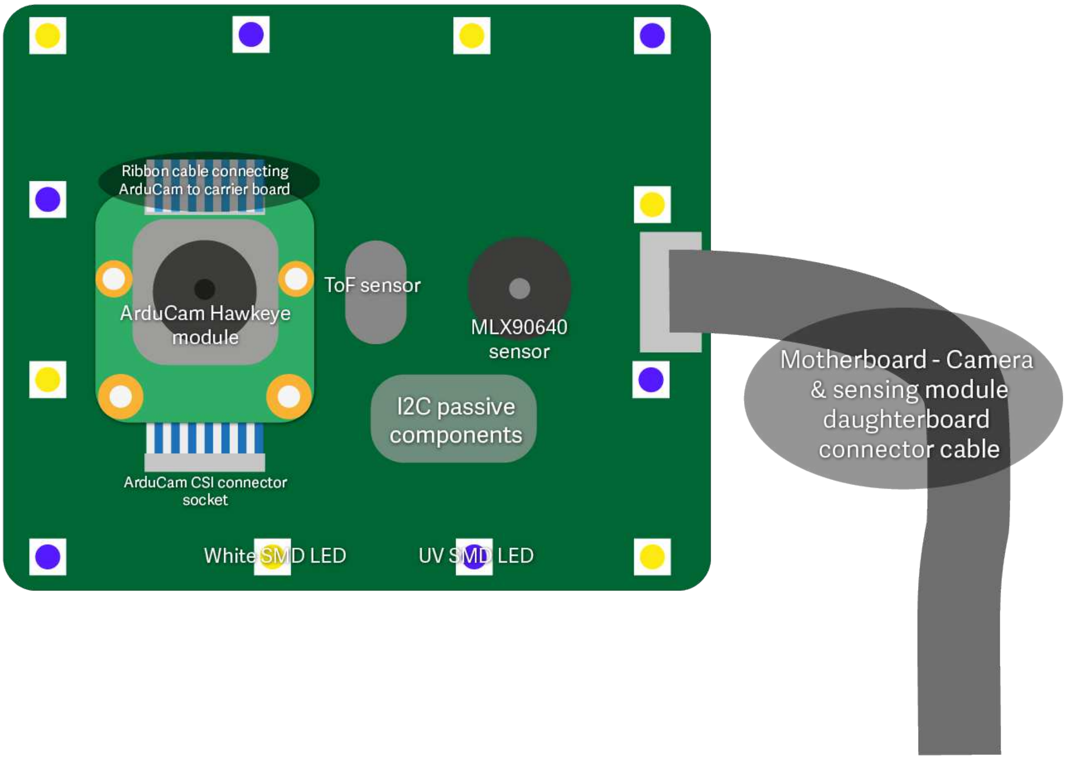

Figure 4.2: A concept of a daughterboard, with embedded sensors and LEDs

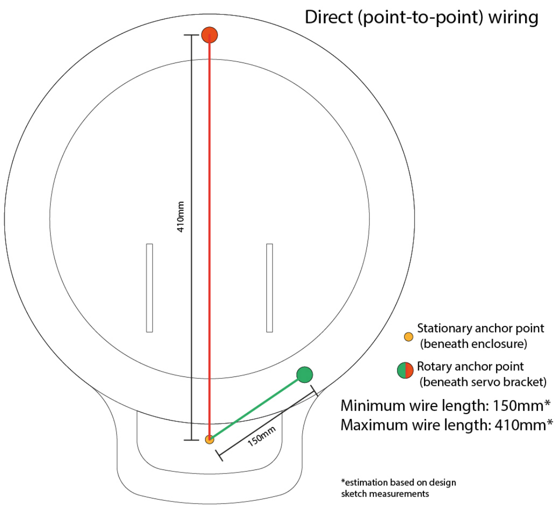

Figure 4.3: Sketch of a point-to-point wiring solution

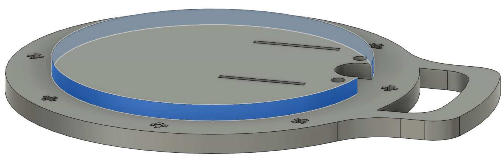

Figure 4.4: Ring "cut" through by a point-to-point wiring solution

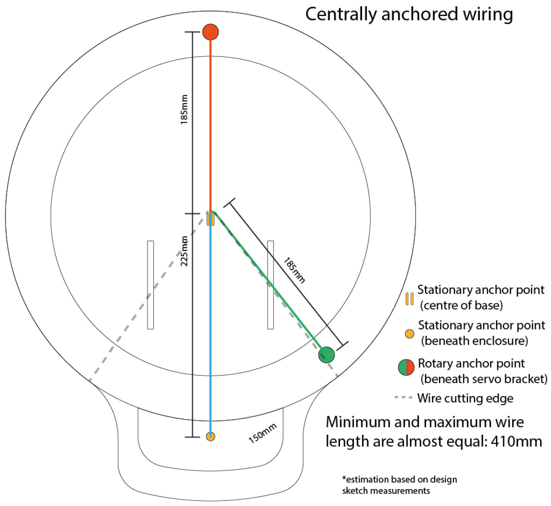

Figure 4.5: Sketch of a centrally anchored wiring solution

Solving this problem is trivial before any other suggestions to improve the cables can be provided. Fortunately, the problem is simplified as there are limits to the angles of rotation that can be achieved with the stepper motor. The servo arm does not rotate a full 360°, as this would cut through the leg. There are clear "start" and "stop" points on the right and left sides of the device, respectively. If the wire is not anchored directly at the electronics enclosure, but instead at the centre of the base, a "pizza slice" shape is left, allowing the top of the base to be supported. Using a central anchor for the wire has the added benefit of fixing the wire length to a set length, regardless of the servo bracket's position. This is illustrated in Figure 4.5.

Of course, the device's design would need to be changed to accommodate a slit for the cable around the stationary base. Figures 4.6 and 4.7 show how this concept might be executed in the design. A loft has been added between the "pizza slice" support and the bottom of the base to improve the structural integrity. After all, the device should still be able to sustain the weight of a person stepping on it. Even with the loft, it is still possible that, depending on the material used, the stationary base is not supported well enough to sustain this weight. A potential workaround for this could be to support the stationary base with the rotary base when pressure is applied, by having it overhang the rotary base slightly.

Another solution would be to embed the wires in the rotary wheel itself by feeding them through a gutter, as shown in Figure 4.8. This leaves the stationary base free from having to consider wiring, which means no sacrifices have to be made to structural integrity, and the

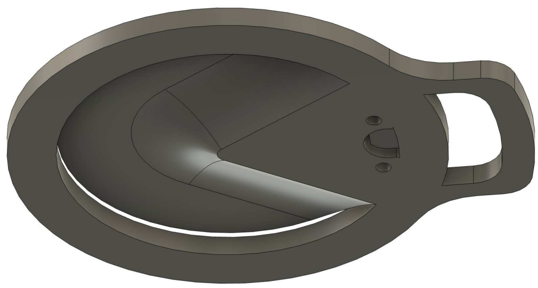

Figure 4.6: Altered stationary base, supported by a lofted "pizza slice" support at the bottom

Figure 4.7: Slits added in the stationary base to allow cables to pass through

space in the centre can be used for other purposes, such as a relocated electronics compartment. The gutter inside the rotary wheel would need to be made out of a material with low friction to ensure the wiring has good durability. As the wire now wraps around the rotary wheel, its length is dependent on the position of the servo bracket, meaning that excess wire needs to be stored away when the servo bracket is in its starting position. To solve this, a spring-loaded spool, similar to those used in many vacuum cleaners, could wind the wire up when it is not in use. This dramatically increases the complexity of the design but is arguably the most elegant solution.

After the cables are routed to the servo bracket, they are still exposed on the outside of the servo arm. Although many industrial-grade robotic arms route their clamped cables on the outside, most medical robots have their cables fully enclosed. Another solution would be to have the wires briefly exit at each servo joint, which would partially expose them but may also provide more slack for the cables to bend without too much strain. All three approaches are illustrated in figures 4.9, 4.10 and 4.11. As the device is intended for medical use, the aim should be to have the wires routed completely internally in the robotic arm. This means some shielding needs to be added around the hinges, or their design needs to be completely redesigned to accommodate this. Although this effectively shields the wires from the user, it may drastically decrease the lifespan of the wires due to excessive strain when the arm is rotated.

4.1.6 Cable Connectors

The Dupont header-based wire connections of the prototype are fragile and easily removable. It is not unreasonable to assume that these connections may come loose due to the device's rapid motor movements. Therefore, different connectors should be used on the PCBs to connect the cables. Connectors like Molex's Micro-Fit 3.0 series come in various sizes and could provide an easily maintainable, reliable connection for the wires [71]. Different types of connectors should be used based on the current cable requirements. The exact selection of connectors will be determined in the Specification phase.

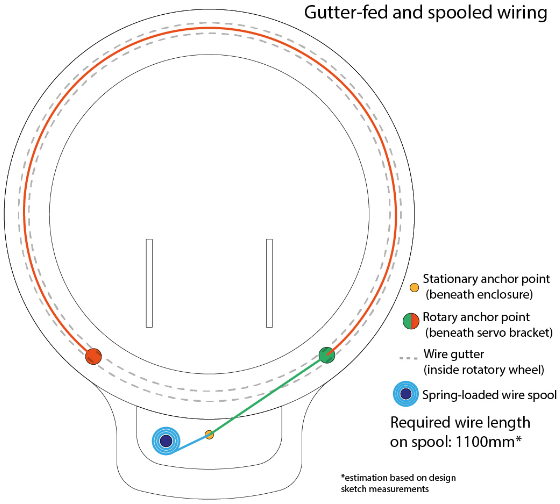

Figure 4.8: Sketch of a gutter-fed wiring solution

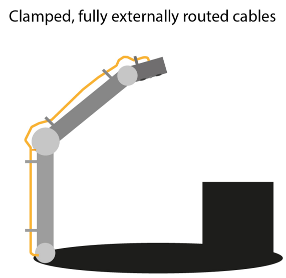

Figure 4.9: External cable routing example

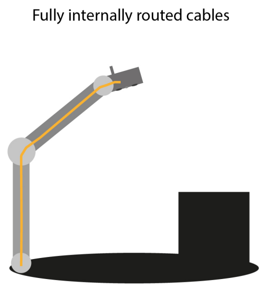

Figure 4.10: Internal cable routing example

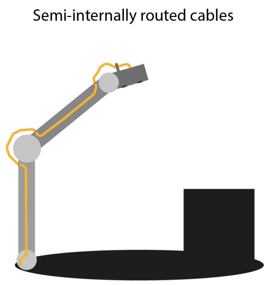

Figure 4.11: Partial internal cable routing example

4.1.7 Other Wiring Improvements

The current prototype has each motor and sensing module wired up separately. The number of necessary wires can be drastically reduced if some wires are combined. A logical starting point is to combine the voltage and ground wires where applicable. For the camera and sensing module, all components use a typical voltage of 3.3 V [55, 65, 69]. In theory, it is possible to power all these components from a single wire, as long as the gauge of the wires and the trace thickness on the PCB are sufficiently thick. The same applies to the ground connections; the CSI connector on the Raspberry Pi specifies four different ground points [41] that can be combined, as long as the current limits of the wires are not exceeded.

A similar approach could be taken for the servo motors, as they all use a nominal voltage of 6 V [REELY SERVO-DATABASE, ABSIMA S150MH MANUAL]. This means that a single 5-wire cable, containing 6 V, ground and one PWM signal for each servo would suffice. However, the benefit of this is questionable, as each servo already requires three separate wires, meaning that the power and ground wires would need to be split at each servo. This approach also requires significant considerations regarding wire gauge, as servos generally have high current usage. Therefore, having a separate, three-wire cable dedicated to each servo seems the most logical approach.

Aside from the voltage and ground wires, it is also possible to combine some of the data signal wires. All three sensors are operated through I^2C [55, 65, 69]. I^2C uses addressing to control multiple devices over just two signal wires: SDA and SCK [72]. These signals can be shared

Cable	No. of wires	Routing
Daughterboard connection cable	12	Through gutter and full servo arm
Top servo cable	3	Through gutter and full servo arm
Middle servo cable	3	Through gutter and half of servo arm
Bottom servo cable	3	Through gutter
Stepper motor cable	6	Through electronics enclosure

Table 4.1: Preliminary overview of wire division and their routing

between devices. This means that, including 3.3 V and ground, a total of just four wires are needed to control both the distance sensor and thermal camera. The Arducam Hawkeye requires eight additional wires for the MIPI protocol [73]. A cable with just twelve wires would, therefore, be enough to power and control the entire camera and sensing module. This assumes that power consumption is not a big concern as long as the wire gauge is thick enough. However, as a preventive measure, it may be wise to include additional 3.3 V and ground wires to handle the current load. This is further worked out in the specification step. For now, it is assumed that twelve wires will suffice.

In total, five cables need to be routed through the device. The number of wires per cable and their routing layout are laid out in Table 4.1. The servo arms require careful consideration for their wiring, as they must accommodate three cables with numerous wires in a constantly moving part.

First of all, the robotic arm requires sufficient space to accommodate all the cables. The upper arm is likely too thin right now, as its diameter of 10 mm needs to accommodate fifteen wires; therefore, the diameter of this arm likely needs to be increased. The bottom arm is significantly thicker and may already have a large enough diameter to accommodate all the wires.

With the previously mentioned fully enclosed approach for the cables, there needs to be sufficient room at the hinges to accommodate the slack in the wires. The cables could be guided at the hinges and shielded with an outer frame to make sure there is enough space without exposing them.

Some cables, such as the one for the daughterboard, may require additional shielding to prevent noise and interference from affecting sensor data. Especially high-bandwidth camera sensors, like the Arducam, may be susceptible to such interference.

4.1.8 Changing Motors

Van der Kroft notes that the device's servo motors are not able to support the weight of the full arm assembly due to insufficient torque [4]. As the arm assembly is already relatively light, using carbon fibre rods for the arms themselves will reduce the weight of the assembly, making it difficult, if not impossible. Therefore, the apparent solution to the low torque is to exchange the servo motors with higher power equivalents. However, the choice of motors should be carefully considered, as higher-torque motors are larger, heavier, and often require a higher voltage to function. This also means that when calculating the required torque for the motors, the weight of all but the topmost motors should be taken into account as well. The Specification phase will go more in-depth into motor selection and torque calculations.

4.1.9 External Power Button

The current prototype lacks a power button as the Raspberry Pi is powered directly from a USB connection. From both a usability and safety standpoint, adding a hardware power button makes a lot of sense. It ensures the device does not consume any power if it is not in use, and the ability to shut down the system if the electronics or motors are malfunctioning minimises potential damage to equipment or the user.

The power button should be located on a stationary part, preferably on the outside of the device, for optimal usability. One of the most logical locations is the outside of the electronics enclosure. The electronics are already located here, so implementing an electrical connection to the power button would be straightforward. It also resides on the same side as the user of the device, so it is easy to reach.

4.2 New Features

4.2.1 Battery

One of the design requirements indicated by van Koolwijk is on-device power storage for a full day of use, with a max of twelve patients per day [3]. This ensures the device can be used without needing to be near a power outlet, reducing setup time. Van der Kroft indicates the current prototype does not contain any kind of battery or other power storage solution, so it could be interesting to investigate the implementation of this in the device.

Lithium-ion (Li-ion) batteries are currently the most common type of batteries for consumer electronics [74, 75], also in the biomedical industry [76]. Although various other technologies are emerging, the energy density and wide-scale adoption of Li-ion-based batteries remain unmatched [74]. Therefore, it makes sense to investigate the feasibility of adding a Li-ion-based battery to the device.

The inclusion of motors in the device, which generally have demanding power requirements, means that a significant amount of energy storage will be required to perform twelve scanning procedures per day. Although Li-ion cells have excellent energy density, the added volume and weight introduced by the addition of a battery still have to be taken into account. Ideally, the device's size should not increase with the addition of a battery, and the added weight should not compromise the device's portability. As Li-ion batteries have a limited lifespan and degrade over time, the battery pack is ideally socketed to be easily replaceable if needed.

The inclusion of a battery also demands the need for a Battery Management System (BMS) to handle the charging, discharging and protection of the battery. This should be located at least somewhat close to the battery for ease of development and minimal power loss. To convert all the battery voltage to the other necessary voltages, a Voltage Regulation Module (VRM) will need to be added to the PCB, which should also be highly efficient to minimise power losses. For this reason, switching voltage converters should be used over linear voltage regulators. These converters must account for the amount of current drawn by each component, which is further investigated during the Specification phase.

For charging the device, a charging port needs to be added near the BMS. Although various sockets and types of ports are available, the recently adopted directive 2022/2380 of the European Parliament highly recommends the use of USB Type-C. It even enforces this for certain types of consumer electronics, such as phones and laptops [77]. Therefore, it makes sense to use this port as well. The USB Power Delivery (PD) standard specifies a range of charging voltages between 3 and 20 volts [78], which should be sufficient to charge the device effectively. According to the standard, the maximum charging wattage available is 240 W [78], which should be higher than the device's power consumption. This will be verified in the Specification phase.

4.2.2 Emergency & Safety Features

The current prototype lacks built-in safety features; however, since it has moving parts that can potentially damage the device or harm the user, it is essential to consider the risk of possible motor malfunctions. Software-based safety features will not be considered here, as they are the developer's responsibility to implement.

Although a proper risk analysis is outside the scope of this project, some simple safety features, such as an easily accessible emergency stop button, can be implemented to mitigate most risks posed by the motors. Unfortunately, implementing this is not as trivial as simply cutting power to the entire system. For servo motors, cutting power also makes the motors lose their torque. This means that if this happened during the device's operation, the arm would come crashing down due to gravity, potentially injuring the user or the operator. For this reason, the device's power button should not immediately cut off power, and strict measures must be taken to prevent this from happening in the event of a power loss.

One solution that covers most problems is the usage of power-off brakes. These brakes halt the motor shafts upon a loss of power using a spring or electromagnetism, and disengage once power is restored. If these brakes are used in the design, a loss of power would immediately lock the motors in place. The emergency stop button can then cut power to the motors, stopping them in place. Unfortunately, these types of brakes are typically only used with higher-power motors than the ones used in this device. Therefore, it is not a viable option in this case.

Another solution, arguably less optimal but easier to implement for the current prototype, is to stop the motors in place once the emergency button is pressed. This would effectively be the same as engaging emergency brakes, without requiring additional hardware. This requires drastic measures to be put in place when the battery is at a low percentage, though, as the user needs enough time to fold the arm back before the motors fail and the arm falls. Therefore, the device should stop functioning at around 1-2% power remaining and automatically fold back using the motors. With the current class of motors, this appears to be the only feasible solution.

The PCB should have reverse current protection for the stepper motor driver to ensure the circuit does not break if, under any circumstances, the motors are manually moved. This may not be necessary for the servo motors, depending on the type of motors used, as some "smart" servos may have built-in protection against reverse currents.

One interesting aspect of the servo motor layout is that it is technically possible for the robotic arm to protrude into the leg rest. For obvious reasons, this should never happen under any circumstances, as it could cause severe damage to both the device and the user. While it is possible to add hardware or design limitations to prevent the robot from reaching this area, it is likely easier to enforce strict software limitations to ensure the motors cannot turn in this direction. For some wounds, it may be necessary to remove the leg rest and have the arm go further than would usually be possible with the leg rest [4], so this should be an option that can be enabled in software.

Safety measures should also be taken with the battery and the BMS. To comply with the IEC 60601-1 standard, the BMS should have over-(dis)charge protection, over-current protection, short-circuit protection, thermal protection and feature cell balancing. The battery itself should be well-shielded and protected from puncture or compression by either the robot arm or the patient's foot stepping on it.

4.2.3 Interface

The device does not yet have a physical user interface, but ideas for implementing one are under development by Arnoud Hartemink. One such idea is to add a small LCD screen with a button interface in a stationary part of the device. As the location of this interface is likely going to be close to the rest of the electronics, the existing processing hardware of the Raspberry Pi could be reused to process the screen data and handle button input. The addition of an interface should not have any further ramifications for the PCB design itself.

4.2.4 Thermal Regulation

Some of the high-power components, such as the Raspberry Pi, stepper motor driver, and battery charging circuit, may produce enough heat that design considerations will have to be made to ensure these components are adequately cooled. Depending on the heat output of the components, simple passive cooling solutions, such as ventilation holes, heat sinks, and large copper pours in the PCB design itself, may already suffice. However, if this fails to sufficiently cool the device, a small fan can be added to provide additional active cooling. If some parts of the exterior are made of metal, such as aluminium, the exterior could also be used to dissipate heat. The heat output will be quantised in the Specification phase, but for now, it is assumed that passive cooling with ventilation and small heat sinks will be enough.

4.3 Final Design Concept

Now that issues have been identified and solutions and new features have been ideated for different individual parts of the device, a concept for a definitive, integrated design that implements these improvements should be created. This section outlines potential candidates for designs that can be developed and selects a single design for further development in the Specification stage. As explained in Section 4.1.1, there is a clear preference for PCB-based designs over breadboard or point-to-point-based designs, so all proposed solutions will assume the use of PCB designs.

4.3.1 Design Idea 1: Raspberry Pi Hat and Daughterboard Solution

The electronics, even after accounting for the potential new features, are mostly centred around two different points:

- The camera and sensing module, housing the cameras, sensors and LEDs
- The electronics enclosure, housing the Raspberry Pi, Arduino development board, stepper driver shield, stepper motor and limit switch. All of the new proposed features would also be located around this area.

Therefore, one potential solution could be to split the design into two separate PCBs, each having the relevant parts and components connected to it. These boards would somehow need to be connected using one or more cables following the layout described in Section 4.1.5. The daughterboard design described in Section 4.1.4 can be used to connect all the components in the camera and sensing module. However, a solution still needs to be presented for the design of the PCB used to connect the components in the electronics enclosure.

For this board, it makes sense to design it around the Raspberry Pi, as it is the most significant and most complex component that resides in the electronics enclosure. Although the Raspberry Pi 4B or Raspberry Pi 5 cannot be embedded directly onto a PCB, a so-called "Raspberry Pi Hardware Attached on Top (HAT)" can be designed that plugs into the GPIO header on the Raspberry Pi, similar to an Arduino Shield. This PCB is a rectangular board with a 65 by 56 mm dimension that also features four mounting holes to screw the board to the Raspberry Pi [79]. The board has the freedom to utilise all 40 GPIO pins as desired. It can even enable the Pi to autonomously download drivers if a specially configured I^2C EEPROM is added to the HAT. Another advantage of this is that the board can draw power from the Raspberry Pi's power supply without requiring its power delivery method.

While this board may have sufficient space to fit all the required electronics, its limited size means that there is no guarantee every component will fit onto it. The options for expandability or implementing features later on also become significantly limited due to its constrained size. As the integrated heat spreader (IHS) of the Raspberry Pi's processor is covered, cooling it sufficiently may prove to be a challenging ordeal. There is also no easy access to the Pi's high-

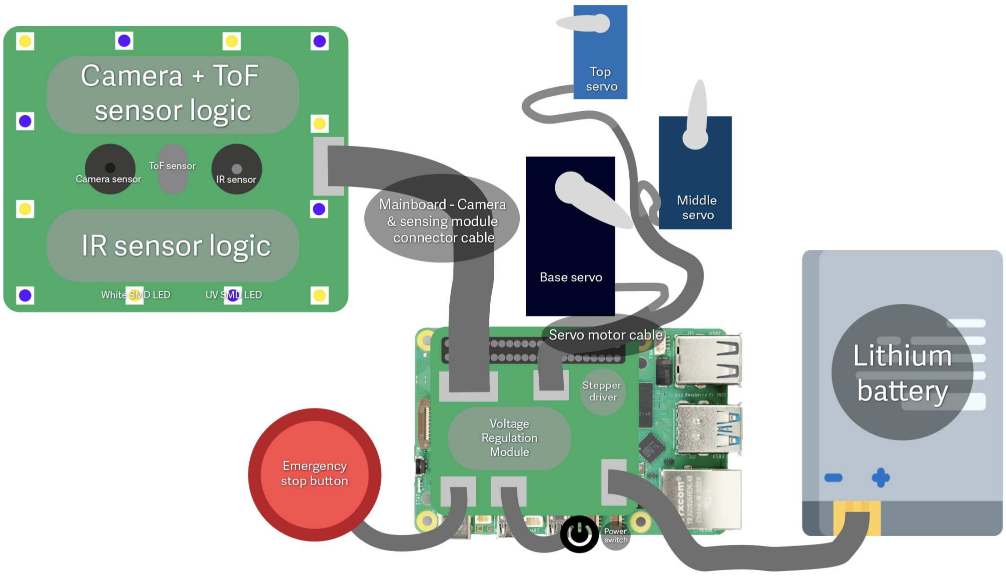

Figure 4.12: Sketch of the Raspberry Pi HAT-based mainboard-daughterboard solution

speed buses, such as USB, but more importantly, the MIPI CSI interface cannot be accessed either. This may have implications for connecting to the camera module.

Although the servo motors are not located near any of the PCBs, it makes more sense to connect them to the mainboard than to the daughterboard, as the logic needed to control them is driven by the Raspberry Pi, which resides on the mainboard. They are, therefore, connected to a PCB header on the mainboard in this design. An illustration of this design is shown in Figure 4.12.

4.3.2 Design Idea 2: Mainboard and Daughterboard Solution

In Section 4.1.2, it was noted that there is also an alternative form factor for the Raspberry Pi, namely the Compute Module (5). As this version of the Raspberry Pi is embedded onto a PCB, the form factor restrictions present in the first design idea do not apply. As the Compute Module 5 exposes all buses on its 200-pin connector [65], there are no concerns regarding accessing the MIPI CSI bus either. Therefore, it could be interesting to develop a PCB that embeds this module instead of using a Raspberry Pi HAT. The daughterboard would not be affected, and the servo motors could still be connected to this PCB.

Unfortunately, using this board over the standard Raspberry Pi also comes with some downsides. Most notably, the absence of a power delivery method to power the Pi and the rest of the electronics. This means that any design would need to implement its power delivery solution on the mainboard, such as USB Type-C power delivery. The CM5 also lacks any form of I/O connectors, such as HDMI or USB-A ports. These ports could be helpful when testing the device. However, they are not necessary to flash software onto the Pi itself, as the Compute Module 5 IO Board, essentially a development kit for the CM5, restores these ports [80]. A sketch of the design is shown in Figure 4.13.

4.3.3 Design Idea 3: Separate Sensing Modules Solution

It is also worth investigating the possibility of using just a single PCB design to handle all the connections. This would centralise all the connections into a single "hub" and create a star topology network [81]. For this, the loose sensor modules would be kept and all individually

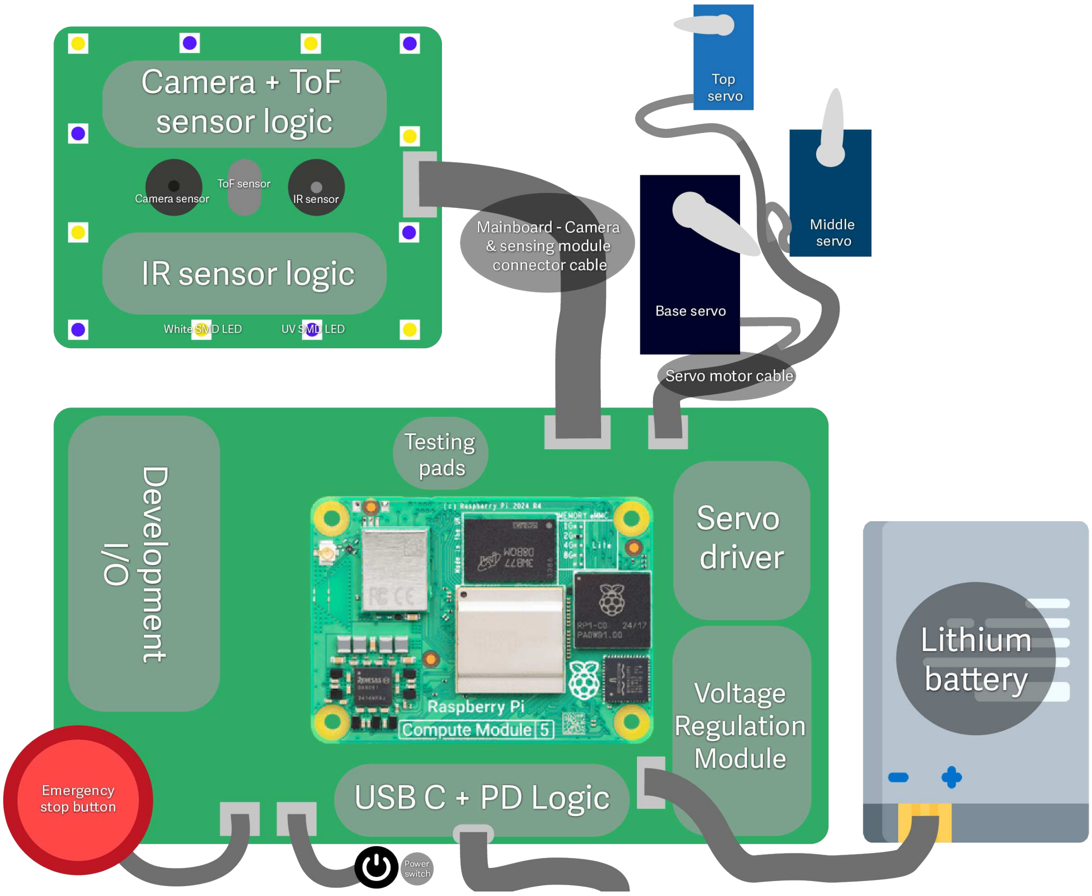

Figure 4.13: Sketch of the Raspberry Pi Compute Module 5-based mainboard-daughterboard solution

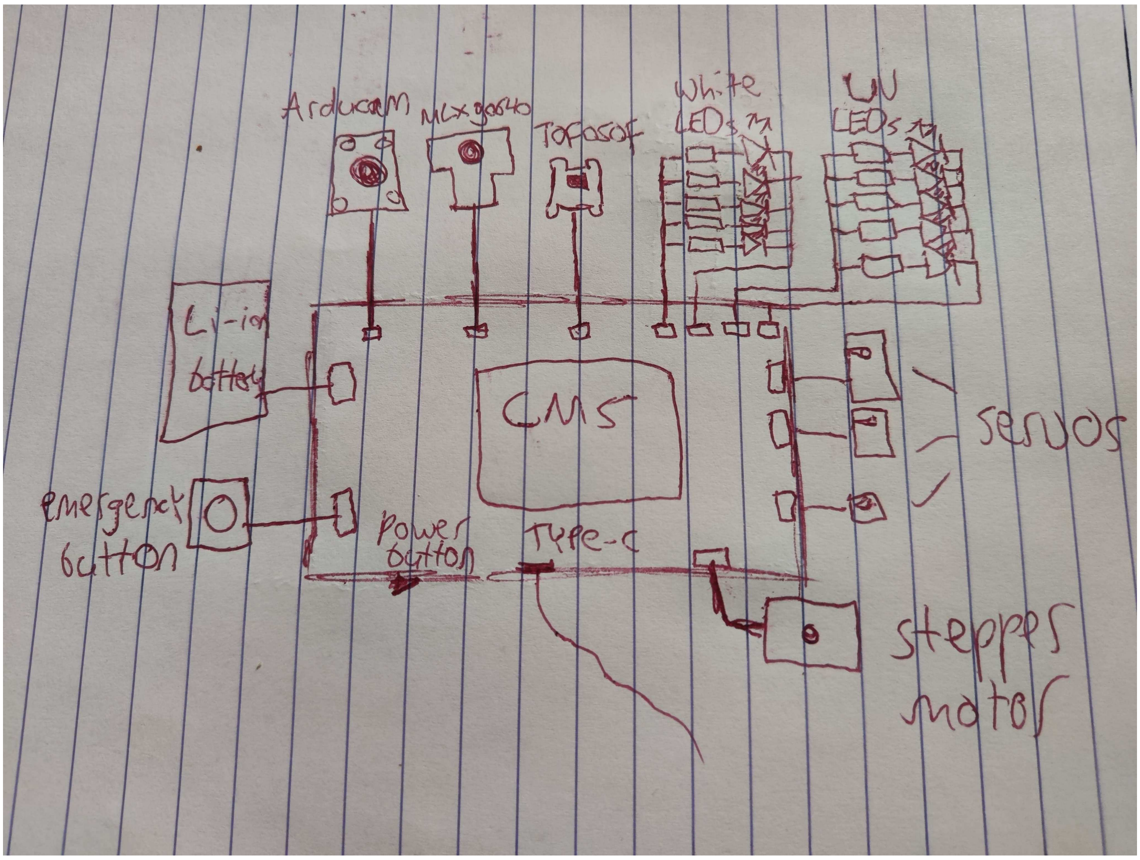

Figure 4.14: Sketch of a star topology solution using sensor modules

wired to the mainboard. This would result in a straightforward layout for the device, making it simple to debug. It would also save effort in the Realisation part of this project as only a single PCB would need to be designed.

This approach, however, has significant downsides compared to a daughterboard-based solution. The camera and sensing module is already quite cramped with the current modules, and it does not even house the LEDs yet. These LEDs would also still need to be wired individually, as the lack of a PCB means it is impossible to use SMDs for them. As the modules need to be individually wired, it is not possible to combine signal and voltage lines, which increases the number of wires required to run these modules. This could be an issue, given that the device is already quite space-constrained. Sensor modules are also generally not favourable for manufacturing, as individual sensors usually have better availability and supply chains. A rough sketch of this approach is represented in Figure 4.14.

4.3.4 Selection of Definitive Design

After evaluating all three designs, it is clear that the final design should be a mainboard-daughterboard-based approach, as this saves a significant amount of space and wires within the device. It is debatable whether the Raspberry Pi HAT or CM5-based mainboard approach should be used; however, as the CM5-based approach provides more flexibility in the design overall, without compromising many features, it makes sense to adopt a strategy that utilises this design to allow for maximum customisability in the future. Although exact power consumption numbers have not been determined yet, it is also possible that the standard Raspberry Pi's power supply cannot deliver sufficient power to the rest of the device's components, causing them to function incorrectly. As this would mandate a separate power delivery method anyway, there is not much reason left to prefer the HAT-based design over the CM5-

based design. The definitive design is therefore determined to be the second design, depicted in Section 4.3.2 and Figure 4.13.

5 Specification

5.1 Component Selection

To delve in-depth into the specification process, it is essential to have an overview of all existing and new components. This section outlines what elements will be added or replaced in the device and justifies the choices for these components.

5.1.1 Single Board Computer & Development Hardware

The Single Board Computer (SBC) is the brain of the device and thus should be considered first. As mentioned in Section 4.1.2, the Raspberry Pi 4B currently housed in the design is a good choice due to its ubiquity and well-documented nature. For this project, however, it makes more sense to use the embedded version of the Raspberry Pi, the Raspberry Pi Compute Module. The most recent and widely available version is the Compute Module 5 (CM5), which primarily features performance improvements over the previous model.

There are similarly sized single-board computers available in the same price range as the Raspberry Pi, including many CM5-compatible Pi-based alternatives, such as the Banana Pi or Radxa Pi. However, the widespread adoption of the Raspberry Pi ecosystem makes it a suitable choice for this project. It ensures good compatibility across all sensors and actuators, as well as long-term software support.

The design for the PCB can primarily be based on the CM5 IO Board. This is a development board for the CM5, which is fully open-source. Basing the PCB design on this board not only speeds up the PCB development but also provides the basis for pin assignment for components like the CSI camera connector. The IO Board itself can act as development hardware for the robot. As the GPIO pins are all exposed on the IO Board, the functionality of the components can be tested and verified by connecting them to the same GPIO pins as the PCB routes to. This allows the developer to develop and test the software and hardware on the IO Board, and then remove the CM5 to transport it to the robot. This eliminates the need for actual development hardware on the device itself. If the developer wishes to upload new code to the CM5 while it is in the robot, this can still be done over Wi-Fi, as the CM5 has this built in.

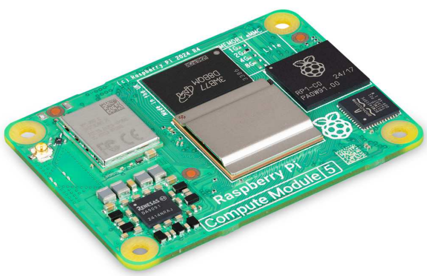

Figure 5.1: Raspberry Pi 5 Compute Module [65]

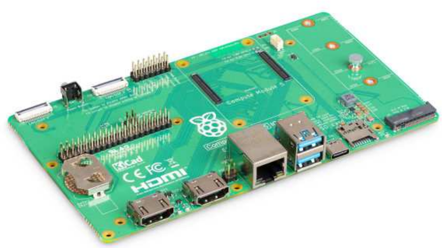

Figure 5.2: Raspberry Pi 5 IO Board [80]

5.1.2 Sensors

The MLX90640 thermal camera module meets the user requirements with sufficient specifications. However, the loose module currently used in the device occupies unnecessary space

Figure 5.3: 15 to 22 pin FFC cable used to connect the Arducam module to the CM5 [82]

that can be saved by embedding the sensor directly on the PCB. The sensor comes in various footprints; however, for this project, the MLX90640ESF-BAB-000-TU will be specifically used.

The distance sensor offers a straightforward method for determining the camera's focus distance. However, the sensor used on the TOF050F module, the VL6180X, is discontinued; therefore, it is better to use the sensor that supersedes it, the VL53L4CD. It has similar specifications and also uses I^2C to communicate, so it should be a drop-in replacement. Similar to the thermal camera, the loose sensor can be directly embedded onto the PCB. The specific component used for the design is the VL53L4CDV0DH.

The Arducam B0399 camera module ensures compatibility with the Raspberry Pi and provides high-quality images that meet the user requirements. Unfortunately, the module is closed-source, making it impossible to determine how to embed its sensor independently without extensive reverse engineering. Therefore, it is easier to use the module and connect it to the PCB using the same 15-pin FFC CSI connector as the Raspberry Pi. One thing to note is that the CM5 IO Board uses a 22-pin connector, whereas a standard Raspberry Pi uses a 15-pin connector. The additional pins do not have any function for this camera, so a simple adapter cable, pictured in Figure 5.3, can be used to plug the camera into the IO Board during development.

It should be noted that the limit switch, used to home the stepper motor on the right side of the electronics enclosure, is a reliable and straightforward solution also employed in 3D printers and does not require replacement. Therefore, this switch will remain the same and will be connected to the PCB through a small two-pin socket.

5.1.3 Actuators

The servo motors need to be swapped for stronger motors to support the weight of the robotic arm. It makes sense to start at the top of the arm and work down from there, as the weight of the servo motors also impacts how much torque the motor below needs to support. The amount of torque the motor needs to provide can be calculated by

$$\tau = Fd$$

where: τ is the torque, F is the force applied, and d is the distance to the motor shaft. As in this case, F will always be equal to the mass multiplied by the gravity, the maximum weight that the motors can support can be calculated based with:

$$m = \frac{gd}{\tau}$$

with m being the weight in kg and g set to 9.81 m/s^2. The current motors are rated for the following stall torques:

Servo motor	Stall torque
Reely S-0008	0.11 Nm
Reely S-0060 MG	0.54 Nm
ABSIMA485 S150MH	1.5 Nm

Table 5.1: Torque ratings of the device's current servo motors

Starting at the top, the servo only has to support the camera and sensing module. While the exact components in this module are not yet fully known, reasonable estimates can be made regarding the weight the motors have to support. While the weight of the sensor PCB is not easily determined, a reasonable assumption for its weight would be the weight of a small microcontroller development board. The Arduino Uno R3 [42] weighs 25 g, which is likely close to the weight of the sensor board. The Arducam module weighs 20 g [52]. The weight of the enclosure depends on the material used, but it should not weigh much more than 150 g, including a potential LED diffuser ring.

The distance to the centre of the module is approximately 10 cm, so using the formula, the required stall torque is 0.17 Nm. Even if the weight of the enclosure is drastically overestimated, the stall torque of the Reely S-0008 is not enough to move the enclosure. An alternative that provides sufficient torque is the Dynamixel XL-320 servo motor. This motor has a stall torque of 0.39 Nm [83], which is still relatively small. The Dynamixel motors are also smart servos that feature several useful functions, including command-based operation and position/velocity tracking, which are beneficial for robotic arm operation.

For the middle servo, the additional weight mainly comes from the distance of the top part of the arm. Additionally, the top servo motor itself, as well as the addition of wires and carbon fibre tubes leading to the top, are estimated to require an additional 0.1 Nm of torque. The distance from the previous calculation increases to 30 cm. Recalculating the torque requirement for this distance, along with the extra 0.1 Nm, yields 0.61 Nm, which means that the Reely S-0060 MG also does not have sufficient torque to support the arm. As it is desirable to use the same brand of motors for each servo due to their shared communication protocol, the Dynamixel XL-430-W250T with a rating of 1.4 Nm should be a suitable candidate [1] [83].

For the bottom servo, the distance of the top part increases to approximately 60 cm, and the additional torque required by the arm is estimated to be around 0.2 Nm (excluding the previously mentioned 0.1 Nm for the top arm). Calculating this yields a required stall torque of 1.3 Nm. While this is within the capability of the ABSIMA485 S150MH, that sensor uses an entirely different control protocol. It, therefore, makes sense to use the same Dynamixel XL-430-W250T here as well.

By replacing the motors with these suggested counterparts, controlling them becomes significantly easier as they all share the same communication protocol. Being smart servos, they come with desirable features like position and velocity tracking. One handy feature is the option to send a command to the motors, allowing them to rotate freely. This means that the arms can be folded away manually, with minimal resistance, if desired.

[1] Unfortunately, new motors were already ordered during the development of this project before these calculations were performed. The electrical designs are based on the usage of an XL-320 motor here instead of an XL-430-W250T

Figure 5.4: Dynamixel XL-320 smart servo motor [83]

Figure 5.5: Dynamixel XL-430-W250T smart servo motor [83]

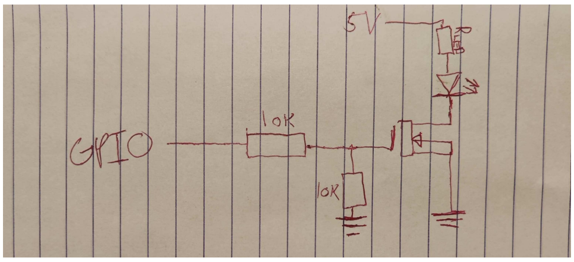

Figure 5.6: An illustration of the MOSFET driver circuit used for the LEDs, with one LED

Both the white and 405 nm UV LEDs, as mentioned earlier, have been replaced by SMD counterparts. However, they still need to be driven somehow. The paper by van der Kroft does not indicate how these LEDs are supposed to be driven. As the LEDs need to be toggleable programmatically, having the CM5's GPIO pins control them makes the most sense. Unfortunately, these pins have a current limit of 16 mA per pin, with a total limit of 50 mA [65]. As the white LEDs require 20 mA per LED and the UV LEDs 30 mA per LED [84, 85], a suitable LED drive circuit needs to be designed to drive them. Fortunately, all LEDs of the same type will always turn on in unison and do not require individual addressing. This makes the drive circuit quite simple, as a single MOSFET can be used to drive an entire string of LEDs. All that is needed is a current-limiting resistor for each LED connected to the source input of the MOSFET. This string of LEDs can then be controlled by pulling the input at the gate, which is connected to one of the CM5's GPIO pins, set to high or low. An example of this circuit demonstrated for a single LED is shown in Figure 5.6.

As for the stepper motor, there is no apparent reason to replace it. It has sufficient torque to rotate the robotic arm around the ring, and it functions properly with the DRV8825 driver. The DRV8825PWPR driver IC, along with the required passive components, will be integrated into the mainboard, replacing the stand-alone module.

Both the white and UV LEDs have a forward voltage of 3.2 V [84, 85]. Using the Raspberry Pi's 3.3 V supply to drive the MOSFETs isn't ideal. This is because 3.3 V is close to the MOSFET's threshold voltage. When the voltage difference across the current-limiting resistor is small, it becomes harder to control the current flowing through the LEDs accurately. Even slight variations between individual LEDs could then cause some to draw significantly more current than others. Therefore, 5 V or 7.4 V is a better choice in this case. However, 5 V will not be available at this point (as explained in Section 5.2.2), so 7.4 V should be used instead. 3.3 V is high enough for most MOSFETs to use as a threshold voltage at the gate, making it suitable to drive this directly from the GPIO pins.

The resistance required for the current-limiting resistors can be calculated using Ohm's Law. First, the voltage that needs to be dropped across the resistors is computed using the forward voltage (same for both LEDs): $U = 7.4 - 3.2 = 4.2V$

Now, the resistances can be calculated. For the white LEDs:

$$R = \frac{4.2}{0.020} = 210\Omega$$

And for the UV LEDs:

$$R = \frac{4.2}{0.030} = 140\Omega$$

5.2 Cable & Wiring Design

To determine the design of the cable connecting the mainboard to the daughterboard, it is essential to establish all the necessary connections that need to be made. In section 4.1.7, this was briefly explored, with estimates for the number of wires and predictions for which signals could be combined into a single wire. In this section, a clear division of these wires is made to create a wiring diagram. Table 5.2 shows all the necessary connections needed between the motherboard and the daughterboard.

5.2.1 Cable Routing

What becomes evident from examining Table 5.2 is that the required number of wires will likely make it challenging to implement the gutter-fed wiring design proposed in Section 4.1.5, as spooling this many wires onto a spool is a complex engineering challenge. Therefore, it would be great if there were a simpler alternative to using a spool that still allows the cable to be fed through a gutter smoothly. Fortunately, the width of the gutter can be increased to enable the wire to fold onto itself. This way, any extra slack in the wire does not have to be spooled up; instead, it can be folded away onto itself. To ensure the wire folds reliably, a cable drag chain can be used to guide the cable, allowing it to fold only in one axis. This solution is not only more straightforward to engineer and manufacture but also likely to have better longevity for the cables, as they don't have to be coiled tightly on a spool. The drag chain itself could even be 3D printed to simplify the manufacturing process and lower the costs of the device. An illustration of this implementation is shown in Figures 5.7 and 5.8.

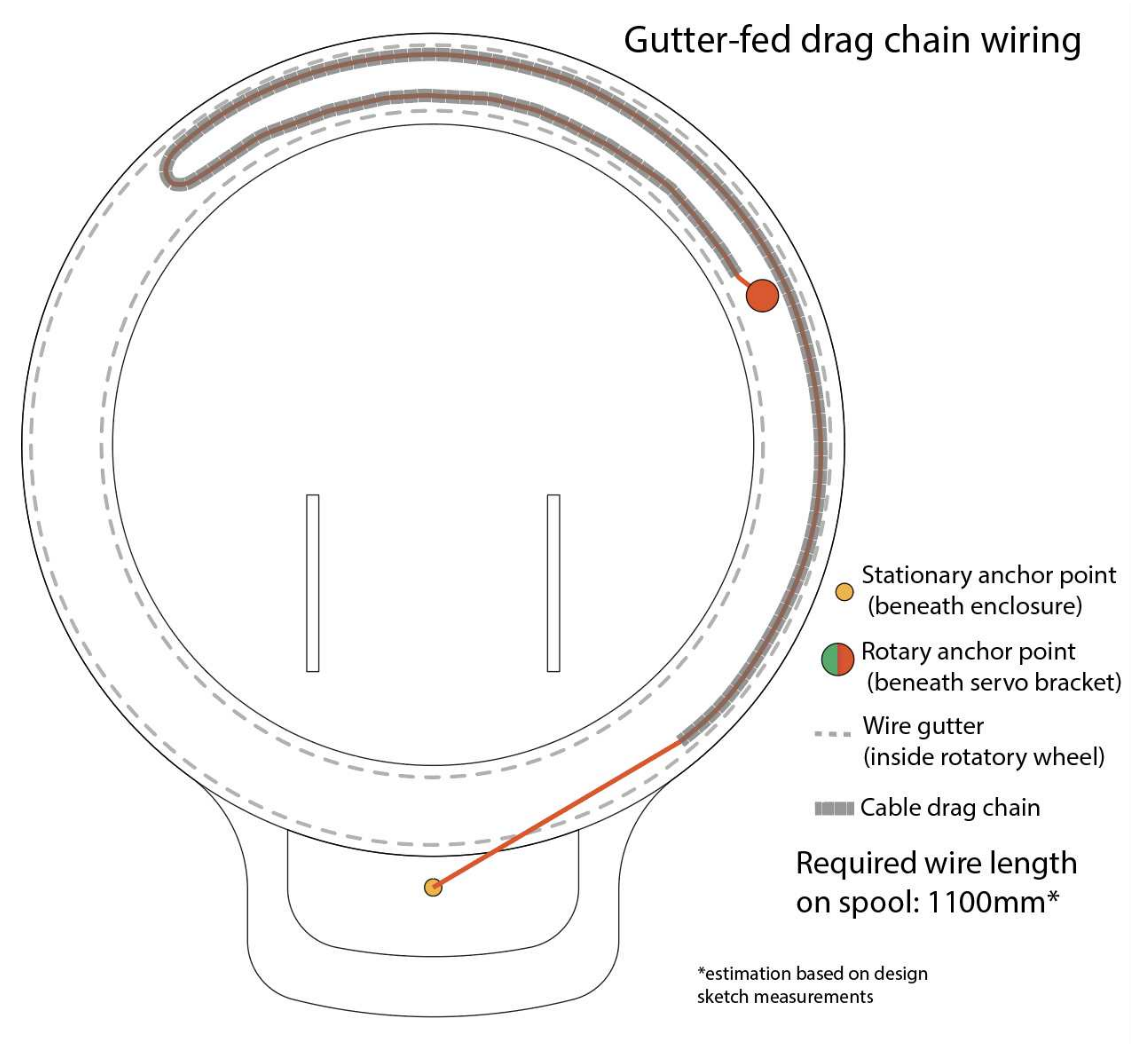

Figure 5.7: Gutter-fed wiring guided by a drag chain

5.2.2 Cable Composition

A distinction is made between regular signal wires (digital logic) and power wires, as these typically have vastly different maximum current ratings. Section 5.3.1 further investigates the current draw for each component. Table 5.2 suggests there are only four power connections. Namely, 3.3 V, 7.4 V, 11.1 V and GND. However, as the 7.4 V lane has a high current draw of 3.3 A (see 5.3.1), it makes sense to add an additional wire for this lane to halve the current running over a single wire and bring it more in line with the 11.1 V line. It is also good practice to have a separate ground connection for each voltage lane, providing a clear return path for each and preventing voltage and current spikes from interfering with logic signals. This also helps to split the current draw. Therefore, the cable will have a total of eight power wires, each with a maximum current rating of 1.65 A.

The required wire thickness can be calculated by combining Ohm's Law with Pouillet's Law and rearranging the terms.

Ohm's Law:

$$V = IR$$

Pouillet's Law:

$$R = \rho \frac{L}{A}$$

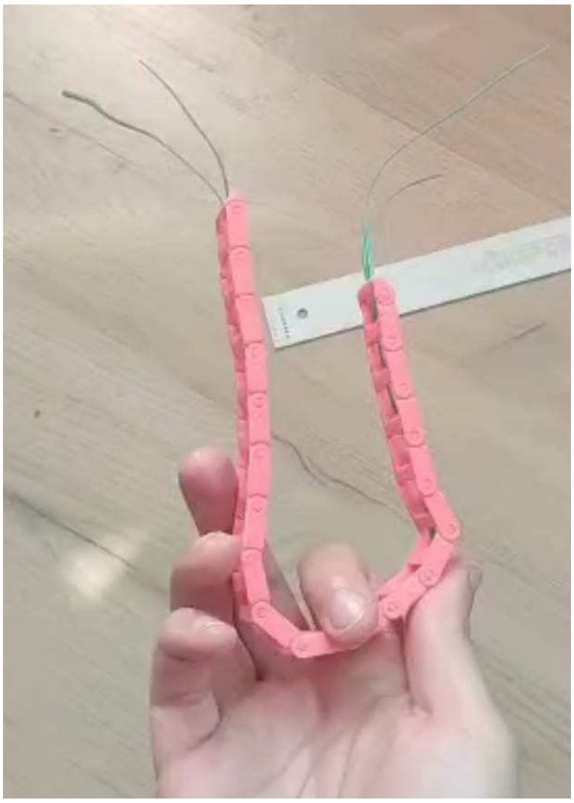

Figure 5.8: Test print of a 3D printed drag chain

Where V is the voltage drop between the source and the end of the wire (V), I is the maximum current running through the wire (A), R is the resistance of the wire (Ω), ρ is the resistivity of the conductor (Ωm, assumed to be copper here), L is the length of the wire and A is the cross-sectional area of the wire (m^2). As the wire thickness is equal to the cross-sectional area of the wire, the equations can be combined and rearranged to get the following equation:

$$A = \frac{I\rho L}{V}$$

To ensure that every sensor continues to work reliably, a maximum voltage drop of 0.2 V (for any voltage) is specified. As previously stated, the maximum current is 1.65 A. The resistivity of copper is 1.72 * 10^8 Ωm at 20° C. The length of the wire is approximately 1 m. By filling in these values in the equation, a cross-sectional area of 0.1419 mm^2 is calculated to be enough. This is close to a wire with an American Wire Gauge (AWG) of 25. To account for potential current spikes, it is good practice to select slightly thicker wires; therefore, the size of these wires is determined to be 22 AWG.

The thickness of the signal wires is less critical, as the low current required over these wires will not significantly impact wire size requirements. Although 22 AWG wire could also be used for these wires, the number of cables warrants a smaller gauge to prevent unnecessary bulk. 30 AWG is a nice balance between the wires being rigid enough to handle the continuous movements made by the robot while still being thin enough not to take up too much space. The number of signal wires is equal to the number in the table, so sixteen.

As the wires will only have to bend in one direction, it makes sense to make the cable flat, as this takes up less space in the drag chain. By stacking the 22 AWG wires next to each other, and doing the same for the 30 AWG wires, two flat cables are created that can be stacked on top of

Connection	Description	Signal Type
GND	System ground	Power
3.3 V	3.3 V power rail	Power
SDA	I^2C data signal	Digital logic
SCL	I^2C clock signal	Digital logic
CAM_D0_N	MIPI data 0 negative	Digital logic
CAM_D0_P	MIPI data 0 positive	Digital logic
CAM_D1_N	MIPI data 1 negative	Digital logic
CAM_D1_P	MIPI data 1 positive	Digital logic
CAM_CK_N	MIPI clock signal negative	Digital logic
CAM_CK_P	MIPI clock signal positive	Digital logic
CAM_IO0	Camera power enable	Digital logic
CAM_IO1	Camera LED indicator	Digital logic
LED_0	White LEDs MOSFET gate	Digital logic
LED_1	UV LEDs MOSFET gate	Digital logic
SRV_0	Bottom servo drive signal	Digital logic
11.1 V	Bottom servo power rail	Power
SRV_1	Middle servo drive signal	Digital logic
SRV_2	Top pitch servo drive signal	Digital logic
SRV_3	Top yaw servo drive signal	Digital logic
7.4 V	Arm servos power rail	Power

Table 5.2: Daughterboard cable signal division

each other to make the final cable, which is illustrated in Figure 5.9. To ensure the cables can be repeatedly bent for a long time, stranded copper wire is used in place of solid wire.

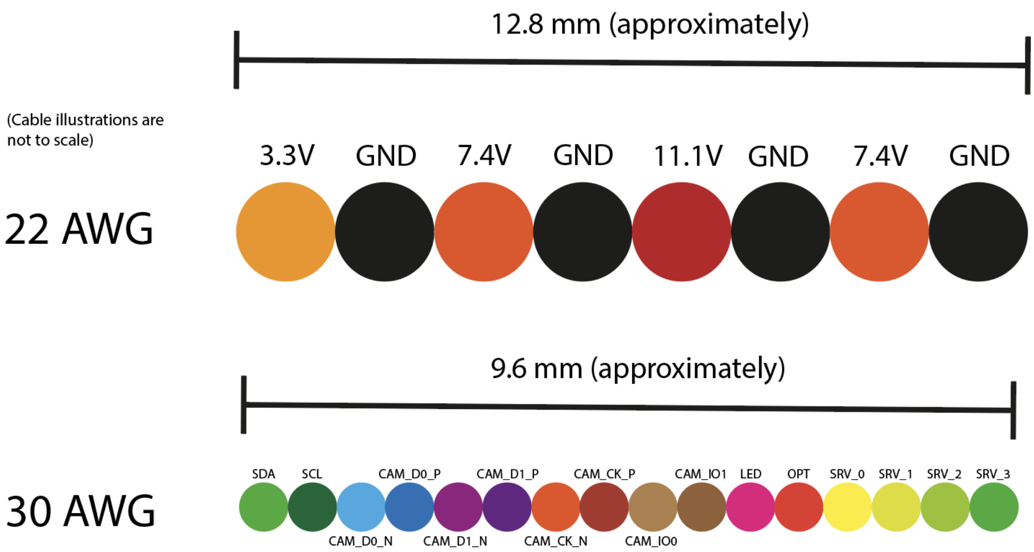

Figure 5.9: Dual flat cable design and wire division

5.3 Power Design

5.3.1 Power Draw

Table 5.3 lists the required voltage for each component and its expected maximum current draw. Values are taken from the components' respective data sheets, or estimated based on other data [44, 47, 52, 55, 65, 69, 84–86].

Component	Voltage	Max. Current Draw
Arducam Hawkeye 64 MP camera	3.3 V	250 mA[1]
MLX90640ESF-BAB-000-TU thermal sensor	3.3 V	23 mA
VL53L4CD distance sensor	3.3 V	1 mA
Raspberry Pi Compute Module 5	5 V	5 A[2]
White LEDs (5x)	5 V[3]	100 mA
UV LEDs (5x)	5 V[3]	150 mA
Dynamixel XL320 servo (3x)	7.4 V	3.3 A
Dynamixel XL430-W250-T servo	11.1 V	1.3 A
SF-2423-10B41 stepper motor	24 V	2 A[4]
DRV8825PWPR stepper motor driver	24 V	1 mA

Table 5.3: Voltage and maximum current ratings for all major components

Together, these components draw a maximum of 114 W. However, in practice, most components will not continuously draw their maximum current ratings, so the actual power consumption is likely a lot lower.

5.3.2 DC-DC conversion

To convert the (yet undetermined) supply voltage to the correct voltages required for each component, the PCB must perform DC-to-DC conversion using a voltage regulation method. Before designing the circuits, it is essential to determine the supply voltage first. Ideally, this supply voltage is higher than or equal to the highest voltage required by the components, as conversion to a lower voltage is generally more efficient.

As the device is to be powered by a Li-ion battery pack, it is crucial to consider a battery configuration that always provides a minimum voltage of 24 V. A safe cut-off voltage for a Li-ion battery, without the cell becoming over-discharged, is 3 V. This means that a battery pack of 8 Li-ion cells in series would have a minimum voltage of $3 \times 8 = 24$ V, with a maximum voltage of $4.2 \times 8 = 33.6$ V when the cells are fully charged. This is consequently the charging voltage of the battery pack.

As mentioned before, the goal is to use USB Type-C Power Delivery for charging or powering the device. PD supports multiple voltage levels. Although the maximum voltage for the Standard Power Range (SPR) mode is 20 V, the Extended Power Range (EPR) mode supports voltages up to 48 V [78]. The closest voltage to 33.6 V in EPR mode is 36 V, which yields a low buck ratio of only 93.3%. In this mode, the standard supports a maximum charging current of 5 A, meaning the battery can be charged with a total of $33.6 * 5 = 168$ W. The total power consumed by the main system components was determined to be 114 W in Section 5.3.1. This means there is an excess power budget of 54 W available for peripheral components and voltage conversion power losses.

[1] Exact current usage is not specified in the data sheet; this is an estimate based on typical MIPI CSI devices.

[2] The CM5 is likely to use significantly less current than 5 A, but this is the current rating of the recommended power supply.

[3] MOSFET driver uses 5 V despite LED forward voltage being less.

[4] 1 A per phase; this assumes both phases of the motor are used.

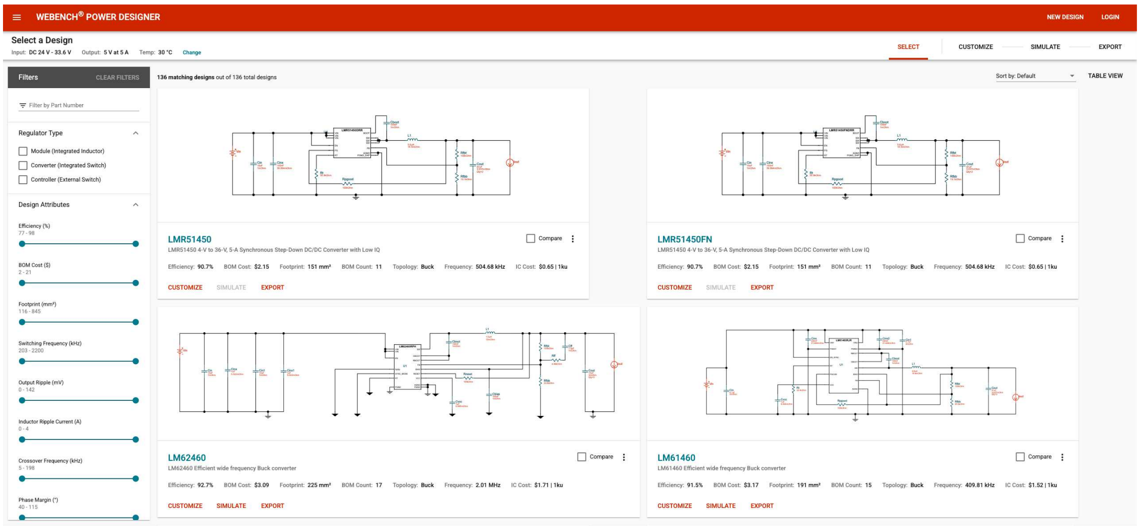

Figure 5.10: Example of generating a buck converter design with Texas Instruments' WEBENCH Power Designer tool [87]

For voltage conversion, the most efficient option is to use buck converters. These switching converters generally have a higher efficiency than linear regulators. While off-the-shelf buck converters could be used, the WEBENCH DC-DC Power Designer web tool created by Texas Instruments simplifies the design process of creating a buck converter design that can be used on a PCB [87]. All the tool needs is a supply voltage input range, output voltage and the maximum current rating for the output. This drastically simplifies the design process of power systems and will be used for designing the voltage conversion in the Realisation phase of this project.

All designs will convert the 24-33.6 V provided by the battery directly to the necessary voltage. Even for the conversion from 24-33.6 V to 5 V, the efficiency remains above 90% [87]. While it is technically possible to compound the conversions, which would, e.g. convert 24-33.6 V to 24 V first, then to 11.1 V, then to 7.4 V, etc., this would result in a compounded loss of power. For 5 V, the efficiency could drop to as low as $0.9^4 = 66\%$. Therefore, it is better to convert directly from the supply range to the necessary voltages. It is not needed to convert to 3.3 V, as the Raspberry Pi already does this, and the current required by the device's components on the 3.3 V rail is less than the maximum rating of the CM5 (500 mA).

Although the efficiency of each conversion will differ slightly depending on the buck ratio and current load, it is fair to assume an average efficiency of 90% accross the entire system. This means that 168*0.1 = 16.8 W will be lost due to the conversion process. This is well within the remaining power budget of 54 W, so in theory, the power lost should not be an issue.

5.3.3 Battery & BMS Design

As mentioned in section 5.3.2, the battery should ideally be an 8S Li-ion cell battery pack. This means that any configuration of cells should be a multiple of eight cells. To determine how many cells are needed, it is important to establish the total power required for the battery. As many variables influence this, a typical use scenario needs to be established first.

According to the design requirements, the device should be able to perform scans on twelve patients per day [3]. It can reasonably be assumed that one day is equal to a single charge, as it is unlikely that medical personnel would charge the device more than once per day. How much power is consumed during a single scan is difficult to determine, as this is likely to be different per patient. For this analysis, we will assume a mean time of five minutes per scan. That means the device should be able to be powered for at least an hour after a full charge.

Figure 5.11: Samsung INR18650-30Q Li-ion battery cell [89]

Although the components were determined to use a maximum of 114 W, this number is likely not realistic for the majority of the time, as components like the Raspberry Pi will not be using their maximum rated current all the time, if ever. Therefore, this analysis will assume that the components use, on average, 100 W of power during regular device operation. This does not include the previously calculated losses due to voltage conversion, which were determined to be approximately 16.8 W. This means the battery should have a capacity of at least 116.8 Wh.

Dividing this number by the nominal voltage of an 8S Li-ion battery pack, which is 29.6 V, the total capacity of the battery pack should be at least 3.95 Ah. However, as the cut-off voltage was set at 3 V, meaning the batteries will not be discharged entirely when used, it is fair to assume that only 80% of a cell's nominal capacity should be considered usable. Besides this, Li-ion cells tend to drop to around 80% of usable capacity left within 500-2000 charge cycles [75]. It is essential to ensure that the batteries do not need to be replaced frequently. Aside from extending the device's service life, it also keeps costs and maintenance efforts low for device users. This last part is particularly relevant for stakeholders, as diabetes is generally more common among lower-income groups, who may not have the means to replace this battery easily [40]. To ensure the batteries do not need to be replaced frequently, this is also taken into account when determining the necessary capacity. This means that in total the battery should have a capacity of 3.95 / (0.80 * 0.80) = 6.17 Ah.

The design of the battery pack will utilise standard 18650 battery cells, as these are widely available and a widespread form factor for battery cells. Although these cells come with various capacities and Continuous Discharge Ratings (CDRs), practically every cell has a minimum CDR high enough to meet the project's needs, and thus, this can be neglected. The Samsung INR18650-30Q is a well-regarded 3000 mAh cell that offers a good balance of price and capacity, making it the cell of choice for this design.

Table 5.4 presents various battery configurations, utilising multiples of eight INR18650-30Q cells. The charge time assumes a charging current of 5.67 A (168 W). The datasheet specifies a weight of 48 g per cell [88], which can be used to determine the total weight of the battery pack (excluding cell holders). Minimising weight is important to keep the device portable.

It is immediately clear that eight cells are not enough to provide sufficient power for twelve scans. Although according to the table, sixteen cells are still not enough, it is so close that it can be reasonably assumed that this is sufficient for twelve scans, mainly because the power con-

Number of cells	Total capacity	No. scans on a single charge	Est. charge time	Est. weight
8	3 Ah	5.8	32 minutes	384 g
16	6 Ah	11.7	64 minutes	768 g
24	9 Ah	17.5	96 minutes	1152 g

Table 5.4: Different configurations of Samsung INR18650 Li-ion cells

sumption estimates are relatively conservative. The cells will have more than 80% capacity for the majority of their lifetime. To be safe, a configuration of 24 cells could also be used; however, as this takes up a considerable amount of space and weighs over 1 kg, it is likely better to use a sixteen-cell battery pack. If needed, the cells could also be exchanged for higher-capacity ones to ensure that the twelve scans are always possible. Thanks to the high-wattage charging, the charging time is relatively low, regardless of the battery pack size, so this does not impact the decision on which configuration to use. For the rest of this project, the sixteen-cell configuration is chosen.

Although designing a BMS for this device is possible, there are so many off-the-shelf solutions available already with many protection and safety features included that, for this project, a pre-existing BMS module will be used. The battery will remain purely theoretical for this project, so an exact module is not determined here. A small circuit board still needs to be added, regardless, to handle the USB-C PD charging and the buck conversion down to 29.6 V, but this board will also stay theoretical for the sake of this project.

5.4 Safety Features

As explained in Section 4.2.2, the emergency button will be implemented as a button that stalls the motors in place, rather than as a hardware power switch. Therefore, it is connected to one of the GPIO pins of the CM5 and can be configured as an interrupt [65] that immediately stops the motors from turning. EN ISO 13850, a European and international standard that specifies the design and functional requirements of an emergency stop button for machinery, mandates the use of a red, "mushroom"- shaped button on a yellow background. The button should be large, unlabelled and easily actuated [90]. The easiest way to conform to these standards is the use of pre-manufactured emergency buttons that are readily available for purchase online.

The standard also specifies that the location of the button should be easily accessible for the operator at all times [90]. As it may be challenging for the operator to reach the device when it is in use, since it is likely stationed on the ground, this button should be attached to a long cable so it can be held in the hand or placed down somewhere easily reachable. This cable should exit on the same side of the leg so as not to interfere with the robotic arm. As there is a possibility that the user may overlap the cable with the arm's path, the device should be marked with a warning that informs the user not to cross the cable over the device. The cable itself can be a coiled cable, similar to what is used for landline phones, allowing it to be stored compactly without occupying much space. This implementation is illustrated in Figure 5.12.

One concern that is always relevant with motors is regenerative current, also known as back EMF. Both the XL-320 and XL-430-W250T servo motors, having their driver circuits fully embedded, are protected against this. The DRV8825 stepper motor driver features built-in protection against the regenerative current, as specified in its data sheet [44]. Therefore, it does not seem necessary to have any additional protection embedded in the PCB.

As mentioned in section 5.3.3, the battery is protected by a BMS. As a pre-existing module will be used for the design, it already incorporates all the necessary safety features for batteries, as mentioned in Section 4.2.2.

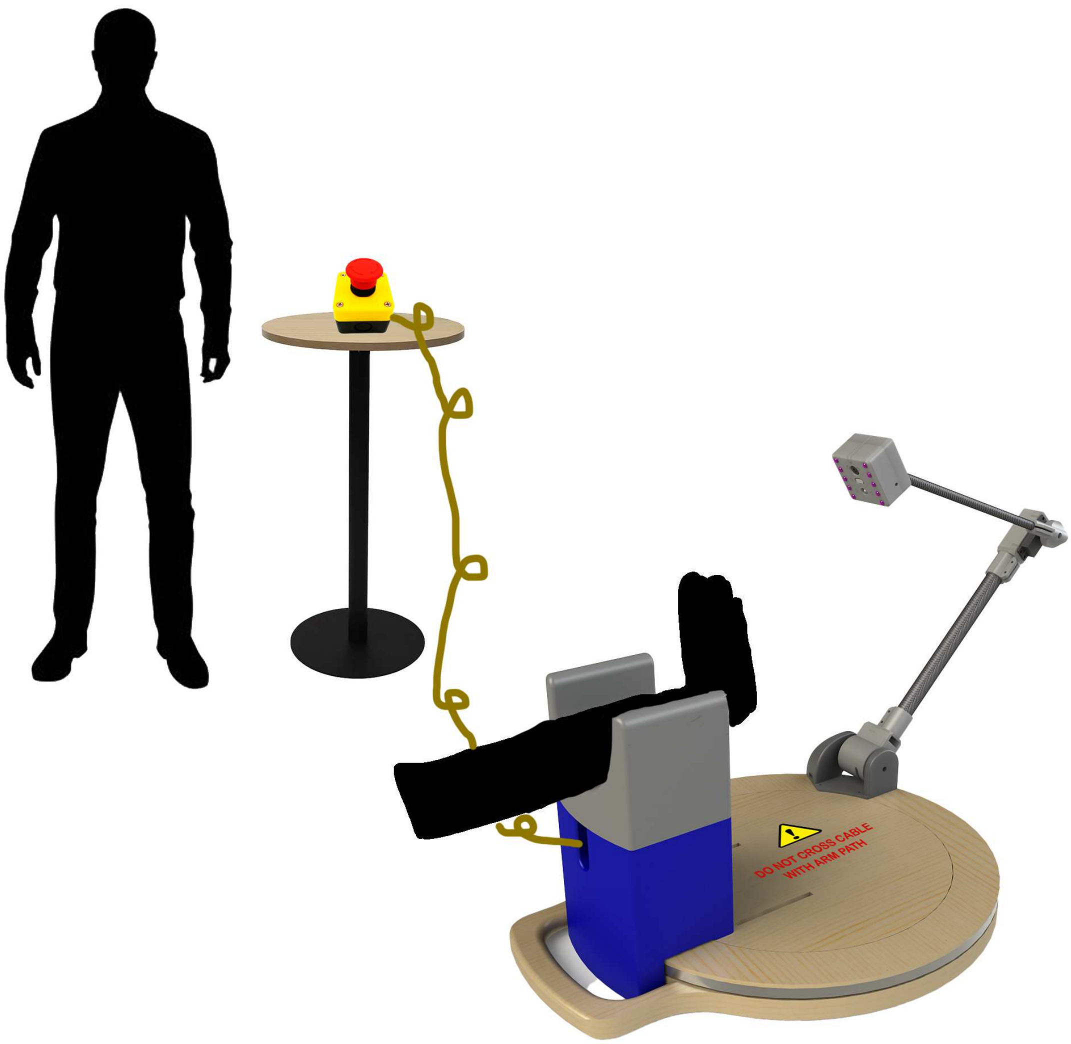

Figure 5.12: Emergency button implementation

Figure 5.13: Bambu P1 series screen and button interface module [46]

5.5 Interface Considerations

The addition of a screen and buttons to control the device later in the development cycle requires some pre-emptive planning to allow these devices to be added seamlessly later. As the specifications of this screen and the button interface are still unknown, it is challenging to add headers for specific screens or buttons on the PCB.

A more straightforward and future-proof approach is to make the screen a separate, standalone module that can communicate with the Raspberry Pi over a specific protocol. Depending on the protocol used, this means only a VCC, GND, and one or two signal wires need to be exposed on a header on the PCB. Suppose the module handles all the button and screen logic independently. In that case, it does not matter what the specifications of the button and screen components are, as a microprocessor on board this module can process the communication to and from these components.

To communicate with the Raspberry Pi, a specific protocol must be selected. In theory, any communication protocol is suitable for this purpose. All the other sensors already use I^2C, so using it for the screen module, too, would make sense. Other protocols, such as SPI or other types of serial protocols, are also options. This is essentially a matter of preference for the interface developer. For this project, it will be assumed that the chosen protocol for communicating with the screen module is I^2C.

Although it is not yet possible to create a design for the interface, as the specifications have not been finalised, some suggestions for the design can be provided. For example, a microprocessor needs to be embedded into the screen module to process the input and communication. This microprocessor should be relatively powerful as it needs to drive a display, so the often-used Atmel ATmega328P, which only has a frequency of 16 MHz [42], might not be powerful enough. Instead, more powerful alternatives, such as an RP2040 (the processor used for Raspberry Pi Pico development boards) or an ESP-32, might be better options.

For an example of what this separate module would look like, the interface of the Bambu P1 series of 3D printers is taken, illustrated in Figure 5.13.

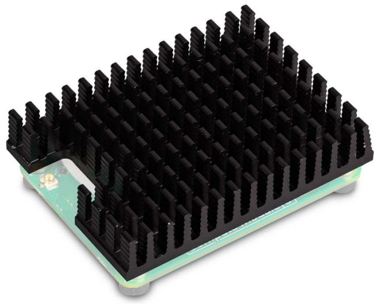

Figure 5.14: The CM5, cooled by a specially designed heat sink [91]

5.6 Thermal Design

According to the data sheet of the CM5, it does not sink as much heat as a standard Raspberry Pi due to containing less metal and fewer connectors [65]. As the Raspberry Pi's processing load can be pretty high when dealing with image analysis algorithms required for wound imaging processing, it is safe to say that some extra cooling would likely benefit the CM5. Especially considering it is contained within an enclosed space. While the data sheet does not specify any specific wattage for the heat output, making it difficult to determine precisely what cooling method would be suitable, Raspberry Pi manufactures and sells a passive heat sink for the CM5 that should be able to handle the heat output. As active cooling is undesirable due to added noise, moving parts and electronic complexity, this seems like a logical solution to regulate the thermals.

The other heat-generating components, such as the DRV8825PWPR stepper driver IC and the battery board, should be able to dissipate enough heat to prevent the need for additional cooling. The DRV8825 features an exposed cooling pad designed to facilitate effective heatsinking. The data sheet suggests connecting it to a ground plane if the PCB on which it is embedded has one [44]. Fortunately, due to the complexity of the mainboard, a ground plane will likely be needed anyway, so this plane can be used to cool the chip. Therefore, an external heat sink should not be necessary as long as sufficient ventilation is provided.

The electronics enclosure, housing all these heat-generating components, should have at least some ventilation holes or grills to allow air to circulate freely. The other components should not generate enough heat to warrant cooling as a significant concern. However, it is still good practice to include a few ventilation holes in areas such as the camera and sensing module, to prevent the inside from slowly heating over time.

5.7 Miscellaneous Design Considerations

5.7.1 Component Layout

The mainboard will be located in the electronics enclosure, just like the Raspberry Pi and Arduino Uno are in the current prototype [4]. On this PCB, all heat-generating components are placed close together, creating a logical space for ventilation holes. The USB Type-C PD port and logic will reside outside the board, as the USB Type-C port needs to be exposed to the outside. As the BMS module will likely not fit next to the PCB in the relatively small electronics enclosure, it will reside below the mainboard. The battery also does not fit in this space, but as there is still a lot of space in the stationary middle part of the base, it could fit there.

The cables connecting the mainboard to the daughterboard are routed through the drag chain in the gutter and then extended throughout the entire arm. The stepper motor and servos remain in the exact locations as before. The daughterboard replaces the sensor modules in the camera and sensing module, with the IR and distance sensor centrally located on the PCB. The camera module is also located at the centre of the PCB, but it will be screwed in on top of the PCB and connected through the CSI connector below. A ring of ten alternating white and UV LEDs is located on the outside of the board along with their MOSFET driver. On the side facing the arm, there are connectors adjacent to the LEDs that facilitate connection to the mainboard, as well as connectors for the motors.

5.7.2 Mechanical Changes

The changes to the electronics also require some mechanical adjustments. Although these will not be addressed during this project, it is still essential to note the necessary changes that impact the mechanical design of the device for future reference.

Some elements of the arm will need to be adjusted to fit the new components. The new servos have a different footprint and are slightly larger than the previous motors. The arms themselves also need to increase in size to accommodate the new cables and provide sufficient slack at the hinges to relieve any stress the wires may be under during arm movement. Although the size of the camera and sensing module can likely remain the same, the new sensors and LEDs' footprints still require a slight redesign of the module's internals. Screw holes also need to be embedded to mount the PCB.

A gutter needs to be created within the ring of the base through which the cables can go. The ring size likely needs to increase for this as well, to make the gutter wide enough for the drag chain to fold smoothly. The thickness of the ring should also be checked and may need to be increased to fit the flat cables, which are lying on their side.

The electronics enclosure primarily requires modifications on the inside to accommodate both the mainboard and the BMS PCBs. There also needs to be holes for the daughterboard cables, the emergency button, the power button, the USB Type-C port, and for ventilation. On the outside, the emergency button should be able to rest or clip in place when not in use, allowing for easy portability.

Finally, the wire connections should all become proper connectors instead of requiring soldered connections. The connector exactly used depends on the wire size. Molex manufactures connectors for various applications, and their connectors have become a global standard; therefore, it makes sense to utilise these connectors for the thinner 30 AWG wires, like the daughterboard sensor wires, Molex's PicoBlade connectors provide a solid, friction-based connection that should be able to withstand the wires moving around a bit [92]. As an extra measure, wire guides could be embedded into the mechanical design next to the connectors to provide some strain relief.

For the larger 22 AWG wires, such as the power wires, Molex's Micro-Fit 3.0 connectors should be able to handle the required current and provide a solid friction-based connection [93]. Once again, some strain relief could be provided by adding wire guides to the mechanical design. For the wires themselves, flexible, stranded copper wire should be used to ensure the cables are durable and can withstand numerous bends in the drag chain or robotic arm.

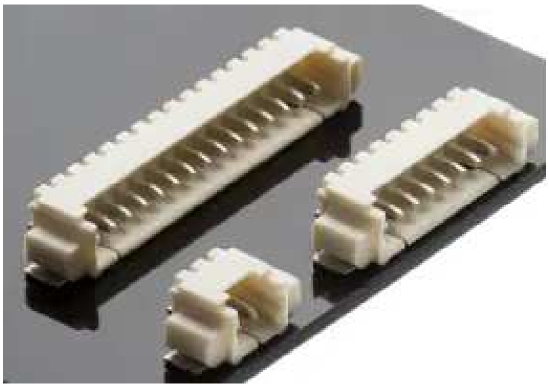

Figure 5.15: Molex PicoBlade female connectors in different sizes [94]

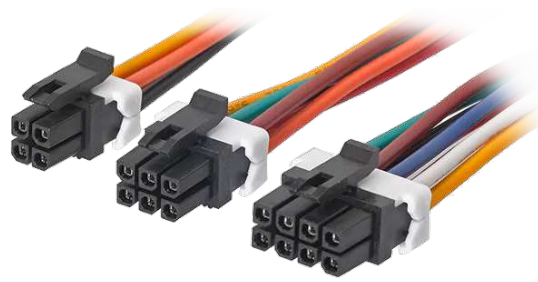

Figure 5.16: Molex Micro-Fit 3.0 male connectors in different sizes [95]

6 Realisation

6.1 Method

As most of the proposed improvements are facilitated by PCB designs, it makes sense to start with creating circuit schematics that implement the design changes. For designing these schematics, Autodesk Fusion 360's electronics design suite is used. As the design for the mainboard is the most complex, this is the first design to be developed. This design is primarily based on the Raspberry Pi Compute Module 5 IO Board, which was developed in-house by the Raspberry Pi Foundation and is entirely open-source [80]. CAD models of this board are also available for download, which, along with the pin-outs detailed in the data sheet, form the basis for the mainboard. Similar pin assignments are also used in the design of the mainboard to ensure that the IO Board can serve as a development board for anyone wanting to test the device's functionalities. GPIO pin assignments are mostly arbitrarily chosen, unless these pins provide a specific functionality necessary for a sensor or other peripheral. Libraries for all components are imported from UltraLibrarian and SnapMagic, services that offer CAD files of these components for download. Any passive components added to the design are not explicitly mentioned here, but they are generally regular 0603 footprint SMD components.

6.2 Design Overhaul

Early into the design of the mainboard, the author realised that there were strict restrictions for the signal integrity of the MIPI CSI-2 interface used for the Arducam module, with a maximum cable length of approximately 30 cm [96]. This has considerable implications for the suggested design of the motherboard/mainboard-daughterboard solution, as it means the camera module must be close to the mainboard. Although Arducam offers solutions to overcome this problem, such as a CSI-to-HDMI adapter, which, as the name suggests, can carry CSI signals over an HDMI cable for long [97], the author was not aware of the existence of these modules when designing the schematics.

Therefore, to solve this problem, the layout of the PCBs was modified to relocate the CM5 directly onto the back side of the daughterboard, thereby integrating it into the camera and sensing module. This also helped to drastically reduce the number of wires that needed to be fed through the drag chain in the base, which was another concern the author had. As most logic is now located inside this area, the PCB inside the camera and sensing module becomes the new mainboard. The servo motors can then also be connected to this board, as the wires only have to run through the robotic arm. Voltage conversion for the CM5 and servo motors is consequently also moved to this board.

During the stage of redesigning the PCB layout, van der Kroft, who was simultaneously working on redesigning the mechanical part of the device, suggested moving the stepper motor from its stationary position next to the electronics enclosure to the right below the servo bracket at the bottom of the arm. Preferably, the stepper motor's control logic would also be moved to the mainboard to simplify wiring. However, due to concerns that the combined footprint of 24 V conversion and the stepper driver logic would be too large for the mainboard to fit within the camera and sensing module, it was decided to place all of the stepper motor logic on a separate PCB located directly above the motor.

As there still needs to be logic to handle peripherals such as the emergency button, power button, and screen button, as well as logic to handle the USB Type-C PD and battery charging, the PCB residing in the electronics enclosure, previously the mainboard, now solely fulfils these functions. To communicate with the mainboard, two wires carrying I^2C are propagated from the mainboard down to the battery and IO board. To process the communication, this board

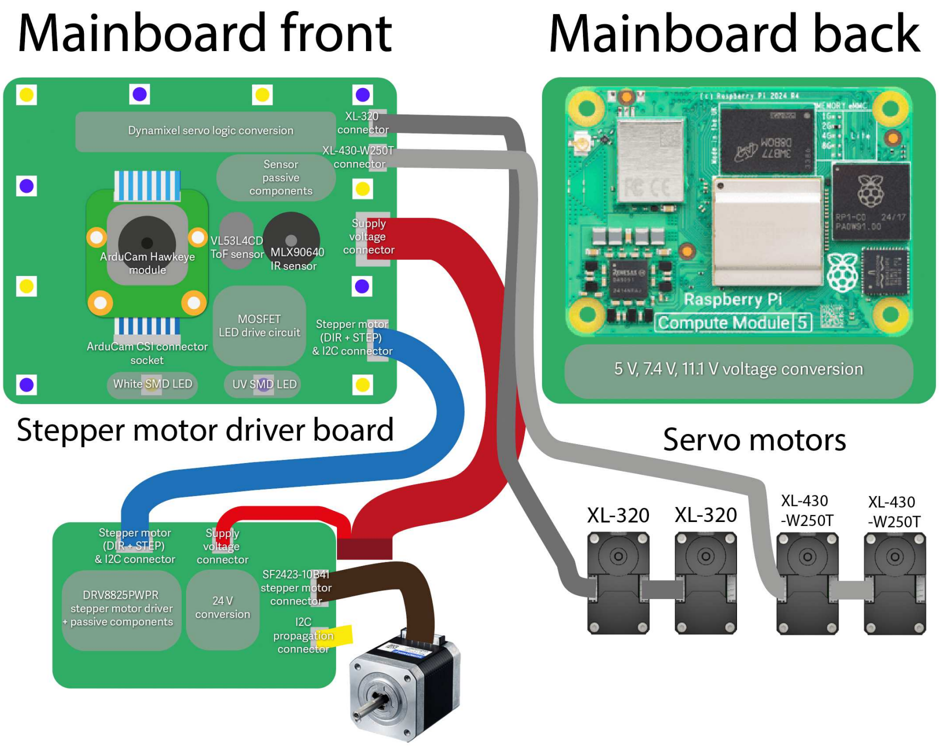

Figure 6.1: The mainboard, stepper motor driver board, and servo motor connections after overhauling the design

has its own microprocessor. This means that the screen module, which was previously designed to require a microprocessor, can now utilise the processing power from the battery and IO board to display graphics on the screen and handle button inputs. As the supply voltage is autonomously converted on the mainboard and stepper driver PCBs, this is the only voltage that needs to go through the base. Like before, the cable is split up into multiple 22 AWG wires to handle the current load. The wire thickness for data wires consequently remains 30 AWG. Molex Micro-Fit 3.0 and Molex PicoBlade connectors are still used for the connectors as described in the Specification phase. The batteries are moved to the centre of the base as they are continuously stationary and have sufficient space to fit there. An illustration of the redesign is shown in Figures 6.1 and 6.2.

6.3 Notable Differences from Overhaul Design

The designs for the PCB layout depicted in Figures 6.1 and 6.2 can be considered "ideal designs", and although they are for the most part replicated in the schematics, there are some differences in the realised designs due to the Realisation phase coinciding with the Specification phase in practise. One notable difference is that the schematics assume a supply voltage of 9-12.6 V. This is because the battery was initially designed to be a 3S Li-ion battery. This was later changed to an 8S battery for efficiency reasons, but this change was not reflected in the schematic design. Although the buck converter designs used in the schematic may still work with the higher supply voltage, this is not confirmed. The 11.1 V regulator is designed as a buck-boost converter in the schematic; however, with an 8S supply voltage of 29.6 V, it would need to be a buck converter only. The same applies to the 24 V conversion, which is handled by a boost converter in the schematic, but would also require a buck converter if 29.6 V is used.

Another change is the switch to a four-servo robotic arm design, replacing the three-servo design. Van der Kroft suggested this change during the realisation phase after the designs for

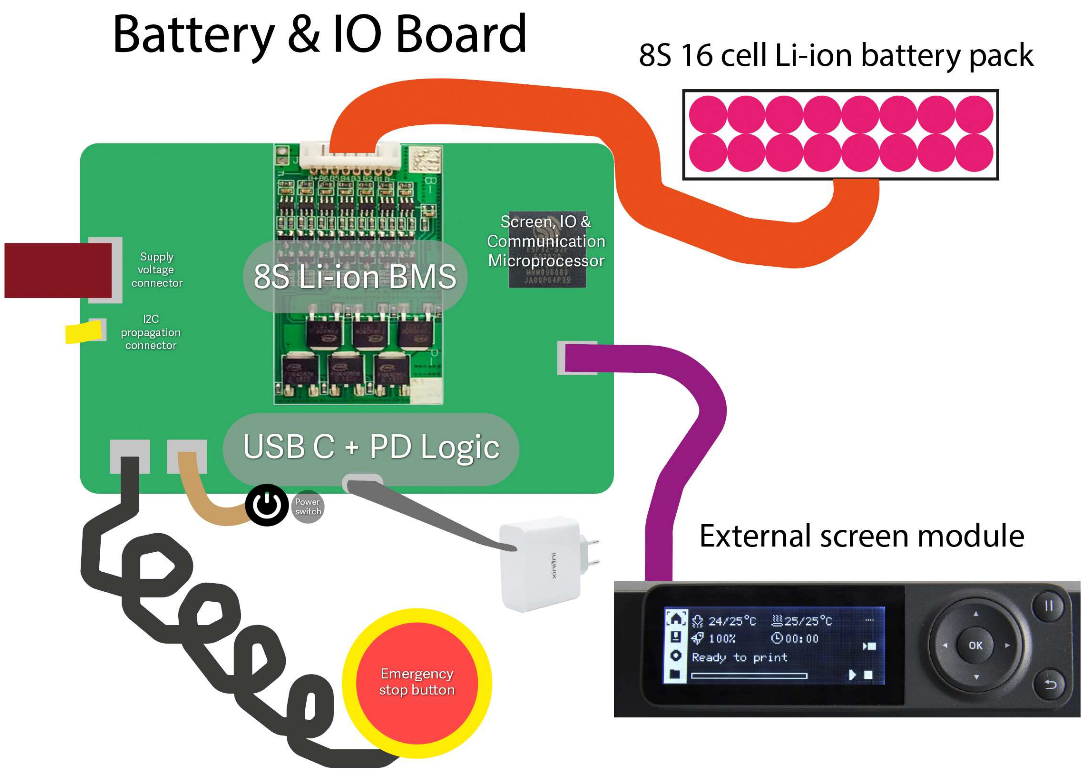

Figure 6.2: The battery board and its connected peripherals after overhauling the design

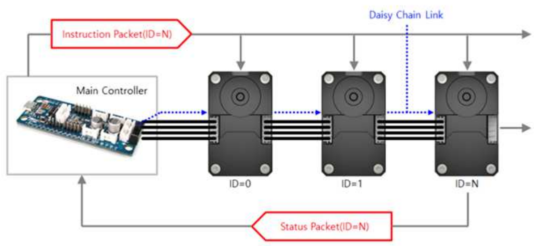

Figure 6.3: Using a daisy chain connection to control multiple Dynamixel servos from a single connection [98]

the motors were already finished. Fortunately, this change did not impact the design, as it was already rated for sufficient current. The daisy-chaining feature of the motors, explained in Section 6.4, meant that no additional headers needed to be added.

6.4 Daisy-Chaining Servo Motors

It was realised during the development of the schematic that the Dynamixel servo motors have an interesting feature that will save some wires and connectors. The motors were designed to pass their power and data connections to up to five other motors, allowing them to be powered and controlled simultaneously. The motors can still be controlled independently, as the smart servos use address-based communication [98]. By daisy-chaining the XL-320 motors and XL-430-W250T motors, two headers and pairs of wires can be eliminated from the design, resulting in a significant space savings. Due to the nature of the shared communication protocol used by the motors, the XL-320 and XL-430-W250T can utilise the same data connection, thereby requiring only one logic converter on the PCB [83].

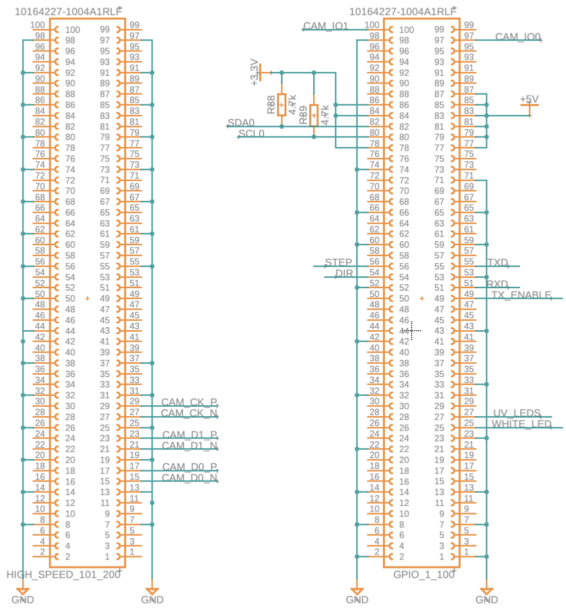

Figure 6.4: Raspberry Pi Compute Module 5 socket implementation

6.5 Mainboard Circuit Schematic Design

This section will explain the design choices behind the schematic of the mainboard. The complete schematic can be found in Appendix B. This section primarily highlights the steps and decisions taken to design the board.

6.5.1 Raspberry Pi Compute Module 5

The design starts with the sockets for the CM5. The CM5 IO Board and the pinout reference in the data sheet are referenced to connect the main voltage lines and specific pins, such as the I^2 pins and CSI data pins [65, 80].

6.5.2 Sensors

Next, all of the sensors are implemented based on the Typical Application sections of their data sheets [55, 69]. The pull-up resistors for the I^2C lines are only required once for those signals, so they are added at the CM5 connector socket. The CSI connector is also added at this stage, with its connections being directly taken from the CM5 IO Board.

6.5.3 Actuators

The LED drive circuits both use the same A03400A N-channel MOSFET to drive the white and UV LEDs. The resistances used differ from those specified in 5.1.3, as the overhaul of the design has made it possible to access 5 V in this area, which is preferred over 7.4 V due to increased efficiency.

The servo motors' UART logic needs to be converted to half-duplex TTL communication. Fortunately, Robotis provides an example signal conversion circuit based on the 74LVC2G241 dual-buffer IC that can be directly copied and implemented into the design [83]. Only one of these circuits is necessary to drive both the XL-320 and XL-430-W250T motors, as they share the same protocol. The sockets used are the Molex Micro-Latch header (model no. 532530370JST) for the XL-320 and the B3B-EH-A for the XL-430-W250T, which are the standard connectors for these motors.

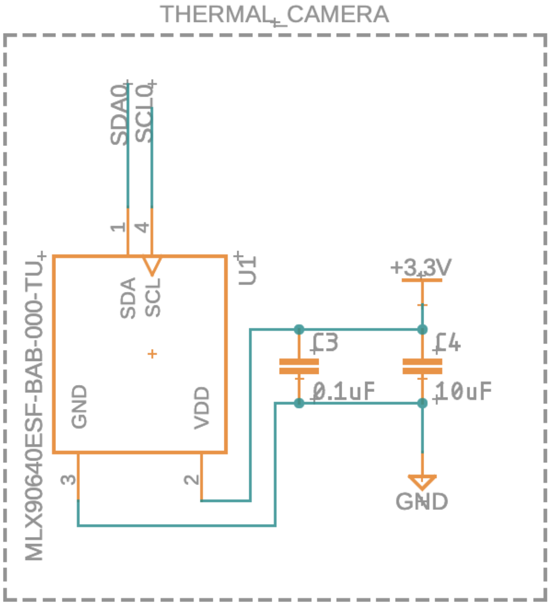

Figure 6.5: MLX90640 thermal sensor implementation

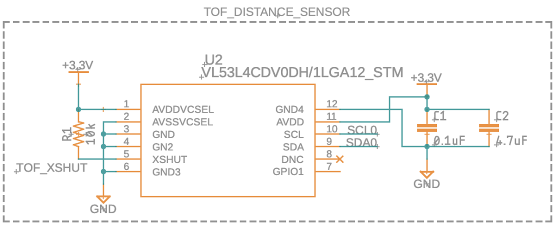

Figure 6.6: VL53L4CDV0DH distance sensor implementation

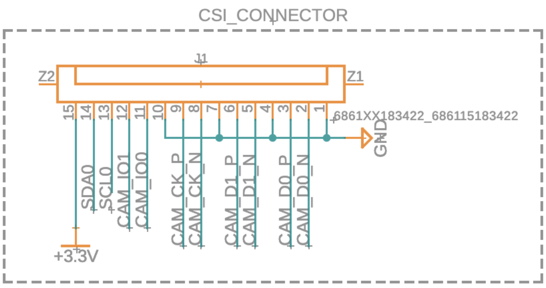

Figure 6.7: MIPI CSI-2 connector implementation

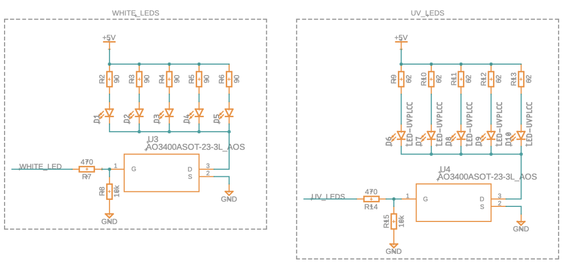

Figure 6.8: MOSFET LED driver circuits implementation for both white and 405 nm UV LEDs

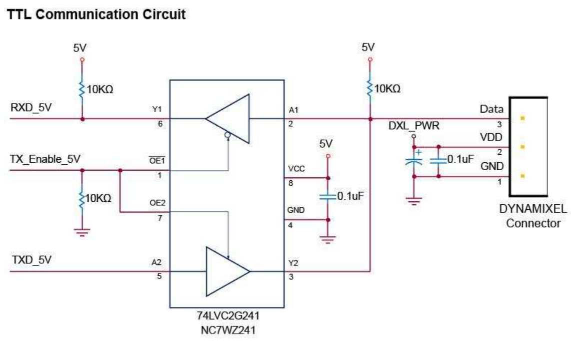

Figure 6.9: UART to TTL communication conversion example by Robotis [83]

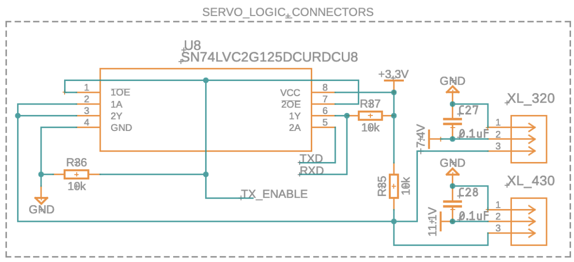

Figure 6.10: Servo data conversion logic and connectors implementation

6.6 5 V, 7.4 V, 11.1 V Voltage Conversion

The designs for the voltage conversion from the supply voltage (9-12.6 V) were based on designs provided by the Texas Instruments WEBENCH Power Designer tool [87]. The desired input and output voltages were used in conjunction with the expected power draw per voltage rail defined in Section 5.3.1. All circuits were also double-checked by verifying the design with the typical application specified in the chip's data sheet. For the 5 V rail, the TPS56637 synchronous buck converter was used. For 7.4 V, the TPS564257 synchronous buck converter and for 11.1 V, the TPS552892RYQR buck-boost converter. The Analogue Ground (AGND) and Power Ground (PGND) of the 5 V and 11.1 V converter are connected to GND through an isolated region in the PCB later.

6.7 Power and stepper driver board connectors

The chosen power connector is the Molex Micro-Fit 3.0 6-pin right-angle connector (model no. 430450600). This connector can support three pairs of 22 AWG wires with a supply voltage. It

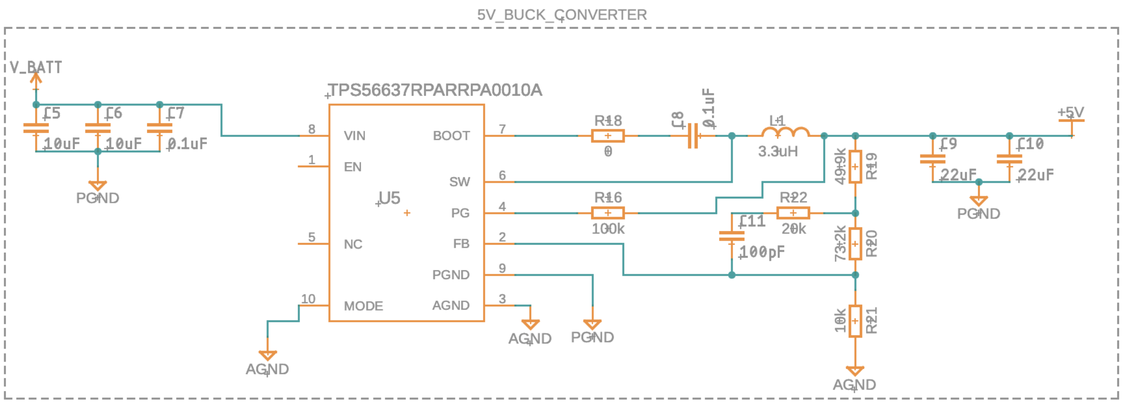

Figure 6.11: 5 V buck converter implementation

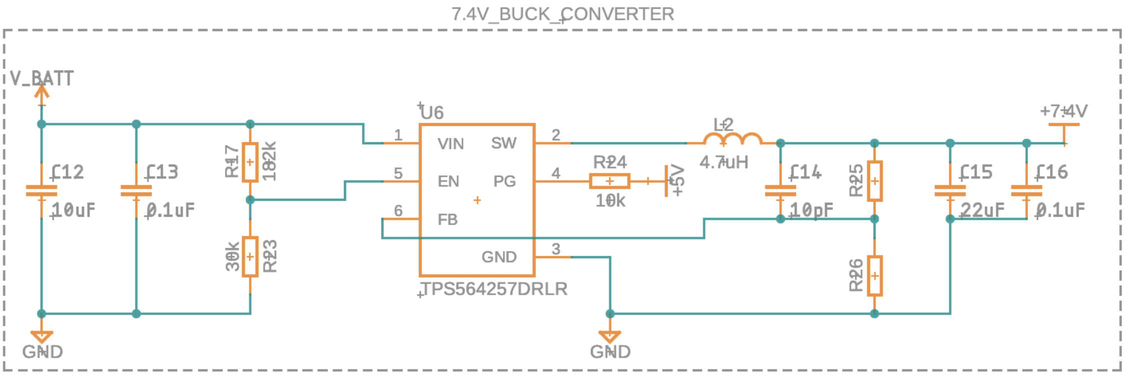

Figure 6.12: 7.4 V buck converter implementation

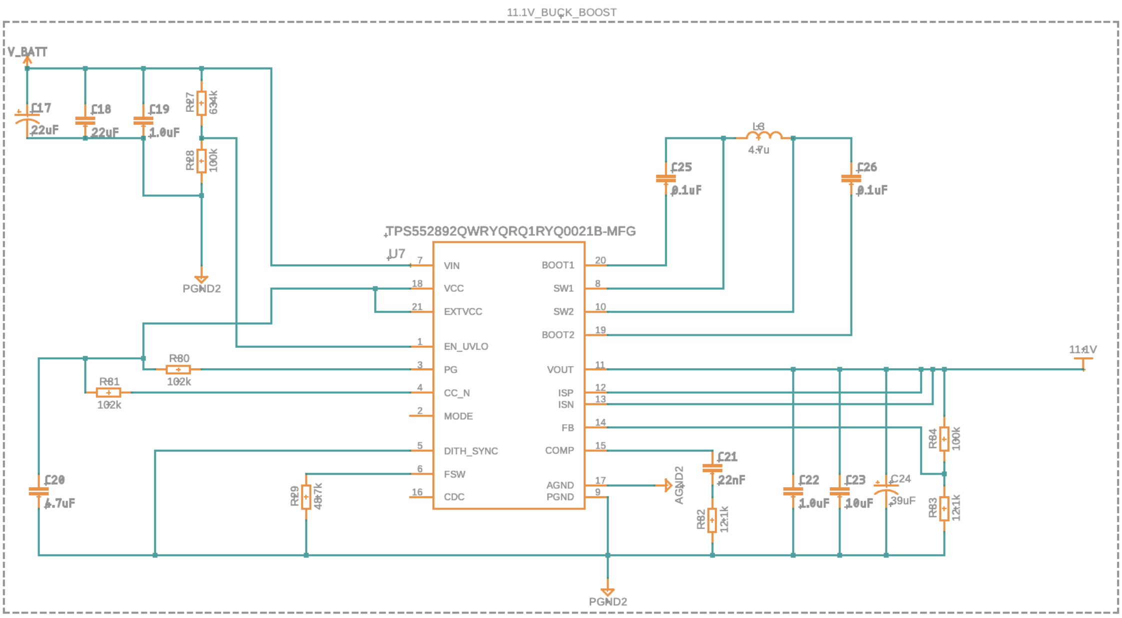

Figure 6.13: 11.1 V buck-boost converter implementation

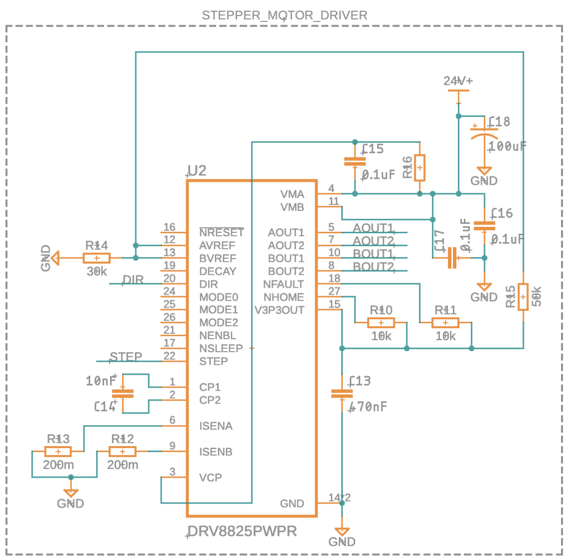

Figure 6.14: DRV8825 stepper motor driver implementation

features a sturdy friction lock to prevent the wires from coming loose during robot use. The stepper driver board is connected through a 4-pin Molex Pico-Clasp right-angle connector (model no. 2023960407). The connector exposes the STEP and DIR signals necessary for the stepper motor driver, as well as the I^2C signals that get propagated to the battery board.

6.8 Stepper Driver Board Circuit Schematic Design

6.8.1 Stepper Motor & Driver

The DRV8825PWPR IC is implemented according to its data sheet's typical application schematic. The motor voltage powers this IC, and thus it does not need a separate VCC supply to operate. The stepper motor is connected through a 4-pin Molex Micro-Fit 3.0 connector (model no. 430450400) to ensure a solid connection.

6.8.2 24 V Conversion

The 24 V voltage conversion necessary for the motor follows the same steps as the conversions in Section 6.6. It is a boost converter based on the TPS43061 boost controller IC. It was not possible to use a standalone boost converter IC, as these are generally not available at these high power ratings.

6.9 Battery Board and IO Board Design

Unfortunately, it was not possible to design a schematic for the battery & IO board due to time constraints. However, the theoretical design shown in Figure 6.2 accurately depicts the elements that would be on this board. A USB Type-C PD controller, such as the TPS26750 from Texas Instruments, can be used in conjunction with a 29.6V buck converter design to handle the USB Type-C charging logic. For the BMS, either a custom design can be created or an existing 8S Li-ion BMS module can be mounted on top of the PCB to ensure all necessary safety features are present. The microprocessor required for the screen, IO and communication should be powerful enough to handle all these tasks, so a chip like the previously mentioned ESP-32 or RP2040 should suffice for this. The external peripherals, such as the emergency button, power button, and screen module, all require connectors. The board powers the other PCBs through the supply voltage connector and communicates to the processor of the CM5 over the I^2C socket.

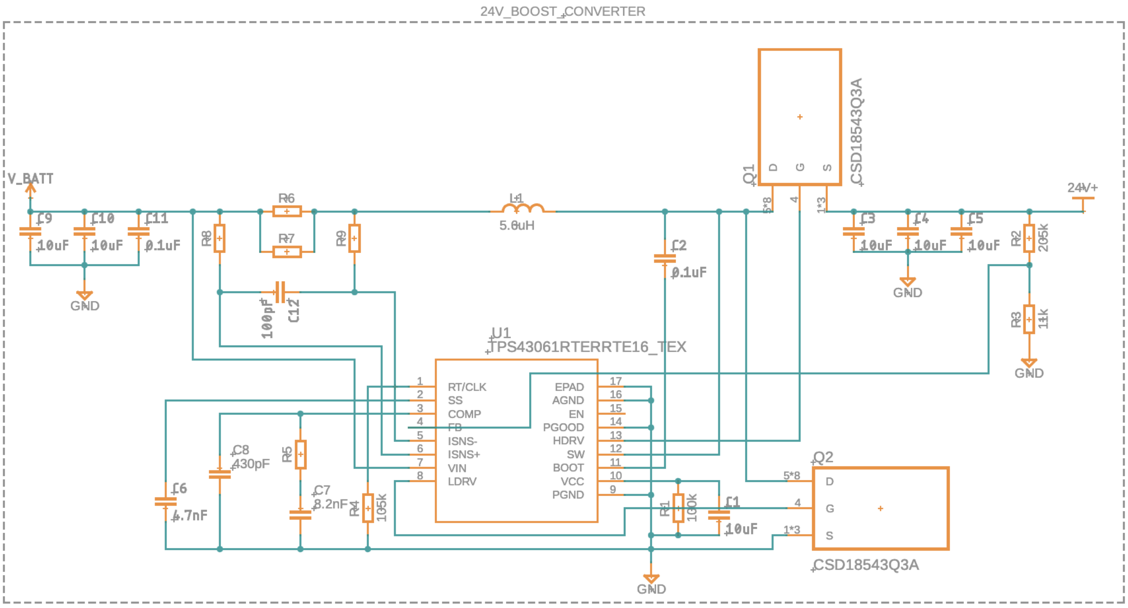

Figure 6.15: 24 V boost converter implementation

6.10 Printed Circuit Board Designs

Although the project's goal was to design and implement a set of PCBs that could be tested, the limited timeframe unfortunately prevented this from becoming a reality. However, some educated guesses and suggestions can be made for the design of these boards. The mainboard is quite complex, space-constrained, and two-sided. This means that it is very likely this PCB needs to be a 4-layer or even 6-layer PCB to allow sufficient space for all the connections to be placed. As the CM5 and servos are likely to consume a significant amount of power, careful attention must be paid to the thickness of the power traces to ensure they're thick enough to handle the current load.

The stepper driver board is not very complex and should easily be able to get away with being a 2-layer board. As there is a lot of space on the board, a ground plane could be used to allow the DRV8825PWPR IC to dissipate its heat through the ground plane as suggested in its data sheet [44]. The battery & IO board, while more complex, also has a lot of space available on the PCB and should therefore be able to get by with a 2-layer PCB as well. Like the mainboard, the power traces should be thick enough to handle the high current requirements.

7 Evaluation

7.1 Evaluating User & Design Requirements

Before evaluating the changes to the design directly, it is wise to verify that all user requirements that were satisfied by the design before are still fulfilled. Table 7.1 provides an analysis of the requirements detailed in Chapter 2. While the table suggests that over five requirements are now satisfied, it is worth noting that no designs have physical implementations. This is further elaborated upon in section 7.2.

Table 7.1: Evaluation of User & Design Requirements established in Chapter 2

Functional Requirement	**Technical Requirement**	**Requirement Satisfied?**	**Remark**
High-resolution images of the wound	Minimum camera resolution of 12.3 MP	Yes	Arducam 64 MP module is still used
High-resolution images of the wound	Camera with built-in autofocus	Yes	Arducam 64 MP module is still used
No impact of variations of lighting	Built-in illumination	Yes	Still a ring of white LEDs (now SMD) that illuminate the wound
Capability to accurately determine the surface area of the wound	Adequate processing power or external processing device	Yes	Can be handled by Raspberry Pi Compute Module 5
Capability to determine the percentage of colour corresponding to the three different tissue types	Adequate processing power or external processing device	Yes	Can be handled by Raspberry Pi Compute Module 5
Display with the possibility to input data	Mobile user interface or built-in touch display	Partially	I^2C socket embedded into the design along with 3.3 V and GND pins to allow a (still to be developed) screen module to be attached
On-board storage space to store multiple images and analysis results	Sufficient amount of internal or external flash storage	Yes	Sufficient flash storage embedded into Raspberry Pi Compute Module 5
Wireless functionality	WiFi or Bluetooth connectivity	Yes	Both present on Raspberry Pi Compute Module 5
Sending updates on wound status remotely	WiFi connectivity	Yes	Present on Raspberry Pi Compute Module 5
The device should last throughout a full day of use	On-board power storage	Yes	Designs for a sixteen-cell 8S Li-ion-based battery pack and charging circuit have been made, but there is no physical prototype yet

Table 7.1: Evaluation of User & Design Requirements established in Chapter 2

Functional Requirement	**Technical Requirement**	**Requirement Satisfied?**	**Remark**
Capability to measure temperature	Infrared thermal camera with an accuracy of +/-0.2°C ideally, a minimum of +/-1.0°C	Yes	The MLX90640 IR array, now embedded onto the PCB, has an accuracy of +/-0.1°C
Capability to measure bacteria presence in wound	High-efficiency UV LEDs with a wavelength of 405 nm	Yes	Still a ring of UV LEDs (now SMD) that shine on the wound tissue
Accurate positioning	Accurate stepper and servo motors	Yes	Two Dynamixel XL-320 motors for the top of the arm and a Dynamixel XL-430-W250T for the bottom, same Sanyo Denki SF2423-10B41 stepper motor as before
Easy (automatic) alignment of camera with the wound	Ranger finder sensor with a minimum sensing distance of 8 cm and an accuracy of +/-5 mm	Yes	TOF050F Time-of-Flight distance sensor has been replaced by the VL53L4CD sensor, which is embedded onto the PCB.
Monitoring all areas of the foot	4 degrees of freedom servo arm with a wide range of motion	Yes	Similar allocation of motors with the servos even having a theoretically higher range than before (full 360°) and an extra servo, providing an additional degree of freedom
Monitoring all areas of the foot	Ability for the camera to be positioned perpendicular to every surface of the foot	Yes	Extra degree of freedom thanks to the additional servo motor
Sufficient safety measures	No contact with wound necessary	Yes	No sensing instruments that require contact
Sufficient safety measures	(Hardware) emergency stop features	Yes	Design and electrical connections for emergency stop button following ISO 13850 standard are in place, but no physical button is present.
Sufficient safety measures	Hardware stops for the servo motors	No	A power failure or shutdown of the device makes the servos lose their torque and makes the arm fall

Table 7.1: Evaluation of User & Design Requirements established in Chapter 2

Functional Requirement	Technical Requirement	Requirement Satisfied?	Remark
Robust power delivery solution	Power supply able to handle the amount of current used by the device's components	Yes	Theoretical design for USB Type-C Power Delivery configured for 180 W, with the ability to charge the battery at 168 W, no physical implementation
Ability to drive the LEDs	A driver circuit to toggle the LEDs on demand	Yes	MOSFET-based LED driver circuit that can toggle both the white and UV LEDs using the CM5 GPIO pins. No physical implementation
Lightweight	Weight in between 1 kg and 15 kg according to ARBO regulations	Yes	Despite new components adding about 1 kg of weight to the device, it still weighs less than 5 kg
Sufficient electrical protection	No exposed wires or electrical contacts with risk of shorting	Yes	Current design does not have any contacts or wires in risk of shorting exposed (except for USB Type-C charging cable when being charged)
Proper thermal regulation and protection measures	Sufficient cooling to handle the heat output of every component	Yes	Cooling measures integrated into designs, but no physical implementation yet

7.2 Realisation of Proposed Improvements

To provide a realistic overview of the progress made in each design during this project, Table 7.2 presents the improvements implemented, along with their current status.

7.3 PCB Layout Changes

The layout of the PCBs has changed drastically throughout the Realisation stage compared to the Specification stage. The motherboard-daughterboard layout was discarded due to the restricted signal integrity of the Arducam camera module over long distances. Instead, the new design integrates the CM5 directly into the camera and sensing module on the same board as the sensors. As the stepper motor is now positioned below the servo bracket, the logic for the stepper motor has been relocated to a new PCB that resides here. The PCB located in the main electronics enclosure is now only responsible for Type-C charging and handling the input of the screen module.

7.4 Motor Torque

A notable issue with the original version of the device was the lack of torque in the servo motors, which meant the robotic arms were unable to support the weight and would fall. In Chapter 5, calculations were performed to determine the required torque and new motors were selec-

Table 7.2: Implementation Overview

Improvement/Addition	**Stage of implementation**
Replacing development boards and hats with PCBs	Schematics for the mainboard and the stepper motor module is finished
Change from Raspberry Pi 4 to CM5	Embedded into mainboard schematic
Change from the thermal camera module to embedded sensor	Embedded into mainboard schematic
Change from distance sensor module to embedded sensor	Embedded into mainboard schematic
Arducam module connected directly to mainboard	Embedded into mainboard schematic
LED driver circuits	Embedded into mainboard schematic
Change from LED THT footprints to SMD	Embedded into mainboard schematic
Voltage conversion logic from supply voltage to 5 V, 7.4 V, 11.1 V	Embedded into mainboard schematic
Servo motor logic converter and connection sockets	Embedded into mainboard schematic
Supply voltage/battery connector	Embedded into mainboard schematic
IO and stepper motor logic propagation connector	Embedded into mainboard schematic
Voltage conversion logic from the supply voltage to 24 V	Embedded into stepper motor board schematic
Change from stepper motor driver shield to embedded IC	Embedded into stepper motor board schematic
Stepper motor connector	Embedded into stepper motor board schematic
Supply voltage/battery connector	Embedded into stepper motor board schematic
IO propagation connector	Embedded into stepper motor board schematic
Type-C charging & IO PCB	Only theoretical layout
Li-ion battery	Full theoretical design, but no physical implementation
Emergency stop button	Full theoretical design, but no physical implementation
System wiring	Full theoretical design, but no physical implementation
Upgraded servo motors	Electrical theoretical design, but no physical implementation
Changes to mechanical design	Only theoretical design, but no changes made to CAD files

Location	Required Torque	Max Old Motor	Max New Motor
Top	0.17Nm	0.11Nm	0.39Nm
Middle	0.61Nm	0.54Nm	0.39Nm [1]
Bottom	1.3Nm	1.5Nm	1.4Nm

Table 7.3: Comparison of torque ratings of new and old motors

ted accordingly. Table 7.3 shows the old and new servo motor's torque ratings along with the required torque. As can be seen, two of the old motors lacked sufficient torque to support the weight of the robotic arm. Out of the new motors, two motors have sufficient torque to support the arm; however, as the XL-320 was accidentally used for the middle servo instead of the XL-430-W250T, the middle motor still lacks enough torque to support the robot.

7.5 Power Consumption & Delivery

Section 5.3.1 inspected the power draw of the various components of the system. The maximum power consumption of the system was calculated to be 114 W. As the previous prototype was not developed to the point where power draw and voltage conversion were considered [4], it is not possible to compare the consumption with that of the previous prototype. However, it can be shown that the prior way of powering the device, which was directly through the Raspberry Pi power supply, would not have been sufficient for the selected components. The recommended Raspberry Pi 4 power supply is rated for 15 W [99], which is much less than what is required. Therefore, it is safe to assume the device would have never functioned previously without a different power supply solution. The chosen USB Type-C Power Delivery solution is rated for 180 W, which is twelve times the amount of current the previous solution could deliver.

7.6 Unrealised Improvements

Unfortunately, the designs of the battery, cooling features, emergency features and the cables and wiring specified in Chapter 5 have not been realised, and therefore their functionality cannot be verified. The wiring design specified in 5.2.2 will need to be altered if implemented in reality, as the sensor board and mainboard have been combined into a single board, now requiring wires for power, the stepper motor module, and the Type-C charging & IO board.

7.7 Manufacturability & Maintainability

One of the primary goals of transitioning to a PCB-based design is to enhance the device's manufacturability. While this is a complex metric to measure, a somewhat methodical analysis can be performed by examining standard Design for Manufacturing (DFM) principles and comparing the previous iteration of the design with the new design based on these metrics.

7.7.1 Product Design & Complexity

A higher number of individual parts generally increases assembly complexity, labour time, potential for errors, and inventory management [100]. Defining "individual parts" is crucial here, as one may wonder whether small components, such as a resistor, are also considered "individual parts". For the sake of this analysis, it is assumed that all elements that can be soldered onto the PCB are assembled by an outsourced company, meaning each assembled PCB is considered a single part.

One significant advantage of the new design is the fact that the LEDs are embedded on the PCB. With the old design, each LED had to be inserted and connected individually. This significantly reduces the number of individual parts that have to be installed. The number of parts is also slightly reduced by the fact that some modules are now integrated into the PCBs. On the other hand, the introduction of these PCBs also increases the number of parts. Additionally, new features, such as the battery, emergency button, power button, and screen module, add to the number of parts. Overall, however, the total number of individual electronic parts that need to be assembled has decreased from twenty to fourteen. This excludes any wiring that may have to be done between the parts.

Reducing design complexity is also crucial. This entails minimising intricate geometries and features that require specialised tooling or multiple manufacturing steps [101]. The design complexity has increased slightly overall, thanks to the new features requiring more intricate geometries, the relocation of the stepper motor, and the gutter needed for the drag chain. However, the layout of the camera and sensing module can be significantly simplified compared to the old design, making it much easier to manufacture and repair the device.

Modularity also helps make designs easier to assemble and maintain. Some components of the old design, such as the Arducam module, were soldered, which means it would be difficult to replace if the design ever failed. For the most part, however, the design utilised modular components that could be easily replaced individually. The new design also adopts a modular approach, particularly in the wiring, with each wire being connected through a PCB header instead of being soldered. The main drawback is that, as many components are now embedded on the PCB, replacing components like the thermal camera or stepper motor driver IC requires more advanced soldering techniques.

7.7.2 Supply Chain & Logistics

Simplifying the supply chain and thus the logistics required for assembly is also beneficial for guaranteeing the prolonged ability to manufacture the device. The old device utilised numerous individual modules, shields, and development boards, all designed by different manufacturers. If the production of one of these development boards were halted, it would be challenging to replace it, as most of these modules are closed-source. Using these modules also increases the device's cost due to the manufacturer's markup on these modules. Using individual sensors may ensure a longer availability for these components, as they are used more widely across the industry. Especially the TOF050F distance sensor of the old prototype is worrisome, as the VL6180X sensor it uses has already been discontinued by the manufacturer [68]. On the other hand, if a single crucial component is not available for the new prototype, it would mean that the entire PCB would not be ready for production. This is somewhat mitigated by the fact that there are multiple PCB designs spread across the device. The use of off-the-shelf, standard components makes it easier for both versions of the prototype to have a decent guarantee of component availability, though.

7.7.3 Verification & Testing

While no specific testing methodology was developed for either prototype, it is still insightful for manufacturing to compare the ability of the components to be tested. The modular approach of the device allows each component to be tested individually before assembly. This is harder for the new prototype, as the PCBs themselves will need to be tested rather than individual modules. Since the new design lacks test pads, it is challenging to test these PCBs. However, the electronic layout of the PCB could still be verified by copying the circuit on a breadboard in conjunction with the CM5 IO Board development kit.

7.8 Mechanical Design Characteristics & Safety Risks

The exposed wires of the old design have been rerouted and enclosed in the new design. This means any potential hazards regarding these wires are now gone. The increased torque of the new motor design also prevents the robotic arm from collapsing onto itself as long as it has power. The measures taken for thermal regulation in the design, like the addition of heat sinks and ventilation holes, also ensure the device cannot overheat. The addition of the emergency button guarantees a way for the user to stop the motors if something goes wrong.

Unfortunately, the new design also adds some new safety hazards. For example, the wire attached to the emergency button can cross over the path of the robotic arm, which could be a problem if the device is in motion. The addition of the battery introduced a potential fire hazard if the battery is punctured or if charging is mismanaged. The location of the battery is also not ideal, as it is situated in the same area where a patient with a wound on the top of the foot would step, necessitating drastic protection measures.

8 Discussion

This chapter reiterates the goal of this research, interprets the evaluation results and highlights the project's strengths and limitations. Recommendations for the future development of the prototype are also presented.

8.1 Key Findings

The project's goal was to identify problems and limitations with the wound monitoring device and design possible solutions for them. The areas of interest outlined in the main and sub-research questions were the *integration, manufacturability, safety, and functionality* of the hardware. Before focusing on any of these aspects, it was essential to gain a thorough understanding of the project's background by understanding the growing problem of DFUs and reviewing current DFU and chronic wound analysis methods, as well as their strengths and weaknesses. Then, the hardware and functions of the previously designed prototype were documented to provide a clear overview of the current state of the electronics. After establishing design requirements based on the previously established stakeholder analysis and user requirements noted in the projects by Ebben, van Koolwijk and van der Kroft, a slightly modified version of the Creative Technology design cycle designed by Mader & Eggink was used to ideate, design and implement improvements to the electronics iteratively.

The results of these efforts were evaluated primarily using qualitative observations. Although physical prototypes of the proposed PCB designs were not developed, the rigorous approach to designing the schematics and theoretical designs enabled a thorough assessment against established design requirements. For certain aspects, such as motor torque and the number of parts, quantitative metrics could be compared to those of the previous prototype iteration. For the most part, however, it was not easy to compare the designs against the prior iteration of the device due to their theoretical nature and the fact that some features did not exist yet on the previous prototype.

Despite this, the qualitative observations and evaluation of the design requirements reveal that most areas of interest highlighted in the research question showed improvements. It is important to note that, except for one, all design requirements would be satisfied by physical implementations of the proposed designs. The only requirement not satisfied is the need for motors with sufficient torque to support the robotic arm. This issue can easily be mitigated by adjusting the design to use the Dynamixel XL-430-W250T servo for the middle motor. It should be noted, however, that the calculations performed for the motor torque did not account for any inertia that may impact the robotic arm during movement. It may be worthwhile to include this in some additional calculations first, before modifying the design, to verify that the motors are sufficient.

Zooming in specifically on the areas focused on in the research question, the integration of the device's components was improved by designing all devices to fit together on the PCBs, sharing voltage and data lines where possible. The reduced footprint for many components, made possible by the use of PCB designs, ensures a more efficient use of space, a reduction in design complexity, and a theoretical decrease in weight. Integrating these components also significantly improved the device's manufacturability by reducing the number of parts required for installation. Manufacturability was also enhanced by simplifying the supply chain through the integration of loose sensors onto the PCB designs. To ensure the device could still be easily assembled and serviced, a modular approach using Molex connectors was chosen to connect the parts, rather than a more fixed design with soldered connections. Unfortunately, the integration of sensors does make it harder to test and verify the device's functionality, but this can be mitigated by incorporating testing features into later revisions of the design.

The new designs retained all the functionality of the previous prototype while adding numerous new features to meet various design requirements. These new features include the addition of a battery, emergency button, USB Type-C Power Delivery, LED drive functionality, a power button, and the option to connect a screen module. While none of these features have physical implementations, all except the USB Type-C power delivery have theoretical designs that should be easy to implement physically in future renditions of the prototype.

While improvements to the device's safety were envisioned, such as the introduction of an emergency stop button, the proposed design also introduced new safety considerations. Specifically, the coiled cable for the emergency stop poses a potential entanglement risk with the robotic arm, and the Li-ion battery introduces a new safety hazard. Furthermore, the lack of a fail-safe mechanism to prevent the robotic arms from crashing in the event of a power failure means that, overall, the device's safety cannot realistically be claimed to have improved in this iteration without further design adjustments.

Overall, the project's findings suggest that applying the proposed designs to the prototype would significantly enhance its capabilities, bringing it a step closer to becoming a device that can provide accurate, real-world wound measurement data. This, in turn, would benefit the training of wound segmentation algorithms and, ultimately, the well-being of patients with DFUs globally. However, the mostly theoretical designs mandate further verification and testing of physical implementations before any of this can be realised.

8.2 Strengths & Limitations

One of the project's strengths was its continuous commitment to evaluating every design choice in the context of the user. By conducting thorough background research on DFUs, chronic wound analysis, and the relevant professional standards, it was ensured that only design choices would be made that could benefit the end user or patient.

The ideation and specification phase covered a broad range of issues, features and possible improvements. Despite the breadth of the problems, most solutions presented in these chapters were based on realistic observations, data-backed calculations, and real-world electronic components. They were also mostly worked out to a detailed extent. This ensures that, even though the designs remained schematic or theoretical, their implementation is straightforward for any developer looking to adapt the designs into the prototype.

Unfortunately, the realisation stage saw the need for a significant redesign of the device. This means that some designs developed in the Specification phase had or will have to be altered and adapted to accommodate the new PCB layout. The theoretical nature of the designs, primarily due to the limited timeframe for the project, made it challenging to conduct well-structured qualitative and quantitative analyses during the Evaluation stage. The lack of statistical evidence for improvements in efficiency, weight reduction, and safety makes it difficult to draw confident conclusions on these areas. It was not possible to test the designs to verify the function of the circuits, making it also difficult to confidently state that they work and are therefore an improvement to the current prototype. Ideally, the design would also have been user-tested to verify the device's potential in the real world. It could be argued that this was not part of the project's goals, however.

In retrospect, it might also have been interesting to focus more on the financial aspect of the electronics. As diabetes is generally more common in low-income areas [SOURCE], ensuring the device's electronics are optimised for a low cost could mean broadening its reach and potential user base. For this, a cost-benefit analysis could have been performed to determine what components would be most relevant for the device to incorporate. The actual mechanical design of the prototype was also not evaluated. Evaluating this before the ideation phase could have resulted in a simpler, more straightforward design for the device and its electronics; however, as this was already explored by van der Kroft [4], the choice was made not to evaluate it in this paper.

8.3 Future Work

One of the obvious steps for future developments of the prototype is to finalise the designs of each PCB and verify their functionality in the real world. To achieve this, a testing methodology should be developed, possibly incorporating features such as test pads directly on the PCBs themselves to simplify the process. Although the theoretical designs are well-documented in this paper, actual documentation for the device is not yet available, which could facilitate software developers' testing and development of the device's functions more easily. As mentioned in Section 8.2, conducting a cost-benefit analysis and evaluating the actual prototype design further could also lead to more straightforward and cost-effective designs. Although this project identified areas of the mechanical design that required modification, such as the holders for the servo motors, the displacement of the stepper motor, and the ventilation holes, no updates were made to the CAD models. Consequently, these modifications will also need to be implemented. After these changes are implemented, the designs can be user-tested to verify that they serve their purpose and help improve the quality of wound measurement data for DFUs.

9 Conclusion

This project explored the potential for enhancing the electronics of a wound care monitoring device for patients with diabetic foot ulcers, to answer the main research question:

"How can the electronics of the wound care monitoring device be modified to improve the integration, manufacturability, safety and functionality of the hardware?"

Through background research, established design requirements and an iterative ideation and specification process, two schematics, along with various theoretical designs for new features, were created. Qualitative observations were then used to evaluate these designs and their contributions to improving the categories outlined in the research question. The switch from individually connected modules to Printed Circuit Board design with embedded sensors significantly enhanced the integration of the components. This led to a reduction in the overall number of components needed for assembly, which, along with the modular approach of using connectors to connect each PCB and loose component, benefited the manufacturability of the device. Aside from refining existing components, the project also laid the groundwork for the addition of new features, including an emergency button, battery, USB Type-C charging, and an optional screen module, to enhance the device's functionalities. Efforts were also made to improve the safety of the device by consulting international professional standards. Although some advancements were made regarding the device's safety, the introduction of new features has also revealed new safety risks that require further investigation in future renditions of the prototype. The new designs successfully fulfilled several design requirements while ensuring that previously fulfilled requirements were still met.

Overall, the enhancements proposed in this project lay a strong foundation for a more capable and integrated wound monitoring device, bringing it closer to being a valuable tool for researchers, home care workers, and DFU patients in chronic wound analysis.

9.1 Significance and Implications

While the advancements made by this project specifically focused on the specific wound care prototype as designed by van der Kroft [4], the physical implementation of these improvements, and thus the ability for the device to become functional, is very relevant for providing accurate, consistent measurements of chronic wound data to DFU patients, healthcare professionals, researchers in medical development and the developers of algorithms for (AI) wound analysis. Additionally, the motivation and design process behind the selection and implementation of each component in this project may aid researchers looking to build a similar device of their own.

9.2 Lessons Learned and Future Perspectives

It became evident during the realisation that the vast number of changes, while theoretically worked out to the full extent, were difficult to realise within the given timeframe of the project. As no physical prototype was realised, a structured evaluation became difficult to achieve, and ultimately, most results ended up being speculative and not based on significant data. In retrospect, it might have been better to focus solely on a few specific areas of improvement, ensuring they could be fully developed into a real-world prototype. Therefore, the following steps for this project involve validating the designs by developing them into physical prototypes, after which the device can be further tested and developed. This would also allow for evaluating the design with quantifiable data, such as energy efficiency and weight. It would also be insightful to research possible solutions to tackle the safety hazards introduced by the new features.

9.3 Final Thoughts

This research lays the groundwork for necessary advances in the next stage of development of an advanced wound monitoring device, offering a promising approach to enhance DFU data acquisition and improve the lives of countless individuals affected by this challenging condition.

A Use of Generative AI

During the preparation of this work, the author utilised Grammarly to assist with grammar and enhance sentence structure. Furthermore, the author used Google Gemini to suggest research paths during the Ideation and Specification phases of the project. After using these tools, the author reviewed and edited the content as needed and takes full responsibility for the content of the work.

B Circuit Schematics

The full circuit schematics can be viewed and downloaded here:

- **Mainboard** Schematic | Image export
- **Stepper Driver Board** Schematic | Image export

References

[1] David G. Armstrong et al. 'Diabetic Foot Ulcers: A Review'. In: *JAMA* 330.1 (July 2023), pp. 62–75. ISSN: 0098-7484. DOI: 10.1001/jama.2023.10578. URL: https://doi.org/10.1001/jama.2023.10578 (visited on 14/03/2025).

[2] Laura Bolton. 'Diabetic foot ulcer: treatment challenges'. eng. In: *Wounds* 34.6 (June 2022), pp. 175–177. ISSN: 1943-2704. DOI: 10.25270/wnds/2022.175177. URL: https://doi.org/10.25270/wnds/2022.175177 (visited on 14/03/2025).

[3] René van Koolwijk. 'Designing an at-home wound monitoring device to address the needs of patients with diabetic feet and their healthcare providers'. Bachelor thesis. Enschede: University of Twente, Jan. 2024.

[4] Filip van der Kroft. 'Automated at-home wound monitoring system design and prototype'. Bachelor thesis. Enschede: University of Twente, Jan. 2024.

[5] Publisher:Open Science Company et al. 'A Comparison of Wound Area Measurement Techniques: Visitrak Versus Photography'. en. In: *ePlasty* 11 (Mar. 2021). URL: https://www.hmpgloballearningnetwork.com/site/eplasty/comparison-wound-area-measurement-techniques-visitrak-versus-photography (visited on 04/07/2025).

[6] Domagoj Marijanović and Damir Filko. 'A Systematic Overview of Recent Methods for Non-Contact Chronic Wound Analysis'. en. In: *Applied Sciences* 10.21 (Jan. 2020). Number: 21 Publisher: Multidisciplinary Digital Publishing Institute, p. 7613. ISSN: 2076-3417. DOI: 10.3390/app10217613. URL: https://www.mdpi.com/2076-3417/10/21/7613 (visited on 25/02/2025).

[7] Shuxin Li et al. 'Imaging in Chronic Wound Diagnostics'. en. In: *Advances in Wound Care* 9.5 (May 2020), pp. 245–263. ISSN: 2162-1918, 2162-1934. DOI: 10.1089/wound.2019.0967. URL: https://www.liebertpub.com/doi/10.1089/wound.2019.0967 (visited on 26/02/2025).

[8] Laura Martinengo et al. 'Prevalence of chronic wounds in the general population: systematic review and meta-analysis of observational studies'. In: *Annals of Epidemiology* 29 (Jan. 2019), pp. 8–15. ISSN: 1047-2797. DOI: 10.1016/j.annepidem.2018.10.005. URL: https://www.sciencedirect.com/science/article/pii/S1047279717310311 (visited on 25/02/2025).

[9] Maheshwari. *(PDF) Chronic wounds: a rising public health concern*. en. URL: https://www.researchgate.net/publication/380074370_Chronic_wounds_a_rising_public_health_concern (visited on 25/02/2025).

[10] *Rapport Innovatie van complexe wondzorg - Nederlandse Zorgautoriteit*. URL: https://puc.overheid.nl/nza/doc/PUC_3196_22/1/ (visited on 25/02/2025).

[11] Imme Ebben. 'Developing an instrument prototype for a wound care computersystem'. en. Bachelor thesis. Enschede: University of Twente, Nov. 2023.

[12] Mark Swerdlow, Jessica Lo and David G. Armstrong. 'Reliability of an AI-Powered Application Across Different Mobile Devices for Assessment of Chronic Wounds'. In: *Advances in Wound Care* 13.1 (Jan. 2024). Publisher: Mary Ann Liebert, Inc., publishers, pp. 14–21. ISSN: 2162-1918. DOI: 10.1089/wound.2022.0095. URL: https://www.liebertpub.com/doi/full/10.1089/wound.2022.0095 (visited on 04/04/2025).

[13] Yves Lucas et al. 'Wound Size Imaging: Ready for Smart Assessment and Monitoring'. In: *Advances in Wound Care* 10.11 (Nov. 2021). Publisher: Mary Ann Liebert, Inc., publishers, pp. 641–661. ISSN: 2162-1918. DOI: 10.1089/wound.2018.0937. URL: https://www.liebertpub.com/doi/full/10.1089/wound.2018.0937 (visited on 23/03/2025).

[14] Rashmi Mukherjee, Suman Tewary and Aurobinda Routray. 'Diagnostic and Prognostic Utility of Non-Invasive Multimodal Imaging in Chronic Wound Monitoring: a Systematic Review'. eng. In: *Journal of Medical Systems* 41.3 (Mar. 2017), p. 46. ISSN: 1573-689X. DOI: 10.1007/s10916-016-0679-y.

[15] Y. M. Zhao et al. 'Laser scanner for 3D reconstruction of a wound's edge and topology'. en. In: *International Journal of Computer Assisted Radiology and Surgery* 16.10 (Oct. 2021), pp. 1761–1773. ISSN: 1861-6429. DOI: 10.1007/s11548-021-02459-1. URL: https://doi.org/10.1007/s11548-021-02459-1 (visited on 23/03/2025).

[16] Michael S. Chin et al. 'Hyperspectral Imaging for Burn Depth Assessment in an Animal Model'. In: *Plastic and Reconstructive Surgery Global Open* 3.12 (Jan. 2016), e591. ISSN: 2169-7574. DOI: 10.1097/GOX.0000000000000558. URL: https://www.ncbi.nlm.nih.gov/pmc/articles/PMC4727700/ (visited on 04/04/2025).

[17] Monika Kuck et al. 'Evaluation of optical coherence tomography as a non-invasive diagnostic tool in cutaneous wound healing'. eng. In: *Skin research and technology: official journal of International Society for Bioengineering and the Skin (ISBS) [and] International Society for Digital Imaging of Skin (ISDIS) [and] International Society for Skin Imaging (ISSI)* 20.1 (Feb. 2014), pp. 1–7. ISSN: 1600-0846. DOI: 10.1111/srt.12077.

[18] Milos Todorović et al. 'In vivo burn imaging using Mueller optical coherence tomography'. eng. In: *Optics Express* 16.14 (July 2008), pp. 10279–10284. ISSN: 1094-4087. DOI: 10.1364/oe.16.010279.

[19] Anthony J. Deegan et al. 'Optical coherence tomography angiography monitors human cutaneous wound healing over time'. eng. In: *Quantitative Imaging in Medicine and Surgery* 8.2 (Mar. 2018), pp. 135–150. ISSN: 2223-4292. DOI: 10.21037/qims.2018.02.07.

[20] Arjun Chanmugam et al. 'Relative Temperature Maximum in Wound Infection and Inflammation as Compared with a Control Subject Using Long-Wave Infrared Thermography'. eng. In: *Advances in Skin & Wound Care* 30.9 (Sept. 2017), pp. 406–414. ISSN: 1538-8654. DOI: 10.1097/01.ASW.0000522161.13573.62.

[21] S. Yi et al. 'Enhance wound healing monitoring through a thermal imaging based smartphone app'. In: vol. 10579. 2018. DOI: 10.1117/12.2293674.

[22] Alexandra Burke-Smith, Jonathan Collier and Isabel Jones. 'A comparison of non-invasive imaging modalities: Infrared thermography, spectrophotometric intracutaneous analysis and laser Doppler imaging for the assessment of adult burns'. eng. In: *Burns: Journal of the International Society for Burn Injuries* 41.8 (Dec. 2015), pp. 1695–1707. ISSN: 1879-1409. DOI: 10.1016/j.burns.2015.06.023.

[23] Carlos Eduardo Acuña-López et al. 'Testing a ToF (Time of Flight) sensor in an in vivo environment to detect wound depth in specimens with diabetes mellitus'. In: *2024 IEEE International Autumn Meeting on Power, Electronics and Computing (ROPEC)*. Vol. 8. ISSN: 2573-0770. Nov. 2024, pp. 1–9. DOI: 10.1109/ROPEC62734.2024.10876992. URL: https://ieeexplore.ieee.org/abstract/document/10876992 (visited on 27/03/2025).

[24] Maanasa Jayachandran et al. 'Critical Review of Noninvasive Optical Technologies for Wound Imaging'. In: *Advances in Wound Care* 5.8 (Aug. 2016), pp. 349–359. ISSN: 2162-1918. DOI: 10.1089/wound.2015.0678. URL: https://www.ncbi.nlm.nih.gov/pmc/articles/PMC4991615/ (visited on 04/04/2025).

[25] Jay C. Erie. 'Corneal wound healing after photorefractive keratectomy: a 3-year confocal microscopy study'. eng. In: *Transactions of the American Ophthalmological Society* 101 (2003), pp. 293–333. ISSN: 0065-9533.

[26] K. Sahu et al. 'Non-invasive assessment of healing of bacteria infected and uninfected wounds using optical coherence tomography'. eng. In: *Skin research and technology: official journal of International Society for Bioengineering and the Skin (ISBS) [and] International Society for Digital Imaging of Skin (ISDIS) [and] International Society for Skin Imaging (ISSI)* 16.4 (Nov. 2010), pp. 428–437. ISSN: 1600-0846. DOI: 10.1111/j.1600-0846.2010.00451.x.

[27] F. Prati et al. 'Does optical coherence tomography identify arterial healing after stenting? An in vivo comparison with histology, in a rabbit carotid model'. eng. In: *Heart (British Cardiac Society)* 94.2 (Feb. 2008), pp. 217–221. ISSN: 1468-201X. DOI: 10.1136/hrt.2006.112482.

[28] S. A. Pape, C. A. Skouras and P. O. Byrne. 'An audit of the use of laser Doppler imaging (LDI) in the assessment of burns of intermediate depth'. eng. In: *Burns: Journal of the International Society for Burn Injuries* 27.3 (May 2001), pp. 233–239. ISSN: 0305-4179. DOI: 10.1016/s0305-4179(00)00118-2.

[29] Hursit Soyer and Ilhami Uslu. 'A patient with peripheral arterial stenosis diagnosed with lower extremity perfusion scintigraphy'. eng. In: *Clinical Nuclear Medicine* 32.6 (June 2007), pp. 458–459. ISSN: 0363-9762. DOI: 10.1097/RLU.0b013e318059b54a.

[30] M. Hassan Arbab et al. 'Terahertz spectroscopy for the assessment of burn injuries in vivo'. eng. In: *Journal of Biomedical Optics* 18.7 (July 2013), p. 077004. ISSN: 1560-2281. DOI: 10.1117/1.JBO.18.7.077004.

[31] P.H. Siegel. 'Terahertz technology in biology and medicine'. In: *IEEE Transactions on Microwave Theory and Techniques* 52.10 (Oct. 2004). Conference Name: IEEE Transactions on Microwave Theory and Techniques, pp. 2438–2447. ISSN: 1557-9670. DOI: 10.1109/TMTT.2004.835916. URL: https://ieeexplore.ieee.org/document/1341664 (visited on 04/04/2025).

[32] Neha Bajwa et al. 'In vivo confirmation of hydration based contrast mechanisms for terahertz medical imaging using MRI'. In: *Terahertz Emitters, Receivers, and Applications V*. Vol. 9199. SPIE, Sept. 2014, pp. 179–186. DOI: 10.1117/12.2060115. URL: https://photonicsforenergy.spiedigitallibrary.org/conference-proceedings-of-spie/9199/91990U/In-vivo-confirmation-of-hydration-based-contrast-mechanisms-for-terahertz/10.1117/12.2060115.full (visited on 04/04/2025).

[33] Yi-Chun Du et al. 'Implementation of a burn scar assessment system by ultrasound techniques'. eng. In: *Conference proceedings: ... Annual International Conference of the IEEE Engineering in Medicine and Biology Society. IEEE Engineering in Medicine and Biology Society. Annual Conference* 2006 (2006), pp. 2328–2331. ISSN: 1557-170X. DOI: 10.1109/IEMBS.2006.260018.

[34] Benjamin A. Lipsky et al. '2012 Infectious Diseases Society of America clinical practice guideline for the diagnosis and treatment of diabetic foot infections'. eng. In: *Clinical Infectious Diseases: An Official Publication of the Infectious Diseases Society of America* 54.12 (June 2012), e132–173. ISSN: 1537-6591. DOI: 10.1093/cid/cis346.

[35] Ameer M Eltelwany, Ashraf A Zytoon and Elsayed E Elsayed. 'Role of computed tomography angiography and color Doppler ultrasonography in the evaluation of diabetic foot'. en. In: ().

[36] MD Smith Brandon J., MD Buchanan Grant S and MD Shuler Franklin. 'A comparison of imaging modalities for the diagnosis of osteomyelitis'. In: *Marshall Journal of Medicine* (July 2016). DOI: 10.18590/mjm.2016.vol2.iss3.10. URL: https://mds.marshall.edu/mjm/vol2/iss3/10 (visited on 04/04/2025).

[37] Poh Tan, Joanne Lim and Moiemen Naiem. '(PDF) Imaging Techniques Used for Wound Healing Assessment: A Systematic Review Part 1 Chronic Wounds'. en. In: *ResearchGate* (Dec. 2024). DOI: 10.3390/ebj2040015. URL: https://www.researchgate.net/publication/355452091_Imaging_Techniques_Used_for_Wound_Healing_Assessment_A_Systematic_Review_Part_1_Chronic_Wounds (visited on 04/04/2025).

[38] Line Bisgaard Jørgensen et al. 'Methods to assess area and volume of wounds - a systematic review'. eng. In: *International Wound Journal* 13.4 (Aug. 2016), pp. 540–553. ISSN: 1742-481X. DOI: 10.1111/iwj.12472.

[39] Piotr Foltynski et al. 'Accuracy and precision of selected wound area measurement methods in diabetic foot ulceration'. eng. In: *Diabetes Technology & Therapeutics* 15.8 (Aug. 2013), pp. 712–721. ISSN: 1557-8593. DOI: 10.1089/dia.2013.0026.

[40] Katherine McDermott et al. 'Etiology, Epidemiology, and Disparities in the Burden of Diabetic Foot Ulcers'. In: *Diabetes Care* 46.1 (Jan. 2023), pp. 209–221. ISSN: 0149-5992. DOI: 10.2337/dci22-0043. URL: https://www.ncbi.nlm.nih.gov/pmc/articles/PMC9797649/ (visited on 04/04/2025).

[41] *Raspberry Pi hardware - Raspberry Pi Documentation*. en. URL: https://www.raspberrypi.com/documentation/computers/raspberry-pi.html (visited on 24/04/2025).

[42] *Arduino Uno Rev3 - ATMEGA328*. 2025. URL: https://elektronicavoorjou.nl/product/arduino-uno-rev3-atmega328/ (visited on 06/07/2025).

[43] Raspberry Pi Ltd. *Buy a Raspberry Pi 4 Model B*. en-GB. URL: https://www.raspberrypi.com/products/raspberry-pi-4-model-b/ (visited on 06/07/2025).

[44] Texas Instruments. *DRV8825 Stepper Motor Controller IC*. Tech. rep. 2014.

[45] *Arduino CNC-Shield V3.00*. nl. URL: https://www.vngsystems.nl/Arduino-cnc-shield (visited on 06/07/2025).

[46] *123-3D.nl - 3D-printers | kits | parts | filament*. nl-nl. URL: https://www.123-3d.nl (visited on 06/07/2025).

[47] *SF2423-10B41 | SANMOTION F2 (2-phase) | SANMOTION | Product Site | SANYO DENKI*. URL: https://products.sanyodenki.com/en/sanmotion/stepping/f2/SF2423-10B41/ (visited on 06/07/2025).

[48] PCBLinear. *Stepper Motor NEMA 17*. Tech. rep. 2022.

[49] *Absima Servo S150MH 15Kg 25t/JR Metal Gear 2030005*. en. URL: https://www.modelsport.co.uk/product/absima-servo-s150mh-15kg-25t-jr-metal-gear-381462 (visited on 06/07/2025).

[50] *Reely S-0008 Servo Specs and Reviews*. URL: https://servodatabase.com/servo/reely/s-0008 (visited on 06/07/2025).

[51] *Reely S-0060-MG Servo Specs and Reviews*. URL: https://servodatabase.com/servo/reely/s-0060-mg (visited on 06/07/2025).

[52] *Arducam: 64MP Autofocus Camera for Raspberry Pi - B0399*. en. URL: https://instock.pk/arducam-64mp-autofocus-camera-for-raspberry-pi-b0399.html (visited on 28/06/2025).

[53] *Laser Sensor for Depth Measurement of a Hole - Laser-View Technologies*. URL: https://laser-view.com/lasers-sensors-for-hole-depth-measurement/ (visited on 06/07/2025).

[54] *TOF050F Laser Distance Sensor Module — OKY3266 – OKYSTAR*. en-US. URL: https://www.okystar.com/product-item/tof050f-laser-distance-sensor-module-oky3266/ (visited on 06/07/2025).

[55] Melexis. *MLX90640 32x24 IR array*. Tech. rep. 2019.

[56] Monique Y. Rennie et al. 'Understanding Real-Time Fluorescence Signals from Bacteria and Wound Tissues Observed with the MolecuLight i:XTM'. en. In: *Diagnostics* 9.1 (Mar. 2019). Number: 1 Publisher: Multidisciplinary Digital Publishing Institute, p. 22. ISSN: 2075-4418. DOI: 10.3390/diagnostics9010022. URL: https://www.mdpi.com/2075-4418/9/1/22 (visited on 06/07/2025).

[57] *MLX90640-D55 Thermal Camera - Waveshare Wiki*. en. URL: https://www.waveshare.com/wiki/MLX90640-D55_Thermal_Camera (visited on 06/07/2025).

[58] *SS-5GL*. nl-nl. URL: https://www.digikey.nl/nl/products/detail/omron-electronics-inc-emc-div/SS-5GL/272367 (visited on 06/07/2025).

[59] Stacey J. L. Sullivan et al. 'Clinical evaluation of non-contact infrared thermometers'. In: *Scientific Reports* 11 (Nov. 2021), p. 22079. ISSN: 2045-2322. DOI: 10.1038/s41598-021-99300-1. URL: https://www.ncbi.nlm.nih.gov/pmc/articles/PMC8586154/ (visited on 03/07/2025).

[60] *Electrical safety in active medical devices: The IEC 60601-1 standard*. en. URL: https://www.vde.com/topics-en/health/consulting/electrical-safety-in-active-medical-devices--the-iec-60601-1-standard (visited on 03/07/2025).

[61] Angelika H. Mader and Wouter Eggink. 'A Design Process for Creative Technology'. en. In: *Proceedings of the 16th International conference on Engineering and Product Design, E&PDE 2014*. The Design Society, Sept. 2014, pp. 568–573. URL: https://research.utwente.nl/en/publications/a-design-process-for-creative-technology (visited on 22/04/2025).

[62] *What Is a Printed Circuit Board (PCB)? - Technical Articles*. en. URL: https://www.allaboutcircuits.com/technical-articles/what-is-a-printed-circuit-board-pcb/ (visited on 04/07/2025).

[63] Raghbir Singh Khandpur. *Printed circuit boards: design, fabrication, assembly and testing ; [high density interconnects ; CAD/CAM techniques ; laminates ; soldering]*. en. McGraw-Hill electronic engineering. New York, NY: McGraw-Hill, 2006. ISBN: 978-0-07-146420-8.

[64] *Raspberry Pi 5 vs Raspberry Pi 4: A Comparison of Raspberry Pi Benchmarks and More*. en. Nov. 2023. URL: https://www.elektormagazine.com/news/raspberry-pi-5-vs-raspberry-pi-4-a-comparison (visited on 06/07/2025).

[65] Raspberry Pi Ltd. *Raspberry Pi Compute Module 5: A Raspberry Pi for deeply embedded applications*. en. Tech. rep. 2024.

[66] *pigpio library*. URL: https://abyz.me.uk/rpi/pigpio/python.html (visited on 24/04/2025).

[67] NXP. *PCA9685 16-channel, 12-bit PWM Fm+ I2C-bus LED controller*. en. Datasheet. 2015.

[68] *VL6180X - Time-of-Flight (ToF) proximity sensor and ambient light sensing (ALS) module - STMicroelectronics*. en. URL: https://www.st.com/en/imaging-and-photonics-solutions/vl6180x.html (visited on 30/06/2025).

[69] STMicroelectronics. *VL53L4CD Datasheet*. Datasheet. 2024.

[70] Adafruit Industries. *Adafruit VL53L4CD Time of Flight Distance Sensor - ~1 to 1300mm*. en-US. URL: https://www.adafruit.com/product/5396 (visited on 29/04/2025).

[71] Molex. 'Micro-Fit (Compliant Pin) CPI Connectors'. en. In: (2018).

[72] NXP. 'I2C-bus specification and user manual'. en. In: 2021 (2021).

[73] *Raspberry Pi Camera Pinout*. en-US. URL: https://blog.arducam.com/raspberry-pi-camera-pinout/ (visited on 07/05/2025).

[74] Shaik Nyamathulla and C. Dhanamjayulu. 'A review of battery energy storage systems and advanced battery management system for different applications: Challenges and recommendations'. In: *Journal of Energy Storage* 86 (May 2024), p. 111179. ISSN: 2352-152X. DOI: 10.1016/j.est.2024.111179. URL: https://www.sciencedirect.com/science/article/pii/S2352152X24007631 (visited on 25/06/2025).

[75] Yeru Liang et al. 'A review of rechargeable batteries for portable electronic devices'. en. In: *InfoMat* 1.1 (2019). _eprint: https://onlinelibrary.wiley.com/doi/pdf/10.1002/inf2.12000, pp. 6–32. ISSN: 2567-3165. DOI: 10.1002/inf2.12000. URL: https://onlinelibrary.wiley.com/doi/abs/10.1002/inf2.12000 (visited on 11/02/2025).

[76] A Ghafari et al. 'Batteries applications in the biomedical industry: A review'. en. In: 10 (2023).

[77] European Parliament and Council of the European Union. *Directive (EU) 2022/2380 of the European Parliament and of the Council of 23 November 2022 amending Directive 2014/53/EU on the harmonisation of the laws of the Member States relating to the making available on the market of radio equipment*. Issue: 2022/2380 Series: L. Nov. 2022.

[78] Adam McGaffin. 'USB Type-C® and USB Power Delivery: Designing for both Extended Power Range and battery-powered systems'. en. In: (2024).

[79] James Adams. *Introducing Raspberry Pi HATs*. en-GB. July 2014. URL: https://www.raspberrypi.com/news/introducing-raspberry-pi-hats/ (visited on 04/07/2025).

[80] Raspberry Pi Ltd. *Raspberry Pi Compute Module 5 IO Board: An application board for Raspberry Pi Compute Module 5*. en. Datasheet. 2024.

[81] *Star Topology - an overview | ScienceDirect Topics*. URL: https://www.sciencedirect.com/topics/computer-science/star-topology (visited on 04/07/2025).

[82] *Waveshare Raspberry Pi 5 Camera Cable - 22 to 15 pin FPC-FFC flex - 20cm*. en. URL: https://www.tinytronics.nl/en/cables-and-connectors/cables-and-adapters/ffc/waveshare-raspberry-pi-5-camera-cable-22-to-15-pin-fpc-ffc-flex-20cm (visited on 04/07/2025).

[83] Robotis. *ROBOTIS e-Manual*. en. URL: https://emanual.robotis.com/docs/en/dxl/x/xl320/ (visited on 19/05/2025).

[84] OSRAM Opto Semiconductors. *DURIS S 5 White (LW TTSD) Datasheet*. Datasheet Rev. 2.0. 2019. URL: https://assets.osram.info/im/global/assets/Flatfiles/OSRAM_Datasheet_DURIS_S_5_white_LW_TTSD_EN.pdf.

[85] Vishay Semiconductors. *VLMU3100 UV SMD LED PLCC-2 Datasheet*. Datasheet. 2017. URL: https://www.vishay.com/docs/82556/vlmu3100.pdf.

[86] Robotis. *ROBOTIS e-Manual*. en. URL: https://emanual.robotis.com/docs/en/dxl/x/xl430-w250/ (visited on 19/05/2025).

[87] Texas Instruments. *WEBENCH Power Designer*. URL: https://webench.ti.com/power-designer/switching-regulator?powerSupply=0 (visited on 02/06/2025).

[88] Samsung SDI Co., LTD. *INR18650-30Q Cell Specification*. Datasheet Version 1.0. Samsung SDI Co., LTD., Jan. 2015. URL: https://e2e.ti.com/cfs-file/__key/communityserver-discussions-components-files/196/INR18650_2D00_30Q_5F00_datasheet.PDF.

[89] *Samsung INR18650-30Q - 3.6V - 3.7V, 3000mAh (15A)*. nl-NL. URL: https://www.akku-shop.nl/nl/samsung-inr18650-30q-36v-37v-3000mah-15a/ (visited on 04/07/2025).

[90] European Committee for Standardization. *Safety of machinery - Emergency stop function - Principles for design*. European Standard. Brussels, Belgium, 2015.

[91] *Compute Module 5 Passive Cooler*. nl. URL: https://www.kiwi-electronics.com/nl/compute-module-5-passive-cooler-20297 (visited on 04/07/2025).

[92] *PicoBlade Connectors | Molex*. en-US. URL: https://www.molex.com/en-us/products/connectors/wire-to-board-connectors/picoblade-connectors (visited on 28/06/2025).

[93] *Micro-Fit Connectors | Molex*. en-US. URL: https://www.molex.com/en-us/products/connectors/wire-to-board-connectors/micro-fit-connectors (visited on 28/06/2025).

[94] *PicoBlade Standard Connectors*. nl-nl. Sept. 2016. URL: https://nl.mouser.com/molex-picoblade (visited on 04/07/2025).

[95] *Micro-Fit 3.0 OTS Discrete Cable Assemblies*. nl-nl. May 2020. URL: https://nl.mouser.com/molex-microfit-3-dual-row-ots-cable-assemblies (visited on 04/07/2025).

[96] Prabu Kumar. *GMSL Camera over MIPI Camera*. en-US. Nov. 2021. URL: https://www.e-consystems.com/blog/camera/technology/gmsl-camera-over-mipi-camera/ (visited on 03/07/2025).

[97] Lee Jackson. *7 Types of MIPI CSI 2 Converters & Bridges: Turning MIPI-CSI 2 Cameras into Other Interfaces*. en-US. Sept. 2021. URL: https://blog.arducam.com/mipi-csi-2-converters-bridges-other-interfaces/ (visited on 03/07/2025).

[98] *The Ultimate DYNAMIXEL Daisy Chaining Guide*. en. URL: https://www.robotis.us/robotis-ir-pr-blog/the-ultimate-dynamixel-daisy-chaining-guide/ (visited on 03/07/2025).

[99] Raspberry Pi Ltd. *Raspberry Pi 15W USB-C Power Supply*. Tech. rep. Raspberry Pi Foundation, 2024.

[100] Editorial Team. *Design for Manufacturing (DFM): A Guide to Optimizing Product Development*. en-US. Oct. 2024. URL: https://www.6sigma.us/six-sigma-in-focus/design-for-manufacturing-dfm/ (visited on 30/06/2025).

[101] SAE Media Group. *Design for Manufacturability Improves Articulating Instrument Development*. en. May 2019. URL: https://www.medicaldesignbriefs.com/component/content/article/34431-design-for-manufacturability-improves-articulating-instrument-development (visited on 30/06/2025).